Patrick Matthias Perner, BSc

Smart additively manufactured components

Master's Thesis

To achieve the university degree of

Angestrebter akad. Grad

Diplom-Ingenieur/Master of Science

Master's degree programme: Mechanical Engineering and Business Economics

submitted to

Graz University of Technology

Supervisor

Dipl.-Ing. BSc Matthias Helmut Friessnig – Dipl.-Ing. Dr.techn. Hans Peter Schnöll

Institute of Innovation and Industrial Management
Univ.-Prof. Dipl.-Ing. Dr.techn. Christian Ramsauer

Supervisor

Dipl.-Ing. BSc Christoph Monsberger

Institute of Engineering Geodesy and Measurement Systems
Univ.-Prof. Dipl.-Ing. Dr.techn. Werner Lienhart

Graz, September 2018

Affidavit

I declare that I have authored this thesis independently, that I have not used other than the declared sources/resources, and that I have explicitly indicated all material which has been quoted either literally or by content from the sources used. The text document uploaded to TUGRAZonline is identical to the present master's thesis dissertation.

Date

Signature

Acknowledgement

I would like to say thank you to everyone who supported and accompanied me during the past years, especially during the period of education at Graz University of Technology and the concluding master thesis.

Special thanks to the two supporting institutes of my master thesis at Graz University of Technology. Univ.-Prof. Dipl.-Ing. Dr.techn. Christian Ramsauer and Univ.-Prof. Dipl.-Ing. Dr.techn. Werner Lienhart and their staff, especially Dipl.-Ing. BSc Christoph Monsberger, Dipl.-Ing. BSc Matthias Helmut Friessnig and Dipl.-Ing. Dr.techn. Hans Peter Schnöll, were constantly supporting and supervising my thesis and providing the necessary equipment and resources for accomplishing the predefined goals.

Thanks also to all my friends and fellow students with whom I spent the best moments of my life so far. Let us continue having a great time together.

Finally, my biggest thanks go to my parents Ingrid and Matthias, my sister Iris and of course my girlfriend Andrea. They are not only supporting me financially but are constantly holding my back. Without their unfailing support and continuous encouragement throughout my years of study, my accomplishments would have been almost impossible. Thank you!

Abstract

The innovative concept of smart additively manufactured components is a combination of two already existing, future-oriented technologies. Additive manufacturing, a technology that is currently disrupting the manufacturing industry, is used to generate the base structure of these components. Additionally, the continuously improving technology of fiber optic sensing is integrated into the manufactured structure to provide various sensing capabilities.

This master thesis will provide a feasibility study on this described concept. Therefore, a detailed analysis of the combined technologies is conducted. Both technologies, fiber optic sensing and additive manufacturing are especially evaluated concerning their possibility of combining them into smart structures.

This created knowledge base is then used to provide an overview where smart additively manufactured components can be implemented. A future perspective and development ideas can be used as input for further research.

The manufactured smart prototypes are described and detailed guidelines on how these components can be produced is created. Furthermore, laboratory measurements are carried out in order to analyse and validate the characteristics of the manufactured elements. Special equipment is designed to perform tensile and bending tests. A highly accurate optical interferometer is used to perform reference measurements. The necessary equipment for manufacturing and testing the smart components is provided by the two supporting institutes of Graz University of Technology. In that way, essential parameters of the tested smart components can be determined.

The developed concept can be regarded feasible. The collected information, further improvement proposals and the results of the performed laboratory measurements can be used as a solid base for additional research and product development.

Kurzfassung

Das innovative Konzept für “Smart additively manufactured components” ergibt sich aus der Kombination von zwei bestehenden, zukunftsorientieren Technologien. Die Methoden der additiven Fertigung, die bereits jetzt ihren Industriesektor revolutionieren, werden zur Erzeugung der Grundstruktur dieser sensitiven Komponenten verwendet. Zusätzlich wird eine aufstrebende Technologie, die faseroptische Sensorik, in die Bauteile miteingebunden. Dies ermöglicht die Produktion von sensitiven Elementen.

Im Zuge der vorliegenden Masterarbeit wird eine Machbarkeitsstudie für dieses Konzept durchgeführt. Dafür werden zuerst die beiden kombinierten Technologien analysiert und bewertet. Sowohl die faseroptischen Messsysteme als auch die Methoden der generativen Fertigung werden speziell in Bezug auf deren Kombination zu smarten Strukturen überprüft und beurteilt.

Aufbauend auf dieser Wissensgrundlage wird ein Überblick über die möglichen Einsatzgebiete von diesen Bauteilen erstellt. Zukunftsprognosen und Entwicklungsansätze werden als Input für weitere Erforschungen angefügt.

Die Beschreibung der produzierten Prototypen als auch detaillierte Guidelines über die Herstellung dieser dienen als Leitfaden. In Laboruntersuchungen werden diese Bauteile schließlich vermessen und analysiert. Speziell entworfene Aufbauten für die vorhandene Kalibrieranlage werden verwendet um Zug- und Biegeversuche durchzuführen. Referenzmessungen werden dabei mit einem Interferometer aufgezeichnet. Das benötigte Equipment zur Fertigung und Erprobung der sensitiven Komponenten wird von den beiden betreuenden Instituten der Technischen Universität Graz zur Verfügung gestellt. Das ermöglicht die Bestimmung von wesentlichen Kenngrößen der gefertigten Bauteile.

Das entwickelte Konzept kann als realisierbar betrachtet werden. Die gesammelten Informationen, zusätzliche Verbesserungsvorschläge und die Resultate der durchgeführten Labormessungen können als solide Basis für weiterführende Forschung und Produktentwicklung verwendet werden.

Contents

Abbreviations

BJ	Binder Jetting
CDLP	Continuous Digital Light Processing
DLP	Digital Light Processing
DMLS	Direct Metal Laser Sintering
DOD	Drop On Demand
EBAM	Electron Beam Additive Manufacturing
EBM	Electron Beam Melting
FabLab	Fabrication Laboratory
FBG	Fiber Bragg Grating
FDM	Fused Deposition Modelling
FFF	Fused Filament Fabrication
FOS	Fiber Optical Sensors
IGMS	Institute of Engineering Geodesy and Measurement Systems, TU Graz
IIM	Institute of Innovation and Industrial Management, TU Graz
LENS	Laser Engineering Net Shape
LOM	Laminated Object Manufacturing
LUNA OBR 4600	LUNA Optical Backscatter Reflectometer 4600
Mark One	MarkForged Mark One™
MJ	Material Jetting
MJF	Multi Jet Fusion
NASA	National Aeronautics and Space Administration
NPJ	Nanoparticle Jetting
OBR	Optical Backscatter Reflectometer
OFDR	Optical Frequency Domain Reflectometry
OTDR	Optical Frequency Domain Reflectometry
PJ	Photopolymer Jetting
SLA	Stereolithography
SLM;	Selective Laser Melting
SLS	Selective Laser Sintering
TU Graz	Graz University of Technology
UAV	Unmanned aerial vehicle

1. Introduction

Joseph A. Schumpeter defined in one of his books innovation as the process of finding economic applications for the inventions.[1] In case of this thesis, two already existing technologies are combined to create a new use case – additively manufactured smart components. The concept of additive manufacturing, an emerging technology, which has already grown to a multi-billion-dollar market, is used for producing the base structure of these components. To make these components smart, in case of this thesis sensitive to strain and temperature changes, fiber optical sensors (FOS) are integrated into the structure. This integration of FOS can then be applied to produce a variety of sensitive components with highly individual layouts for all sorts of different use cases.

1.1 Concept and idea development

In cooperation with the Institute of Innovation and Industrial Management (IIM) and the Institute of Engineering Geodesy and Measurement Systems (IGMS), both from Graz University of Technology (TU Graz), a concept for manufacturing smart elements by combining the technologies of additive manufacturing and fiber optic sensing is developed. An analysis of the technical capabilities available within this thesis is necessary to verify the feasibility of producing these smart components. An optical fiber needs to be integrated into the structure of an additively manufactured element without being damaged. The exact location and positioning of the fiber needs to be known to interpret the measurement data correctly. This concept for manufacturing smart elements is put to practice and validated within this master thesis.

1.2 Objectives

The concept of producing smart elements by integrating a FOS into an additively manufactured component should be evaluated, validated and a number of these smart elements should be produced. An analysis of existing additive manufacturing technologies, especially fused filament fabrication with continuous fiber reinforcement, serves as a basis for realizing this concept within the thesis. A manufacturing strategy should be developed in order to produce functional smart elements with embedded FOS. Furthermore, various guidelines on how these smart components need to be designed and manufactured will enable the reader of this thesis to produce smart components on their own.

1.3 Structure

The first part of the master thesis provides an overview of the technologies used to produce smart additively manufactured components.

A detailed analysis of the technologies used to manufacture these smart elements is done to create a knowledge base for further procedure. The theoretical research provides a better understanding of

[1] Joseph Schumpeter, *Theorie Der Wirtschaftlichen Entwicklung*, 7. Auflage, 1987, p. 120.

the crucial aspects of the two combined technologies. By identifying the boundary conditions and by evaluating the limits of the additive manufacturing processes and the fiber optical sensing methods, the following practical steps can be made. Chapter 2 describes the used sensing technology and the important physical properties which should be taken into consideration for this special use case. An analysis of different additive manufacturing methods is performed within chapter 3 as well as an evaluation regarding the feasibility to produce these sensitive components.

Chapter 4 provides an overview of the possibilities within this innovative concept. The advantages of this method of manufacturing highly individual sensitive components are described and a concept of an ideal printer is proposed. Furthermore, some interesting developments in this sector of technology are mentioned and possible future developments are presented.

The realized prototypes within this thesis and a detailed description on how to manufacture them is presented in chapter 5. An overview of the different stages of the prototypes is used to provide an impression of the development process.

The prove of concept is accomplished with some early stage prototypes. Laboratory measurements, detailed within chapter 6, are performed. The results and interpretation of those tests can be found in this part of the thesis.

A conclusion and further perspectives are included in chapter 7. Those will be used to suggest strategies for further improving the developed concept of smart additively manufactured components.

The described structure of the thesis is illustrated in Figure 1-1.

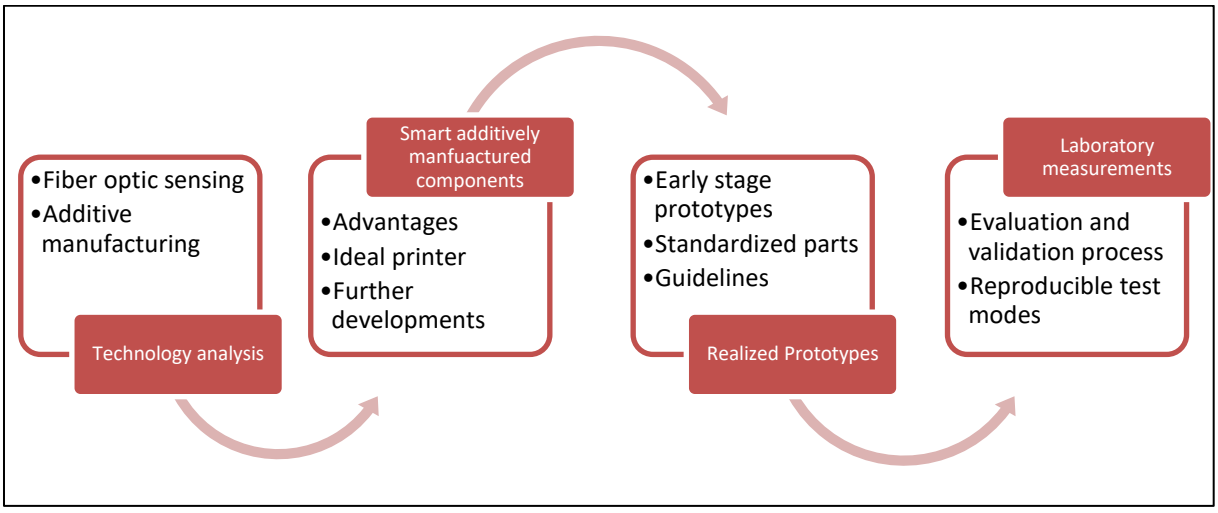

Figure 1-1 Structure of the master thesis

2. Fiber optic sensing

The realisation of additively manufactured smart elements is accomplished by the integration of FOS into the produced components. Therefore, a technology overview is created. As there are different types of FOS, the most suitable sensing system has to be chosen according to certain boundary conditions within the process of additive manufacturing.

2.1 Optical fiber technology

In order to provide basic knowledge of fiber optic sensing, the following sections will give a short overview of this technology. The focus will be on topics and properties of optical fibers relevant to produce smart components by using the methods of additive manufacturing.

2.1.1 Structure of optical fibers

In general, a standard optical fiber is composed from the core, the cladding and the coating on the outside. This basic construction is shown in the Figure 2-1. The core is usually made from pure silica glass ($SiO2$) while the cladding is doped with Aluminium (Al) and Germanium (Ge). Therefore, the index of reflection of the core n_{core} is slightly bigger than that of the cladding $n_{cladding}$. This difference between the indices of reflection, together with the small diameter of the core enables a total reflection inside the core and a propagation of the optical signal. [2]

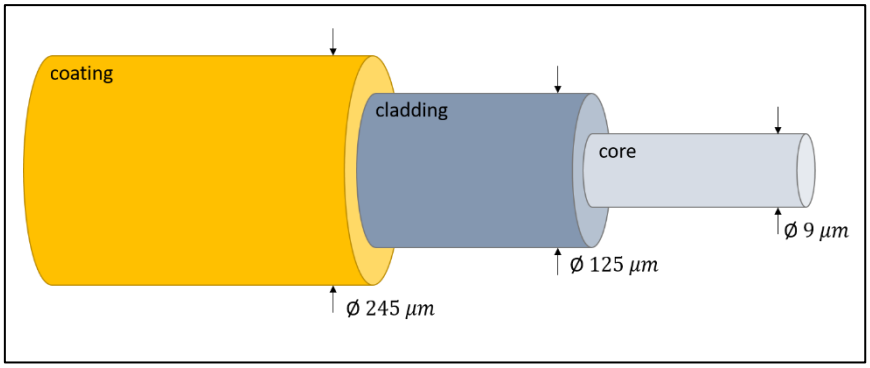

Figure 2-1 Basic construction of a single mode optical fiber [3]

The coating is generally made from a synthetic material (acrylate, polyamide, ORMOCER®, etc.) and works as a protection layer from mechanical damage and humidity. More expansive special coating materials like gold and aluminium can also be applied to the fiber. In this way, some additional properties like increasing the operational temperature range are realised. [4]

[2] cf. Zujie Fang and others, *Fundamentals of Optical Fiber Sensors*, ed. by Kai H Chang, 2012, p. 10 f.
[3] after Corning, *SMF-28e+ Optical Fiber Specification Sheet*, 2014.
[4] cf. Fibercore, *SM1250(10.4/125)Gold*; FBGS International, *DTG-A3*.

A rigid connection between the core and the cladding as well as between the cladding and the coating is crucial for using the optical fiber as a strain-sensing element because the strain must be transferred to the core without losses. [5]

2.1.2 Properties of optical fibers

The characteristics and properties of optical fibers are related to the composition of the glass used for the core and the cladding as well as to the material of the coating. For a given task, an analysis of the existing products needs to be done in order to identify the suitable optical fiber.

The elastic behaviour of optical fibers is classified by using standardized models from engineering mechanics. Therefore, applying the Hooke's law to an optical fiber, its tensile stress σ is linearly proportional to its strain ε by the modulus of elasticity E. Experiments at the IGMS show that the elongation at fracture for optical fibers is between $6{,}4\%$ and $8{,}1\%$. This results in a limitation for using FOS to detect strain directly. By realising an indirect strain measurement system through wrapping around the fiber along the elongated object, the detectable strain maximum can be increased. [6]

Another limiting aspect is the temperature range to which the optical fiber will be exposed while being implemented and used as a sensing element. The limiting factor concerning temperature is the material of the coating. As the core and the cladding are made from glass, their melting point is around $1900°C$ while the most common polymer coatings only have a range of application up to $300°C$. Some special coatings made form metals like gold or aluminium may be exposed to temperatures up to $700°C$. A comparison of the operational temperature range of some optical fibers can be seen in Table 2-1. [7]

Table 2-1 Operational temperature range of various optical fiber sensors; information taken from datasheets [8]

Manufacturer	Sensor	Coating	Temperature range		
Corning	SMF-28e+	Acrylate	-60°C	to	+85°C
FBGS Technologies	DTG-A3	ORMOCER®	-200°C	to	+200°C
Fibercore	SM 980	Polyimide	-55°C	to	+300°C
TAIHAN	ITU-T G.657	UV Acrylate	-60°C	to	+85°C
FIBERCORE	SM 1250(10.4/125)Cu	Copper		to	+450°C
FIBERCORE	SM1250(10.4/125)Gold	Gold		to	+700°C

[5] cf. Christoph Monsberger, 'Verteilte Faseroptische Dehnungsmessung Mit Dem Hochauflösenden Luna OBR 4600', 2015, p. 4.
[6] cf. Monsberger, p. 9.
[7] cf. Casimer M. DeCusatis and Carolyn J. Sher DeCusatis, *Fiber Optic Essentials*, 2006, p. 167 f.
[8] cf. Corning, *SMF-28e+ Optical Fiber Specification Sheet*, 2014; FBGS International; TAIHAN, *Bending Loss Insensitive Fiber ITU-T G.657*; Fibercore, *SM1250(10.4/125)Cu*; Fibercore, *SM1250(10.4/125)Gold*.

2.2 Sensing Technologies

In order to use optical fibers as sensing elements, their sensitivities to strain and temperature changes and the behaviour of the fiber's physical properties must be well understood. Different sensitivities of the optical fibers concerning physical conditions are used to create various sensors. [9]

2.2.1 Optical fibers as sensing elements

Regarding the flexibility of implementing fiber optic sensors, there is a wide field of application for this technology. Fiber optic sensors are currently used in the telecommunication industry, the oil industry, the military, in the fields of medicine, the aviation and aerospace industry, the automotive industry, in civil engineering and in many other different areas. More detailed information on structural and composite monitoring projects can be found in the "Handbook of Optical Fibre Sensing Technology" by José Miguel López-Higuera [10]. An example for the use of optical fibers in the aerospace industry is the National Aeronautics and Space Administration (NASA) project of monitoring the deflection and strain of the wings of an unmanned aerial vehicle (UAV) is described in the case study[11].

In advantage to conventional sensing systems, fiber optic sensors are insensitive to electromagnetic disturbances and do not need any power supply at the sensing element. This provides the possibility to use those sensors in explosive and fire hazardous areas. The measurement system itself may be far away from the sensing unit as signal loss within a supply fiber optical cable is minimal. With different fiber optical sensing methods, it is possible to have more than one sensing element on one single fiber or even use the fiber itself as a continuous and distributed sensing element to perform measurements. This guarantees an easy cabling because only one optical fiber cable is necessary to perform measurements at different locations. In contrast to that, other conventional sensing methods need a separate cabling for each sensor. The small dimensions and the lightness of the optical fibers assure that the sensing element itself hardly influences the object which should be measured. In addition, these optical fibers are easily integrated and embedded into structures and objects. Conventional optical fibers, which are also used for telecommunication purposes, are not just very low cost but also capable to perform measurements within a reasonable temperature range. For more extreme temperatures, there are optical fibers with special coatings available which can operate between $-270°C$ up to $+700°C$ (see Table 2-1). [12]

Fiber optic sensors are either available as ready to use sensors or the bare fiber is specially installed as the sensing element. A ready to use sensor has a protective encapsulation around the fiber optic sensing element and can be directly mounted or welded to an object or embedded into a structure. Installing the bare fiber provides the highest flexibility for arranging the sensor but the installation process must be carefully handled and an additional protection of the bare fiber is necessary. [13]

[9] cf. Fang et al., p. 76.
[10] cf. José Miguel López-higuera, *Handbook of Optical Fibre Sensing Technology*, 2014, p. 488 ff., 517 .
[11] cf. Strain Monitoring, 'NASA UAV Deflection And Strain Monitoring', 2008.
[12] cf. Eric Udd and William Spillman, *Fiber Optic Sensors: An Introduction for Engineers and Scientists*, 2011, p. 409 f.
[13] cf. Ginu Rajan, *Optical Fiber Sensors: Advanced Techniques and Applications*, 2015, pp. 19, 20.

2.2.2 Classification of fiber optical sensors

Based on the different principles used to realize measurements with FOS, the sensing system can be categorized as follows. A short description of the methods provides the foundation for choosing a suitable measurement strategy to be integrated into smart additively manufactured components.

- Single Point Sensors

These sensors are specially designed and perform measurements at specific local points along the optical sensing fiber. Typical single point sensors are microbend and macrobend sensor [14] Fabry-Perot, Mach-Zehnder and Michelson interferometers. These FOS are mostly prefabricated sensor that are directly mounted to measured objects. As the measurement point is predefined with the positioning of the sensor, only this specific area can be supervised using this kind of sensors. [15]

- Quasi distributed sensor array

The integration of so called Fiber Bragg Gratings (FBG) enables to equip a single optical fiber with multiple sensitive areas along the fiber. These embedded FBGs reflect a certain wavelength of the broadband incoming optical signal. If the sensitive area of the optical fiber is deformed, there is a shift in the wavelength of the reflected signal. This shift can be detected and analysed by using an optical spectrometer. It is crucial, that the reflected signals from integrated FBGs along a single optical fiber do not interfere with each other when the fiber is deformed.[16]

- Distributed sensing element

The fundamental mechanisms that enable distributed sensing along an optical fiber are based on different scattering effects which occur when light is propagating through glass. Random inhomogeneities within the core of the optical fiber cause backscattering effects. These effects can be correlated to changes in physical parameters like strain or temperature along the optical fiber. The three main scattering mechanisms optical fiber sensors are based on are Rayleigh-, Raman- and Brillouin-scattering. Table 2-2 shows a comparison of these scattering effects concerning their potential for performing measurements:

Table 2-2: Distributed fiber optic sensor applications [17]

Scattering effect	Measurand	Range	Spatial resolution
Rayleigh	Strain and temperature	Mid-length (70 m)	High (1 cm)
Brillouin	Strain and temperature	Long (2 - 50 km)	Low (20 -1000 cm)
Raman	Temperature	Long (8 km)	Medium (100 cm)

Raman scattering effects can be correlated to functions that represent the physical conditions of temperature changes. Therefore, Raman signals can be used for distributed temperature sensing. But these systems are not sensitive to other physical parameters like strain.[18]

[14] cf. Ginu Rajan, p. 19 f.
[15] cf. Ginu Rajan, p. 16 ff.
[16] cf. Mousumi Majumder et al., 'Fibre Bragg Gratings in Structural Health monitoring—Present Status and Applications' ,2008.
[17] cf. Ginu Rajan, p. 17 f.; cf. FibrisTerre-Systems-GmbH, *fTB 2505 Series*.
[18] cf. Fang et al., p. 302.

Brillouin and Rayleigh scattering effects can be correlated to changes of the physical conditions of temperature and strain. Brillouin scattering systems offer the possibility to measure both strain and temperature over longer distances. The higher intensity of Rayleigh scattering based signals makes those systems the best suitable for strain measurements with high spatial resolution. [19]

As the goal is to accomplish smart elements, which are sensitive along the whole fiber inside the components, a distributed optical sensing system with a high spatial resolution is selected. A suitable measuring instrument available within the limits of this master thesis is the LUNA Optical Backscatter Reflectometer 4600 (LUNA OBR 4600). This system is used to perform measurements with all the additively manufactured components. The measuring device is capable of performing distributed strain and temperature measurements along single mode optical fibers by using Optical Frequency Domain Reflectometry (OFDR).

[19] cf. Ginu Rajan, p. 311 f.

3. Additive manufacturing

The technology of additive manufacturing provides the possibility of using digital models to manufacture products. A three-dimensional, real-life object which was designed and modelled digitally, is created through adding layer-upon-layer to a structure until the geometry of the manufactured component is completed. By dividing the three-dimensional manufacturing problem into multiple two-dimensional production steps, nearly any possible complex geometry can be produced. The processes of generating these layers vary depending on the material used for production. CAD models can be produced immediately without the need of creating special tools and forms beforehand. Various materials, which then define the part's properties, can be used for this way of manufacturing highly complex products. The component's geometry can be generated very precisely in the working x-y-layer. The precision in z-direction depends on the layer thickness. The resulting step-effect is characteristic for additive manufacturing processes. [20] [21]

Nowadays, the demand for highly innovative and individual products for a competitive price is constantly increasing. Additionally, product lifecycles are decreasing which leads to shorter amortization periods for investments in tooling and machines. The methods of additive manufacturing can be used to generate various high-quality products in small batch sizes without the need of big additional investments. Customer-specific components can be manufactured for relatively low costs. In contrast to subtractive manufacturing methods like turning and milling, there is hardly any scrap material during the production process. Furthermore, geometries with indentations that cannot be realized through subtractive methods can be manufactured additively. Considering that computer aided design and manufacturing is gaining more and more importance with the transformation to industry 4.0, the methods of additive manufacturing are a technology driver and enabler. The rising importance of additive manufacturing is also reflected in the forecast of the market volume shown in Figure 3-1.[22]

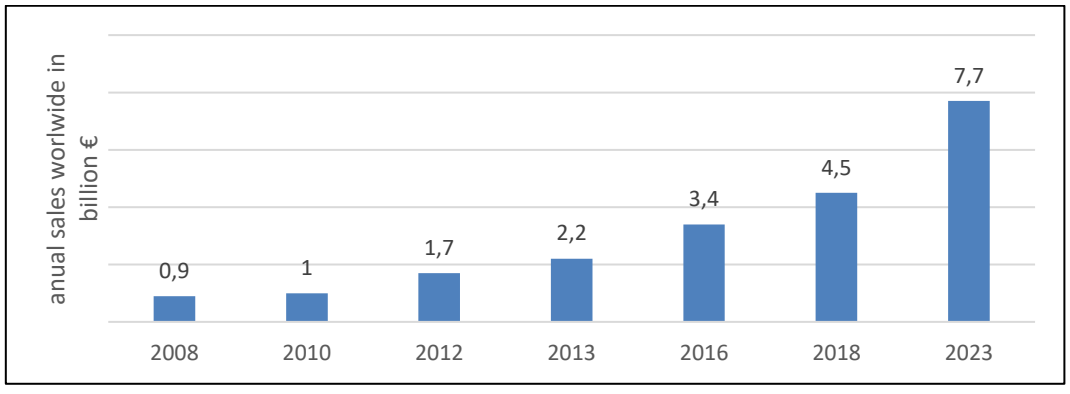

Figure 3-1: Forecast of market volume for additive manufacturing services, systems and materials [23]

[20] cf. Petra Fastermann, *3D-Drucken*, 2016.
[21] cf. Tobias Schmidt, *Potentialbewertung Generativer Fertigungsverfahren Für Leichtbauteile*, 2016.
[22] cf. Carsten Feldmann and Andreas Pumpe, *3D-Druck – Verfahrensauswahl und Wirtschaftlichkeit*, 2016, p. 1 f.
[23] cf. Roland Lachmayer and Rene Bastian Lippert, *Additive Manufacturing Quantifiziert*, 2017, p. 3

The most common additive manufacturing processes will be described and evaluated in the following sections. The focus of the evaluation will be on the aspect that a continuous optical fiber needs to be integrated into the manufactured structure to produce sensitive components.

3.1 Categorization and evaluation of additive manufacturing methods

To provide an overview of the most common additive manufacturing methods currently available, those methods are categorised depending on the raw material production concept used for producing components. This categorisation is shown in the first two columns of Table 3-1. Additionally, a quick overview of the advantages and disadvantages regarding the implementation of a continuous optical fiber into the manufactured structure of the various technologies is provided within this table.

Table 3-1 Categorization and evalution overview of manufacturing methods regarding continuous fiber integration

Method	Concepts	Advantages	Disadvantages
Vat Polymerization	• Stereolithography • Digital Light Processing • Continuous Digital Light Processing	Minimal thermal impacts to the optical fiber due to low manufacturing temperature	Technical difficulties of precisely positioning the fiber within the liquid resin Lack of fusion between fiber coating and additively manufactured structure
Material Extrusion	• Fused Filament Fabrication	Easily adoptable process Printing temperature range compliant with standard optical fiber coating Automated fabrication of complex sensor layouts	Weak mechanical properties of the manufactured components
Material Jetting	• Material Jetting • Nanoparticle Jetting • Drop On Demand	Fiber integration process can be provided by an additional print head	Coating material of the optical fiber has to be aligned with the material used for additive manufacturing
Binder Jetting	• Binder Jetting	No temperature issues Binder can be used to provide a sufficient connection between the fiber and the manufactured component	Fiber needs to be placed into the loose powder No complex sensor geometries possible

Powder Bed Fusion	• Selective Laser Sintering • Multi Jet Fusion • Direct Metal Laser Sintering / Selective Laser Melting • Electron Beam Melting	Possibility to generate metal components with integrated optical fiber sensors	Specially coated fibers are necessary to meet the temperature requirements Fiber needs to be placed into the loose powder No complex sensor geometries possible
Direct Energy Deposition	• Laser Engineering Net Shape • Electron Beam Additive Manufacturing	/	Optical fibers is likely to be damaged during the manufacturing process due to the high temperature
Sheet Lamination	• Laminated Object Manufacturing	Low temperature laminating methods enable the manufacturing of metal components with integrated optical fiber sensors	Fiber channel has to be manufactured before the integration of the sensor between two laminated layers

The differences between all the additive manufacturing methods concerning material properties of the finished components, internal structure, level of detail, speed of fabrication and many more are all influencing the fabrication methods of smart elements. But the most crucial aspect for evaluating these additive manufacturing methods is the feasibility of integrating a continuous optical fiber into the structure of the manufactured component. The optical fiber must not be damaged during this integration process. The core and the cladding of the optical fiber need to stay unharmed, whereas the fiber's coating has to form a strong connection between the additively manufactured structure and the sensitive element. Furthermore, the exact positioning of the optical fiber during the manufacturing process must be guaranteed. Otherwise, the measurement results might be interpreted incorrectly afterwards.

The two most important parameters regarding the fabrication of a functional smart element are on the one hand the temperature the optical fiber is exposed during the integration process and the additive manufacturing process itself. On the other hand, there is the placement method which should provide an accurate fiber positioning while not damaging the optical fiber. Regarding these two aspects, the manufacturing methods are explained and will be evaluated in greater detail.

3.1.1 Vat Polymerization

The effect of photopolymerization occurs when a photoreactive resin is exposed to light of a specific wavelength. As a result, the resin solidifies locally. This is used to build up three-dimensional parts layer by layer. Digital light processing technology is used for mapping the single layers within this process. [24]

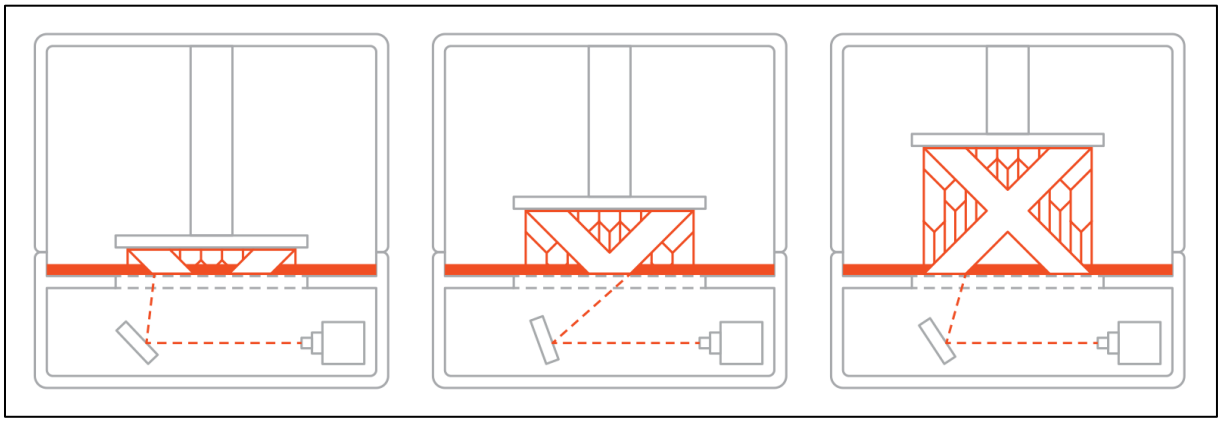

Figure 3-2: Manufacturing concept of Vat polymerization [25]

- Stereolithography (SLA)

A laser beam is used to solidify one layer of a photoreactive polymer. This process uses a build platform submerged into a tank filled with a liquid photopolymer resin. The platform is either submerged into the tank layer by layer and the surface of the resin is mapped by the laser to generate the component or the platform is lifted after each single layer is mapped and solidified through a translucent tank from the bottom. The minimal lateral extension of a single line is limited by the diameter of the laser beam. This makes the manufacturing process of stereolithography the most accurate one which is currently available. To improve the mechanical properties of a finished component it is possible to additionally cure the part using UV irradiation. [26]

- Digital Light Processing (DLP)

An almost similar process to SLA is used with DLP to produce three-dimensional components. Instead of using a laser beam for solidifying a photoreactive polymer, a digital light projector screens the image of each layer onto the resin to harden the liquid photopolymer. As within this method the images of each layer are composed of pixels, the single layers are formed from small rectangular bricks called voxels. Compared to SLA, DLP is able to achieve faster print times, as each layer is exposed all at once rather than mapped with a single laser beam.[27]

[24] cf. Fritz Klocke, *Fertigungsverfahren 5*, 2015, p. 131.
[25] 'SLA Process' <https://s3-eu-west-1.amazonaws.com/3dhubs-knowledgebase/introduction-sla-3d-printing/8-sla-steps.png> [accessed 2 March 2018].
[26] cf. Klocke, p. 135 f.; cf. Andreas Gebhardt and Jan-Steffen Hötter, *Additive Manufacturing: 3D Printing for Prototyping and Manufacturing*, 2016, p. 97 ff.
[27] cf. Gebhardt and Hötter, p. 126 ff.

- Continuous Digital Light Processing (CDLP)

CDLP is sometimes referred to as continuous liquid interface production (CLIP) which is the trademark name of this production process first presented at a TED-conference in 2015. The part production process is the same as with DLP except that the build platform is continuously moved in the Z direction (upwards or downwards). Meanwhile a digital light projector continuously screens the images of the single layers onto the resin which then solidifies through photopolymerization. This allows a 25 up to 100 times increase in build speed compared to conventional additive manufacturing methods. [28]

- **Evaluation:**

As the components are manufactured by solidifying a liquid photoreactive resin, the optical fiber needs to be placed within this liquid resin layer before it is solidified through the exposure to a light source. The exact placement of a continuous fiber inside this liquid resin could lead to difficulties as there is no possibility of temporarily fixing the optical fiber. Furthermore, the connection between the optical fiber and the additively manufactured structure might not be sufficient due to a lack of fusion between the two components.

[28] cf. '3dhubs Knowledge-Base' <https://www.3dhubs.com/knowledge-base/additive-manufacturing-technologies-overview> [accessed 18 July 2017]; cf. Fastermann, *3D-Drucken*, p. 35 f.

3.1.2 Material Extrusion

Developed from conventional extrusion processes, this method of additive manufacturing uses heated nozzles for melting a filament material to produce components layer by layer. Material extrusion is a frequently used production method for rapid prototyping, modelling as well as small batch productions. [29]

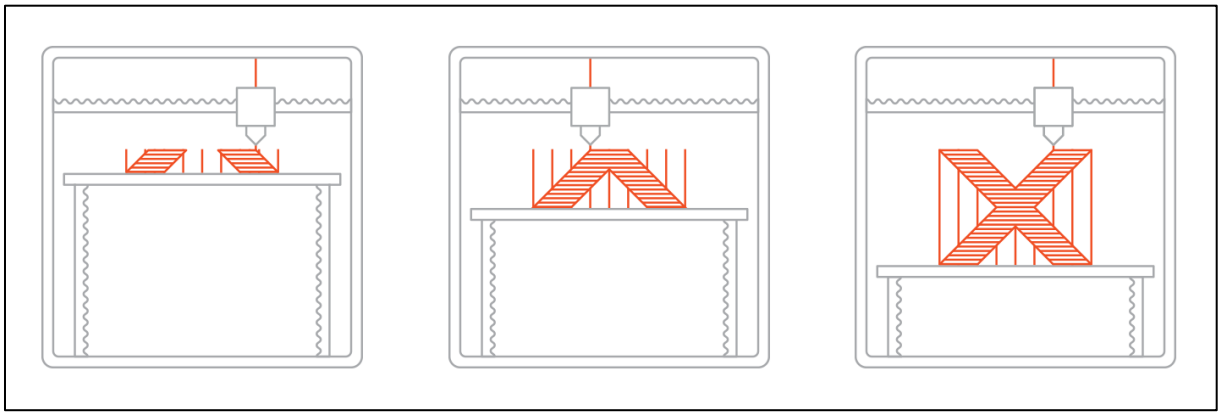

Figure 3-3: Manufacturing concept of Material Extrusion [30]

- Fused Filament Fabrication (FFF) / Fused Deposition Modelling (FDM: registered trademark of Stratyses Ltd., California)

A thermoplastic material (filament) is continuously extruded through an electrically heated nozzle which melts the filament. This nozzle is following a predetermined path along the print bed, laying down the melted material. It instantly cools down due to heat conduction into the component and thermal radiation to the surrounding and thus solidifies. Different filament materials with varying strength and temperature properties like acrylonitrile butadiene styrene (ABS) or polylactide (PLA) are available within this manufacturing process. The flexibility – regarding part design and producible geometries – of this manufacturing process is very high, although temporary supporting structures are needed for overhanging or slanted geometries. [31]

- **Evaluation:**

The possibility of using various extrusion print heads for generating one components provides the possibility of integrating a continuous optical fiber between two layers of filament. The operating temperature range of material extrusion additive manufacturing is within the limits of optical fiber sensors. A sufficient connection between the printed structure and the fiber can be reached by slightly melting the fiber's coating during the integration process. An exact positioning of the optical fiber in between two filament layers can be realized through an additional print head. The fiber can be precisely placed along a predetermined path and covered with an additional layer of filament material.

[29] cf. Richard Hagl, *Das 3D-Druck-Kompendium*, 2015.
[30] 'FDM Process' <https://s3-eu-west-1.amazonaws.com/3dhubs-knowledgebase/intro-fdm-3d-printing/2-fdm-steps.png> [accessed 2 March 2018].
[31] cf. '3dhubs Knowledge-Base'; cf. Klocke.

3.1.3 Material Jetting

Similar to a 2D ink jet printer, the material is deposited as a liquid and then solidified in various ways. The solid three-dimensional components are built up one layer after another. This process provides the possibility to print different materials at the same time, therefore structures with varying properties can be produced.

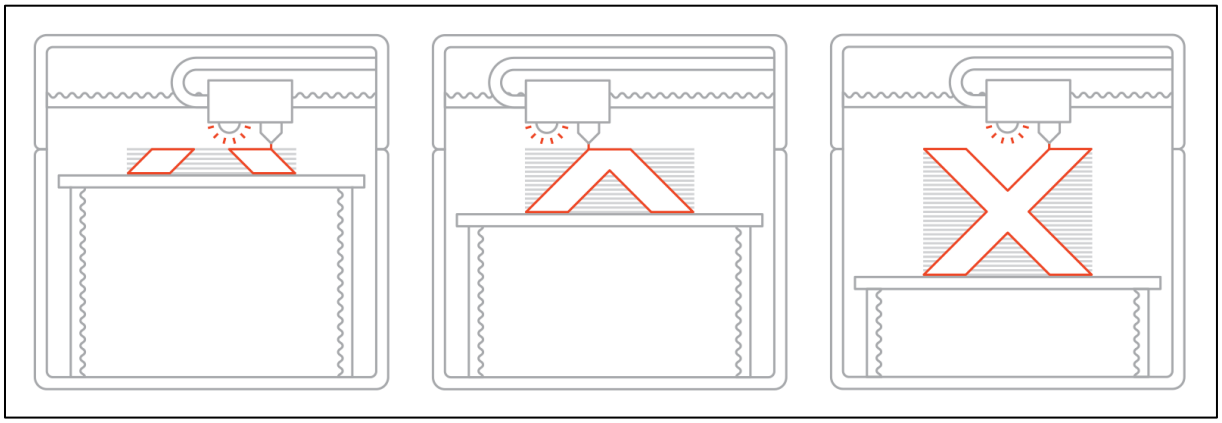

Figure 3-4: Manufacturing concept of Material Jetting [32]

- Material Jetting (MJ) / Photopolymer Jetting (PJ)

A photopolymer jetting machine uses ink jet print heads to dispense liquid droplets of a photopolymer which is then immediately cured with UV lights. In this way three dimensional structures are built up layer by layer. Different materials can be built up simultaneously. This is often used to create special dissolvable support structures for overhanging parts which can be easily removed from the finished components. [33]

- Nanoparticle Jetting (NPJ)

Metal nanoparticles are dissolved within a special liquid suspension. A print head deposits fine droplets to a build platform and the liquid suspension around the metal nanoparticles evaporates due to the high temperature inside the system's enclosed environment. These machines manufacture high detailed pure metal components. [34]

- Drop On Demand (DOD)

A solid structure is generated through depositing a wax-like material. Print jets follow a given path to generate the cross-sectional layers of a component. Between those printing processes of the single layers, a rotating milling blade reworks the surface to ensure a perfectly flat build area for the next layer. As the components are typically build up from a dissolvable wax-like material, they are primarily used for lost-wax castings molds.

[32] 'MJ Process' <https://s3-eu-west-1.amazonaws.com/3dhubs-knowledgebase/introduction-material-jetting/2-mj-steps.png> [accessed 2 March 2018].
[33] cf. Gebhardt and Hötter, p. 108.
[34] cf. Gebhardt and Hötter, p. 61.

- **Evaluation:**

Similar to the material extrusion process, an additional print head for depositing a continuous optical fiber between two layers of the component could be integrated into the manufacturing process. Depending on the material used within the material jetting process, the connection between the optical fiber and the manufactured component will be sufficient. The coating of a standard optical fiber could be fused with a polymer through temperature exposure. For the production of smart metal components, a special coated optical fiber would be needed to meet the temperature constraints.

3.1.4 Binder Jetting

A quite simple concept is used to create three-dimensional structures by using a print head which locally adds a liquid binding agent to powder particle bed. Various powder materials can be used if there is a matching binding agent available. The produced components, especially manufactured from metal powder particles, can be used as form-models but they have different and weaker material properties than conventionally manufactured metals. [35]

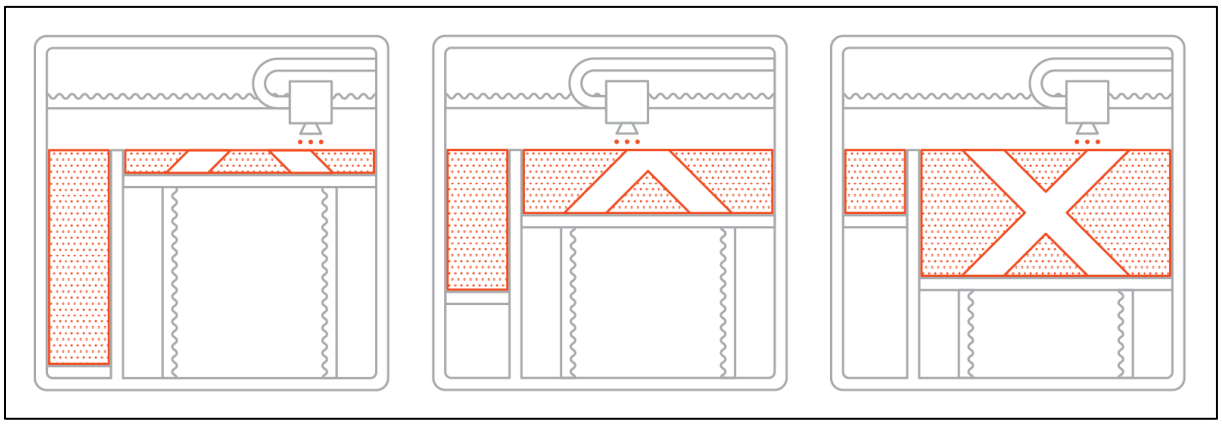

Figure 3-5: Manufacturing concept of Binder Jetting [36]

- Binder Jetting (BJ)

As mentioned before, characteristic for this process is a powder bed which is locally solidified by using a binding agent. After one layer is finished, the build platform is lowered, and a wiping device adds another layer or powder which is then locally solidified again. This process is repeated until the finished component is generated. The binding agent, applied to the surface by a print head similar to an inkjet printer, interconnects the powder particles as well as the single layers. The unbound powder is removed from the finished part. [37]

- **Evaluation:**

Within the binder jetting process, the placement of a continuous optical fiber would need to be done into a layer of not yet solidified powder particles. The binding agent could then be used to generate a connection between the fiber and the manufactured structure. Nevertheless, the fiber might only be placed in straight lines as the loose powder will not be able to keep a more complex fiber layout in place.

[35] cf. Maike Grund, *Implementierung von Schichtadditiven Fertigungsverfahren*, 2015, p. 44.
[36] 'BJ Process' <https://s3-eu-west-1.amazonaws.com/3dhubs-knowledgebase/introduction-binder-jetting/2-bj-steps.png> [accessed 2 March 2018].
[37] cf. '3dhubs Knowledge-Base'; Grund, p. 44.

3.1.5 Powder Bed Fusion

Powder particles are fused together within a predefined area by using a thermal energy source. Adding up one layer of these fused powder particles after another will produce a solid part. At the end of the process, the finished component will be completely encased in powder. After cooling down, the manufactured part can be uncovered and removed from the build platform. The energy sources used in this process are either laser or electron beams. Plastics and metals are used as powder materials. [38]

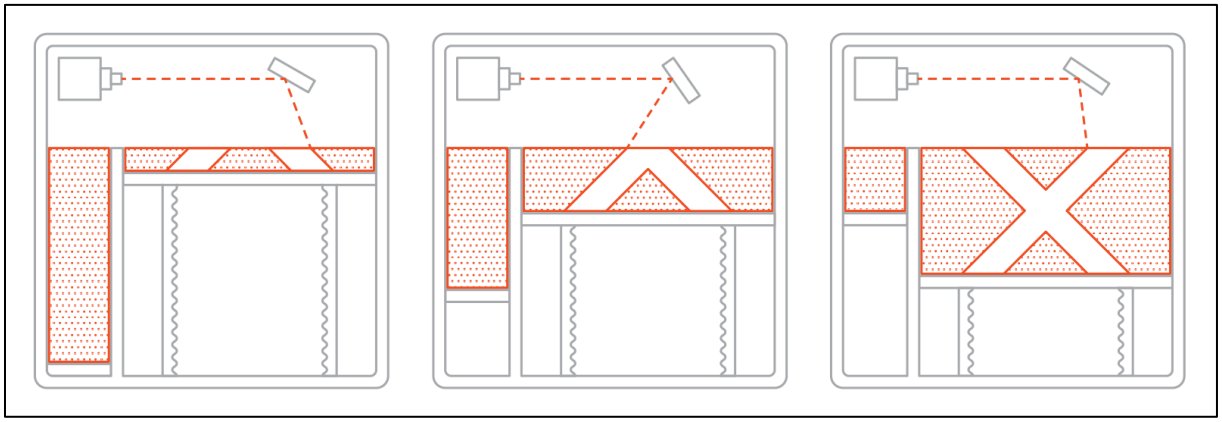

Figure 3-6: Manufacturing concept of Powder Bed Fusion [39]

- Selective Laser Sintering (SLS)

In this process, a laser is used as a thermal source to sinter thin layers of powdered material. At the beginning, the build platform is covered with a thin layer of powder, which is evenly applied by a rotating roller. The building chamber is heated to a certain process temperature slightly below the particle's melting point. The laser beam maps the cross section of the part onto the powder and melts it locally. In this way, a solid shape is generated. The build platform is lowered by the thickness of one layer and another fresh layer of powder is spread across the build platform. This process is repeated until the solid part is finished and can then be removed from the non-solidified powder. Further manual processing as cleaning with pressurized air or surface finishing might be necessary, as the surface will be quite porous due to the manufacturing process. In industry, SLS is mainly used to produce components from nylon powder particles. [40]

- Multi Jet Fusion (MJF)

This process of powder bed fusion is operating an additional ink jet like print head which adds a fusion agent and a detailing agent to the powder particles at the build platform. The powder particles in the area where the fusion agent is applied is then solidified using a thermal source whereas the detailing agent acts as an isolator and prevents those powder particles from solidifying. This technology enables a fast manufacturing process of components with huge precision, dimensional accuracy and smooth and well-defined part edges. [41]

[38] cf. Gebhardt and Hötter, p. 57.
[39] 'SLS Process' <https://s3-eu-west-1.amazonaws.com/3dhubs-knowledgebase/introduction-sls-3d-printing/2-sls-steps.png> [accessed 2 March 2018].
[40] cf. Manfred Schmid, *Additive Fertigung Mit Selektivem Lasersintern (SLS)*, 2015, p. 9 ff.
[41] cf. H P Multi and Jet Fusion, *HP Multi Jet Fusion TM Technology*, *HP Technical White Paper*, 2018.

- Direct Metal Laser Sintering (DMLS) / Selective Laser Melting (SLM)

These two methods use the same principle as described within the process of Selective Laser Sintering, except the components produced are made from metal powder. In comparison to the sinter process used with DMLS to produce solid structures, SLM achieves a full melt of the metal powder in order to generate metal components. The complete fusion process leads to a very high powder density of the components which then have similar material properties compared to conventionally casted metal part. This provides the opportunity to produce working prototypes as well as small batch productions by using this additive manufacturing method. [42]

- Electron Beam Melting (EBM)

A high-energy electron beam is used as a thermal energy source to induce fusion between the metal powder particles rather than using a laser as mentioned in the processes above. The focused electron beam locally melts a thin powder layer and solid structures are created in a similar way to other powder bed fusion technologies. EBM is able to produce components faster than SLM with less energy input needed, but the whole technique is more expensive and complex because the process has to be operated in a vacuum. Furthermore, the achievable focus to the electron beam is larger than that of a laser and therefore the minimum structure size is larger within EBM. [43]

- **Evaluation:**

As within this process, a layer of powder particles is fused together by using a thermal source, the optical fiber needs to be placed inside the loose powder. Therefore, only basic and simple configurations of fiber layout could be implemented. Additionally, the coating of the optical fiber needs to be aligned with the high manufacturing temperature of the powder bed fusion process. More expensive metal coated fibers are available to meet those requirements. In this way, the production of smart additively manufactured metal components could be possible, although the layout of the integrated optical fiber is rather restricted.

[42] cf. Roland Lachmayer and Rene Bastian Lippert, *3D-Druck Beleuchtet*, 2016, p. 25 f.
[43] cf. Lachmayer and Lippert, *3D-Druck Beleuchtet*, p. 27.

3.1.6 Direct Energy Deposition

A solid structure is created by melting material as it is deposited. The materials are either metal powders or a metal wire. Typical applications for this technology can be found in the aerospace sector in case of repairing components made from titanium or other uncommon metals. [44]

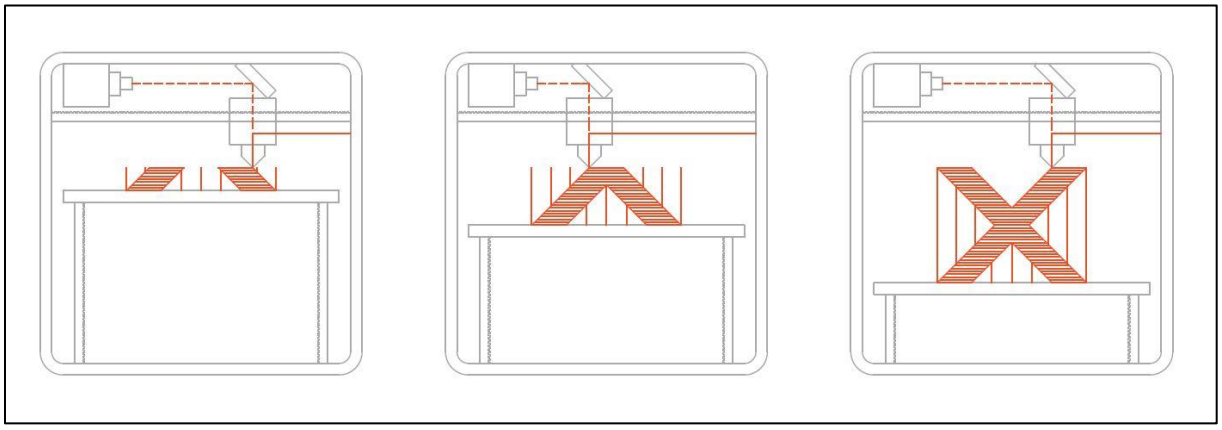

Figure 3-7: Manufacturing concept of Direct Energy Deposition [45]

- Laser Engineering Net Shape (LENS)

A high-energy laser beam is used to create a local weld pool where the metal powder particles are deposited, fused and finally solidified. This deposition head moves along the X-Y-axis to build up a solid structure layer by layer. Various metal powder materials can be used for this process, with titanium being the favourite at the moment. [46]

- Electron Beam Additive Manufacturing (EBAM)

The components are produced in a similar way to LENS, except an electron beam is used to create a molten pool. This method was originally developed for use in space, as electron beams are more efficient than lasers and operate in a vacuum. [47]

- **Evaluation:**

The generation of a local welding pool of molten metal within these methods of manufacturing will most probably cause structural damage to an implemented optical fiber. There are currently no optical fibers available to survive the high temperature of more than $2000°C$ [48] within the welding pool. Therefore, it is not likely to produce functional smart components with this process.

[44] cf. Lachmayer and Lippert, *3D-Druck Beleuchtet*.
[45] cf. 'LENS Process' <https://image.slidesharecdn.com/2015-11-26-slsebmlens-151222115944/95/2015-1126-sls-ebm-lens-52-638.jpg?cb=1450785661> [accessed 15 August 2018].
[46] cf. Hagl, p. 31.
[47] cf. '3dhubs Knowledge-Base'.
[48] cf. Steven Price et al., 'On Process Temperature in Powder-Bed Electron Beam Additive Manufacturing: Process Parameter Effects', *Journal of Manufacturing Science and Engineering*, 2014.

3.1.7 Sheet Lamination

Laminated manufacturing processes are based on a simple principle where two-dimensional contours are cut out of thin sheets which are then glued together to create a three-dimensional structure. [49]

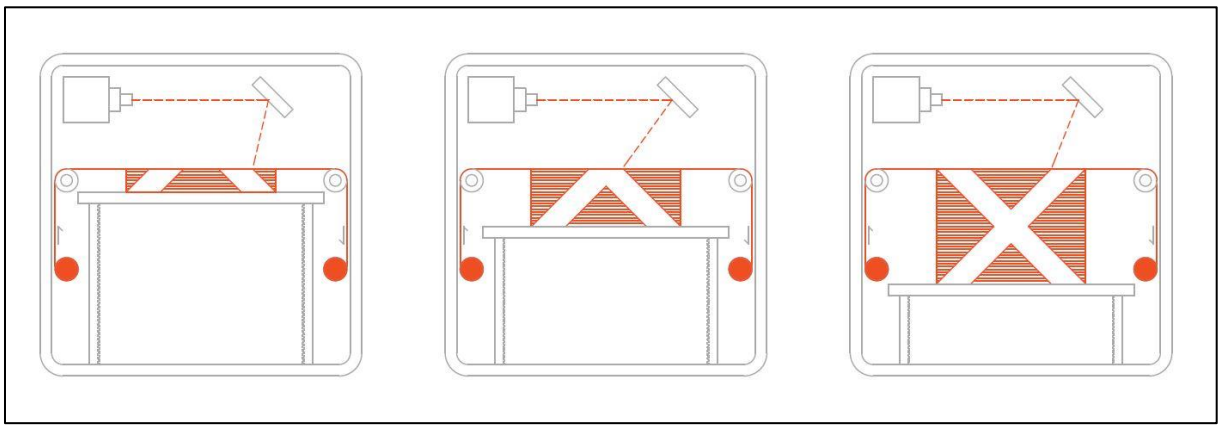

Figure 3-8: Manufacturing concept of Sheet Lamination[50]

- Laminated Object Manufacturing (LOM)

Single layers of material, most commonly paper, are laminated together and glued to a solid structure. The contours of every single layer are cut out after being laminated to the previously built up model. In post processing steps, the excess material is removed manually and must be disposed. Further materials like plastics, ceramics or aluminium might also be used to laminate components with this method. [51]

- **Evaluation:**

When adding an additional channel between two layers of sheets used for this method of manufacturing, an optical fiber can be integrated into the components. The temperature exposure during the lamination process of the single sheets has to match the operating temperature range of the embedded optical fiber. Otherwise, no reliable production of a functional smart object is possible. Aluminium alloy components with an integrated optical fiber with FBGs are manufactured for a study by using the rather new method of ultrasonic additive manufacturing [52].

[49] cf. Grund.
[50] cf.'LOM Process' <http://www.lboro.ac.uk/media/wwwlboroacuk/external/content/research/amrg/Direct Energy Deposition - process.jpg> [accessed 15 August 2018].
[51] cf. Petra Fastermann, *3D-Druck/Rapid Prototyping*, 2012, p. 124.
[52] cf. Adam Hehr et al., *Integrating Fiber Optic Strain Sensors into Metal Using Ultrasonic Additive Manufacturing*, 2018.

3.2 The continuous fiber integrated fused filament fabrication process

As FFF being one additive manufacturing method where the process of integrating a continuous fiber inside the manufactured structure is already developed and established, it is the method of choice for producing smart elements within this thesis. The main purpose of those state of the art machines is to produce stronger parts through integrating continuous reinforcing fibers inside the plastic structure. Nevertheless, the same principle can be used to implement FOS inside the printed components.

The FFF machine operates in addition to the conventional filament printing nozzle a second printing nozzle which is used to place a continuous fiber. The exact path and position of this continuous fiber is defined by a software application prior to the printing process. The conventional plastic filament is extruded through the hot printing nozzle which follows a predetermined path across the printing platform. In this way, three-dimensional objects are created layer upon layer. Between every one of those single layers a continuous fiber can be integrated into the component. Therefore, the continuous fiber is fed through a heated nozzle where the fiber's coating is slightly melted. The fiber nozzle follows a pre-set path across the layer previously printed from filament. Due to the slightly melted coating, the continuous fiber sticks to the filament layer and can be exactly positioned. At some point, the continuous fiber needs to be cut to length by a mechanism inside the printing machine to avoid interferences with the upcoming steps of the printing process. The following layers from plastic filament are simply printed on top of the layer which now contains the continuous fiber. In this way, the fiber is permanently embedded into the structure of the manufactured component.

4. Additively manufactured components with integrated fiber optical sensors

The necessity of implementing additive manufacturing processes is driven by special requirements of certain products. Those requirements are clustered into three different fields shown in Figure 4-1. If a requirement of a component can be assigned to one of these fields, the implementation of an additive manufacturing method can be justified. If all three fields are met, another manufacturing method besides an additive one can be excluded almost certainly. [53]

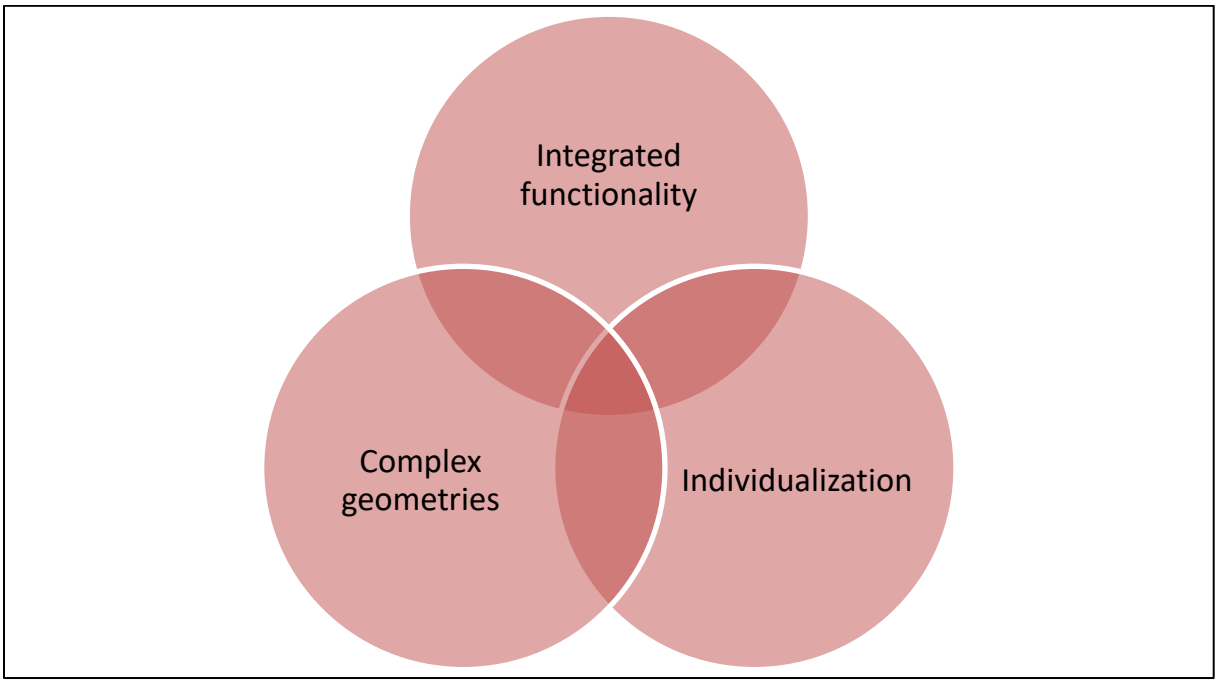

Figure 4-1 Reasons for the necessity of additive manufacturing methods according to Fraunhofer IPA

For producing highly individual smart components, the obvious conclusion is to manufacture those components additively. The combination of a fiber optical sensing technology with an additive manufacturing method provides the possibility to generate sensitive and highly individual components. The sensors can be integrated into the components structure and be placed at critical locations where high loads are expected. The embedded optical sensors can be regarded as minimal invasive to the components structure due to the small size of optical fibers. Nevertheless, even one single integrated optical fiber can be used to perform distributed measurements within an entire component. By utilizing a suitable measurement system, a spatial resolution of $1\ cm$ or even higher can be achieved.

4.1 Advantages

An additively manufactured component with integrated FOS is combining the advantages of both technologies in use. The methods of additive manufacturing provide the possibility of generating

[53] cf. Jannis Breuninger et al., *Generative Fertigung Mit Kunststoffen*, 2013, p. 14 ff.

structures that are not producible with conventional subtractive manufacturing processes. Additionally, the sensors can be integrated inside the component's structure, as the part is build up layer by layer. The small dimensions of the used optical fibers guarantee, that the material properties of the part itself are barely influenced. With a suitable measurement system, a standard single mode optical fiber can be used as a distributed sensing element with a high spatial resolution.

Both, the part's geometry and the sensing fiber layout can be highly customized when designing and producing an additively manufactured component. Some limitations, discussed within chapter 5.3, need to be considered during the design phase of the product. Nevertheless, very specialized sensing elements can be manufactured and used as structural prototypes or operational products. Three-dimensional shape sensing could be realized by integrating multiple fibers in a certain arrangement. The simplest concept could be a rod with three evenly spread optical fibers near the outer shell. A simple algorithm could be used to calculate the rod's shape from the strain measured with the optical fibers when it is deformed.

Additionally, the possibility of an accurate positioning of the sensing fiber inside the structure of a component provides a huge improvement compared to the methods currently used for attaching FOS to tested samples. At the moment, the fiber is mounted mostly by hand onto the object which should be measured by using tape and specialized glue. Another automated fiber-integration method for highly individual components is not available right now.

In comparison to traditional strain sensing methods, like using strain gauges, not only local measurements are possible. By using a distributed optical fiber sensing system, highly sensitive measurements with high spatial resolution are possible by using only one optical fiber. No additional wiring is necessary with this sensing method. This helps reducing the magnitudes of influence that the sensing element itself has on a performed test. Furthermore, the optical fiber can be integrated into the structure and placed exactly at the location where the highest strain is expected. As the sensor is inside the tested element, no additional sensor-protection is necessary.

Another important aspect is the insensitivity of optical fibers against electromagnetic interferences. Therefore, these smart components can be used where standard electric sensors will fail.

4.2 Concept of an ideal manufacturing machine

This section should provide a concept for a 3D printer ideal to produce smart additively manufactured components. The operator should be provided with the possibility of configuring a highly individual fiber layout inside the printed object, so the sensing options as well as the structural properties of the object can be optimized. A guideline for fiber pathing should be considered to avoid configurations which would be of potential malfunction.

At least two independently operating print heads will be used for additively manufacturing smart and sensitive components. One or more print heads are printing the filament by using the traditional method of FFF while another print head is used for printing a continuous optical fiber. Additional print heads for providing features like the production of special support structures or the possibility to add special reinforcing fibers within the components might also be available with this ideal printer. The properties of the printed components can be optimized regarding the expected use case. The print heads are mounted to robotics arms which are situated around a building platform. These arms are guiding the print heads along their predetermined path. The whole printing method will become more

comparable to a three-dimensional weaving process than the standard additive manufacturing process used with FFF at the moment. Complex components can then be equipped with integrated continuous fibers for either sensing or structural improvement. A similar concept is published at Politecnico di Milano University [54]. Figure 4-2 shows their patented apparatus.

As a first step towards this ideal printer, a standard setup of a FFF printer can be modified and extended with a second print head to produce basic smart and sensitive components. The two independently operating print heads are connected to the printer's guiding rails via magnetic couplings. The first print head is printing the filament by using the traditional method of FFF and the second one is used for continuous fiber printing. The magnetic coupling element will be designed in a way that the print heads can be changed automatically during the printing process. The two print heads can be placed on a docking station on the printer's frame which enables a printing process without any interferences of both print heads.

Figure 4-2: Example of a similar concept[55]

4.3 Use cases

As there are major developments and improvements expected in the combined technologies – additive manufacturing and fiber optic sensing – various use cases can be defined and anticipated.

[54] Moi-composites-srl, 'Apparatus and Method for Three-Dimensional Printing of Continuous Fibre Composite Materials', 2015.

[55] 'Moi-composites-srl - Printer Concept' <https://uploads-ssl.webflow.com/5a588c043c31ba0001f32925/5a6db60b10ba58000189f348_project-atrops-img.jpg> [accessed 15 August 2018].

4.3.1 Material and structural testing

This field of application for smart additively manufactured components focuses on testing various materials and structures.

- Small scale prototypes

The production of a sensitive small-scale prototype can be used for testing and for the verification of digital simulations during the product development phase. The integration of FOS can enhance the development workflow, as assumptions concerning a components behaviour can be quickly verified. Additionally, performance tests can be executed with these small-scale prototypes to implement and improve modifications on the developed components. For example, it would be possible to manufacture aerofoil profiles with integrated optical fibers. When putting these profiles into a flow channel, the internal deformations generated through lift and drag can be measured with the optical fibers. In this way, it would be possible to optimize the aerofoil profile. An aerofoil profile with integrated FOS that could be produced with the current manufacturing setup is shown in Figure 4-3.

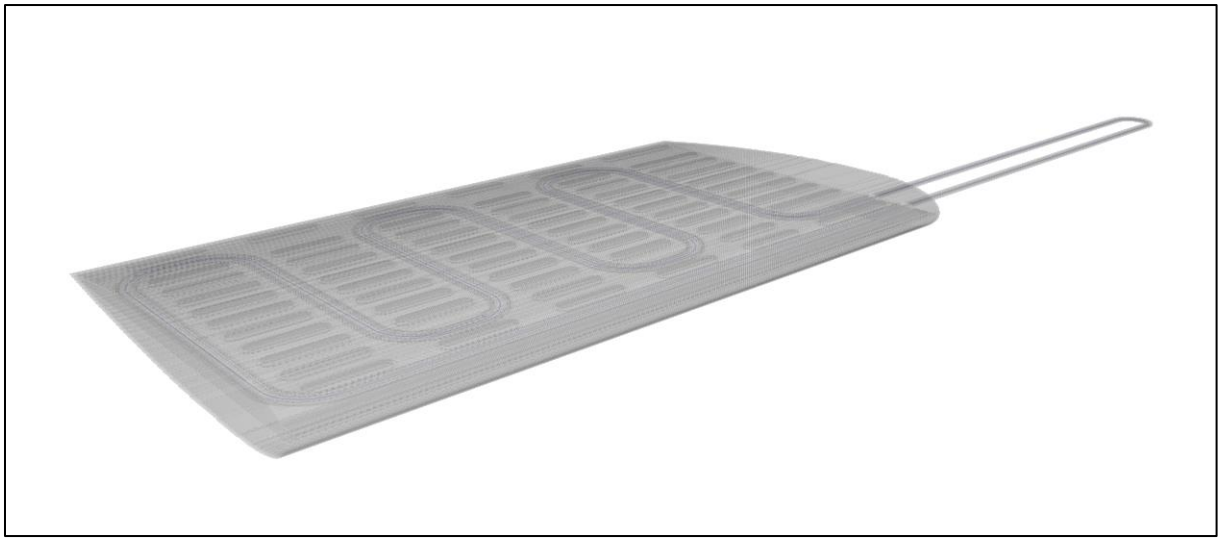

Figure 4-3: Aerofoil profile with integrated FOS

- Crash test optimization

In bigger scale, whole components of vehicles could be produced by using the methods of additive manufacturing. With integrated FOS, an additional sensing opportunity could be realized for performing crash tests. This data can then be used for further improvements concerning vehicle safety.

- Combination with fiber reinforced 3D printing

As the whole sector of additive manufacturing is rapidly growing at the moment, the combination of integrating optical fibers for sensing as well as integrating reinforcing fibers into the additively manufactured structure can provide completely new possibilities for product development. A strong and durable ready to use composite component can be equipped with a highly individual sensor layout and produced with a high end additive manufacturing machine. Additionally, the reinforcing fiber layout can be verified immediately by performing tests and measurements with the integrated FOS.

- Shape sensing

By integrating the optical fibers in a certain predefined arrangement, the shape of the manufactured object could be supervised. Algorithms can be defined that derive the current shape of an object from the strain measured with the FOS. Smart clothing or sensitive prostheses could be developed by implementing this feature.

4.3.2 Product maintenance

When components are produced with integrated FOS, their structural integrity can be supervised over the product's lifetime. In this way, the operational application of a component can be maximized without risking a product failure.

- Sensing pads with highly individualized sensor layouts

The possibility to integrate an optical fiber by using a highly individual layout enables the manufacturing of special sensor pads optimized for a specific use case. In this way, areas of interest can be monitored in detail by using an individually designed sensor pad. Structural overload could be prevented as the component can be supervised precisely.

- Digital Twin

The "Digital Twin" represents a concept which combines a physical model with a virtual one. Information of the physical component is collected through real-time monitoring in order to feed a digital model. Simulations of the future behaviour of the component are then calculated. In this way, a control feedback-loop is generated. The US Air Force implemented this Digital Twin concept to enhance the structural health prediction process for their aircrafts. The concept is becoming increasingly important to the whole industrial sector as products and designs are evolving. Industry 4.0 is a huge driver for generating digital models of physical products for enhancing their performance. Regarding this development, the implementation of optical fiber for strain and temperature measurements into additively manufactured structures will be a crucial improvement in the way the physical counterpart of a digital model is produced. [56]

[56] cf. Hehr et al.; cf. Eric J. Tuegel et al., Reengineering Aircraft Structural Life Prediction Using a Digital Twin, *International Journal of Aerospace Engineering*, 2011

4.3.3 Optimization of the manufacturing process

When starting the measurement process as soon as the optical fiber sensor is integrated into the additively manufactured structure, the material conditions inside the components can be supervised. This provides the possibility to optimize the manufacturing process through adjusting the production parameters. Thermal distortions and shrinkage could be supervised and possible weakness points inside the components could be identified.

5. Realized prototypes within the thesis

Within the framework of this master thesis, several sensitive components were manufactured to proof the concept of smart additively manufactured components. The 3D printer used to produce these parts is the MarkForged Mark One Composite 3D Printer™ (Mark One) at the Fabrication Laboratory (FabLab) Graz. A single mode optical fiber was integrated into the structure of the manufactured components to provide the possibility to perform measurements of strain and temperature changes by using the LUNA OBR 4600 system.

5.1 Material Properties

As the dimension of the integrated optical fibers compared to the printed nylon structure is rather minimal, the material properties of the smart additively manufactured components can be assumed similar to nylon only components. An extract of the mechanical properties of the nylon material used for FFF and the integrated optical fiber are shown in Table 5-1. These values are regarded as valid for the manufactured smart components as well.

Table 5-1: Mechanical Properties of Nylon FFF [57]

Property	Nylon FFF (Test Standard)	ORMOCER® coated optical fiber (Test Standard)
Tensile Strength (MPa)	56(ATSM D3039)	No data available
Tensile Modulus (GPa)	0,38 (ATSM D3039)	No data available
Tensile Strain at Break (%)	>50 (ATSM D3039)	>5 (IEC-60793-1-31)
Flexural Strength (MPa)	No Break (ATSM D790)	No data available
Flexural Modulus (GPa)	0,4 (ATSM D790)	No data available
Flexural Strain at Break (%)	No Break (ATSM D790)	No data available
Heat Deflection Temperature (C°)	44-50 (ATSM D648)	-200 to 200

5.2 Measurement setup

The smart objects manufactured within this thesis are equipped with a distributed sensing element inside the structure. For this purpose, the LUNA OBR 4600 sensing system was selected due to its ability of performing distributed sensing of strain and temperature changes with standard single mode optical fibers. This measurement device is optimal for this application as a high sensitivity for strain as well as a high spatial resolution is needed. The length of the integrated fiber is also compatible with the

[57] cf. MarkForged Inc., 'MarkOne Mechanical Properties Data Sheet', 2015, 1 <http://markforged.com>; FBGS International.

device's sensing range. The whole measurement setup will be described more precisely in the following section.

5.2.1 Setup

The measurement setup consists of a LUNA OBR 4600, the connecting components and the smart additively manufactured component as shown in Figure 5-1. A bare optical fiber is integrated into an additively manufactured component. This process of producing a sensing element will be described in detail within chapter 5.3. The bare optical fiber is spliced to an optical fiber pigtail which can then be connected to the measurement device. By using an additional fiber optical patch cord between the LUNA OBR 4600 and the additively manufactured smart element, the distance between the both can be increased without major deficits concerning the sensing capabilities. Furthermore, when multiple connect-disconnect operations are expected, the wear of the device's connector can be reduced by working with an additional patch cord between the smart element in use and the LUNA OBR 4600. The measurement device is then connected to a personal computer to operate a specialized software for performing measurements.

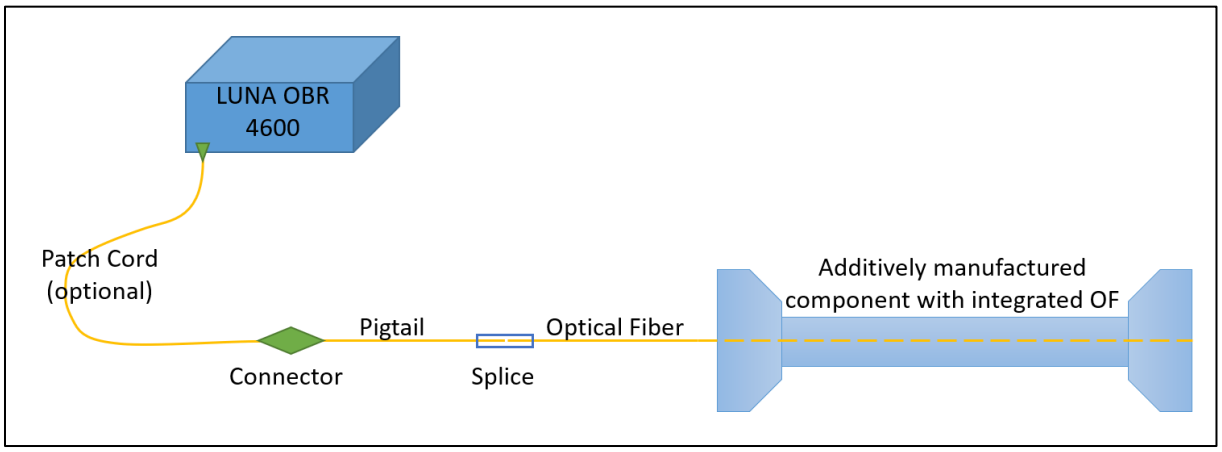

Figure 5-1 Measurement setup including all relevant components used for sensing smart additively manufactured components

5.2.2 Components

Fiber optical measurement systems depend on various components to function properly and to produce high quality and accurate measurement data. All single parts need to be of highest precision and meet the industry's quality standard. The components shown in Figure 5-1 are explained in the upcoming paragraphs:

- Measurement device - LUNA OBR 4600

The measurement principle of a LUNA OBR 4600 is based on Rayleigh scattering effects. They occur when an optical signal interacts with the contaminating particles inside the medium in which it is propagating. Depending on the wavelength of the optical signal, absorption and scattering occurs. Scattering effects in all directions are dominating if the light's wavelength is identical with the size of the contaminating particles inside the medium. Distributed optical fiber sensing systems use the

backscattered part of the signal to derive information concerning strain and temperature changes along the whole fiber.

For detecting the Rayleigh scattering effects, the LUNA OBR 4600 uses an optical frequency domain reflectometer (OFDR).[58]

An analysis of the backscattered Rayleigh signal shows that a commercially available optical fiber has a characteristic fluctuating intensity profile of the Rayleigh scattering along the fiber. This profile will be the same for every measurement performed with the same optical fiber if there are no external impacts to the fiber. A change in temperature or strain of the fiber will not result in a different fluctuating intensity profile but will lead to a frequency shift of the reflected signal in the area of the external mechanical and thermal influences. To analyse this change in the patterns of Rayleigh backscattering, the LUNA OBR 4600 divides the measurement signal which returns from the optical fiber into small segments. After transforming the signals of these segments into the frequency domain, it can be locally compared to a reference measurement. Any local changes concerning strain and temperature cause a frequency shift of these segments. A software algorithm is used to convert these frequency shifts back to local temperature and strain values and to calculate and interpolate a continuous profile along the measured fiber. [59]

- Patch cords and pigtails

Pigtails and patch cords are two terms for fiber optical cable with connectors on either one or both ends. Pigtails have one bare fiber end which is used to splice to an optical sensing fiber which can then be connected to a measurement device. Patch cords work as a fiber optical extension cable.

- Connector

Fiber optical connectors are used to temporarily connect the optical sensing fiber to the measurement device or to another optical fiber. There are multiple different types of connectors available on the market. Besides being practical and robust, a fiber optical connector should be easy to clean and a low attenuation of the signal should be ensured. Another important aspect in regard of fiber optical sensing is to avoid unnecessary reflection at the connection. Therefore, angled physical contact connectors (APC-connectors) are the industry standard used within sensing systems. The difference between a straight physical contact connector (PC-connector) and an APC-connector can be seen in Figure 5-2. To connect two fiber optical connectors together, so called mating sleeves are used in order to align them properly. The limited lifetime of such connectors of around 1000 connection cycles should not be neglected either.[60]

[58] cf. Luna Innovations Inc., 'OPTICAL BACKSCATTER REFLECTOMETER TM (Model OBR 4600)', 2014.
[59] cf. Dirk Samiec and Polytec Gmbh, Distributed Fi Bre-Optic Temperature and Strain Measurement with Extremely High Spatial Resolution, 2011; cf. Xin Lu, Marcelo A. Soto, and Luc Thévenaz, Temperature-Strain Discrimination in Distributed Optical Fiber Sensing Using Phase-Sensitive Optical Time-Domain Reflectometry, 2017.
[60] cf. Martin Löffler-mang, *Optische Sensorik*, 2012, p. 154; cf. Abdul Al-Azzawi, *Fibre Optics Principles and Practices*, 2007, p. 99.

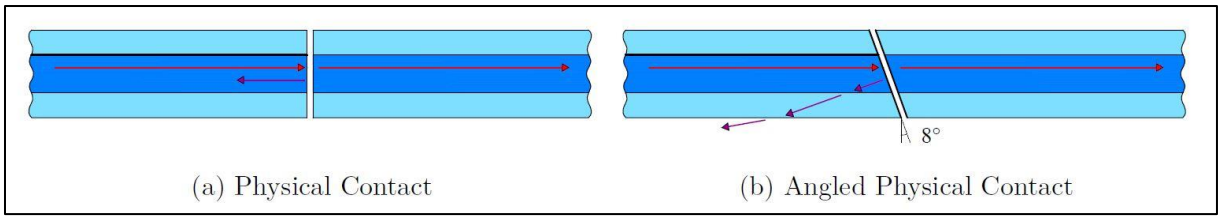

Figure 5-2 Difference between the physical contacts of optical fiber cores [61]

- Splice

For a permanent connection between two optical fibers, a fusion splice is the preferred method. For this process, the coatings of both ends of the optical fibers must be stripped off. The bare fiber ends are then placed into a splicer, where they are aligned and thermally fused together through arc welding. This results in a very low attenuation of the signal when done properly. A splice protection tube is needed because the coating was removed from the fibers prior to the welding process. Mechanical splices would be another way of connecting two fiber ends permanently, but the attenuation is much higher and therefore this process is not preferred.

- Optical fiber

The bare optical fiber is integrated into the additively manufactured component. Strain and temperature changes can be measured along this fiber and therefore a certain analysis of the components is possible. Due to the current production process, parts of the bare optical fiber are outside of the additively manufactured structure. Therefore, an additional protection element might be useful to prevent the optical fiber from damage.

- Smart element

As the additively manufactured components are sensitive to strain and temperature changes, they are referred to as smart elements within this thesis. Various shapes and structures can be produced by the means of additive manufacturing and specialized designs for certain use cases are possible. A more detailed analysis and description of the production process as well as the capabilities of smart elements are provided in chapter 3 and chapter 4.

5.3 Guidelines

These guidelines will enable a technically skilled person to produce smart components on their own. The access to the required tools and material, a Mark One 3D printer, a suitable single mode optical fiber and the equipment to process the bare fiber as well as the measurement device is available at TU Graz. A list with checkpoints and working instructions is attached in the appendix.

[61] cf. Monsberger.

5.3.1 Part design guideline

- Dimensional limitations of the printer:

For designing a component manufactured with this specific additive manufacturing machine, certain boundary conditions need to be considered. The dimensional limits for this printer are $320\ x\ 132\ x\ 154\ mm^3$. The maximal build volume of this printer is shown in Figure 5-3. A minimal fiber length of $\sim 700\ mm$ must be taken under consideration due to the non-changeable standard settings of the used 3D printer. The radius of fiber curves should not be less than $10\ mm$ to avoid unnecessary damage of the optical fiber.

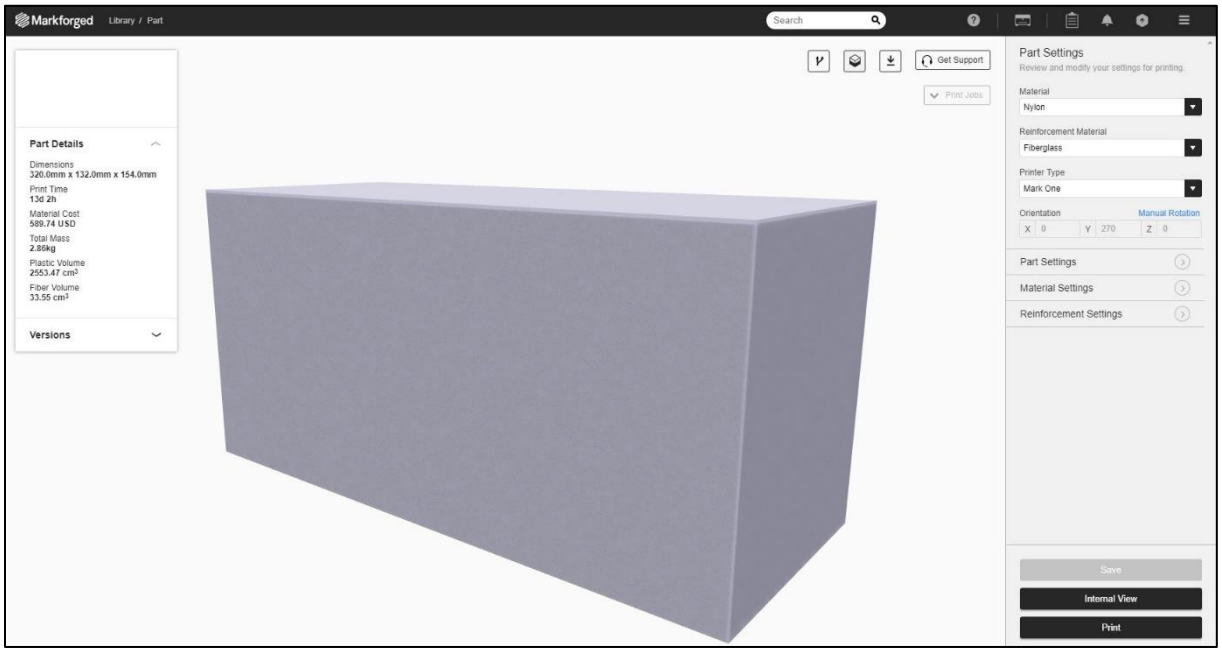

Figure 5-3: Maximal build volume of the MarkForged Mark One™ 3D printer

- Smart component:

To start with the part design, create a 3D element by using a CAD program of choice. Then the desired planes to be equipped with optical fiber for sensing need to be defined. Using the Mark One, only planes parallel to the print bed can be equipped with optical fibers. A minimal distance to the bottom of the part and the sensitive plane of $0{,}4\ mm$ need to be considered. The same space needs to be taken into account at the top of the component.

- Fiber bridge:

The software of the Mark One will try to integrate as much fiber as possible to the pre-defined plane. There is no possibility to set a specific fiber path within the provided software. Therefore, it is necessary to construct an element which exactly defines the path of the optical fiber. This element is called a "fiber bridge" within this thesis and can be seen in Figure 5-4. The fiber bridge needs to be defined inside the smart component as well as outside of it, where it acts as a support structure because the printer is not able to extrude fiber into the air. In addition, this will provide the possibility of splicing the bare optical fiber to a fiber optical pigtail later.

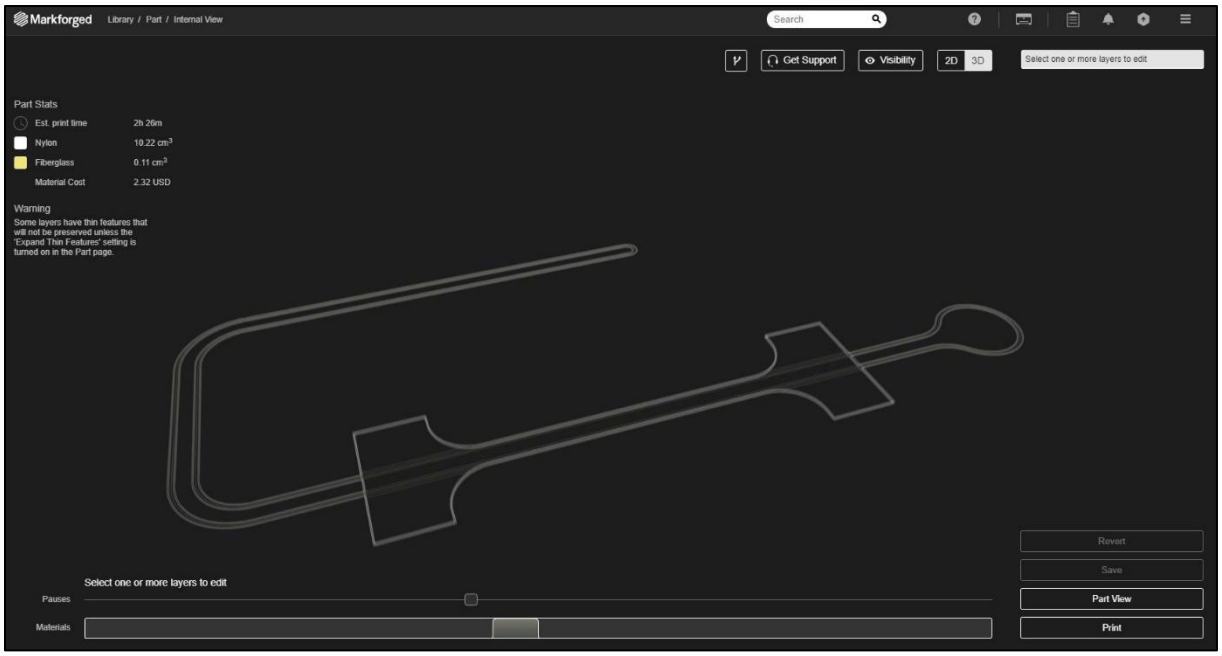

Figure 5-4: Smart component with fiber bridge

The fiber path is constructed with a closed loop drawn onto the pre-defined planes. Inside the smart component small holes need to be generated on the left and right side of the fiber bridge. This is necessary to make the printer place the fiber onto the defined path. The easiest way to accomplish these small holes is by extruding two different-sized rectangles along the drawn fiber path. Both rectangles need to be perpendicular to the fiber path and stay in that orientation when being extruded. Additionally, the centres of both need to be on the fiber path. The dimensions of the first rectangle used for creating an extrusion shape are $3{,}2\ mm\ x\ 0{,}1\ mm$ in width and height. This thin profile needs to be subtracted from the smart components structure. Then a second rectangle with the dimensions of $3\ mm\ x\ 1\ mm$ in width and height is extruded along the fiber path. Through this procedure, the fiber bridge is generated along the pre-defined path. Inside the smart component, two small pockets are created next to the fiber path. This guarantees that the printer will implement the fiber along the pre-defined path.

- Additional pockets

As the printer's software will try to implement as much optical fiber to the pre-defined plane as possible, it is necessary to create additional blank spaces inside the component. The depth of these gaps should be $0{,}1\ mm$ and their distance to walls should be $< 3\ mm$. This guarantees that the only space where an optical fiber can be placed is onto the desired fiber path.

- Eiger.io software

The designed geometry needs to be saved as ".stl" file and uploaded to the online-software tool provided by MarkForged. Access the software by using a Google Chrome Web browser through the URL "www.eiger.io/signin". Enter the service with the access data provided by FabLab Graz (email: fablabgraz; password: fablabgraz). Now, import the designed component and place it to the printer's

bed. The fiber plane needs to be parallel to the print bed. Within the part settings, “Fiberglass” needs to be set as reinforcement material and a layer height of $0{,}1\ mm$ should be defined.

The fiber placement is specified within the “Internal View”. Choose the 2D view and select the layer where the fiber should be placed. Within the menu-box “Edit Layer” the main fiber settings are defined:

- Use Fiber: ON
- Fiber Fill Type: Concentric Fiber
- Walls to Reinforce: Outer Shell Only
- Concentric Fiber Rings: 1
- Start Rotation Percent: outside the smart component

The fiber needs to be used with a concentric fiber fill type within the sensing layer. As the fiber path is defined through the construction of holes inside the component, the printer’s software recognizes this path as an outer shell. Therefore, only the outer shell need to be reinforced with one concentric fiber ring. The start rotation percentage defines where the continuous fiber is cut during the integration process. This position of the cut fiber needs to be outside of the sensitive component. Figure 5-5 shows the described layer settings which are in the top right corner; the fiber is cut inside the red circle.

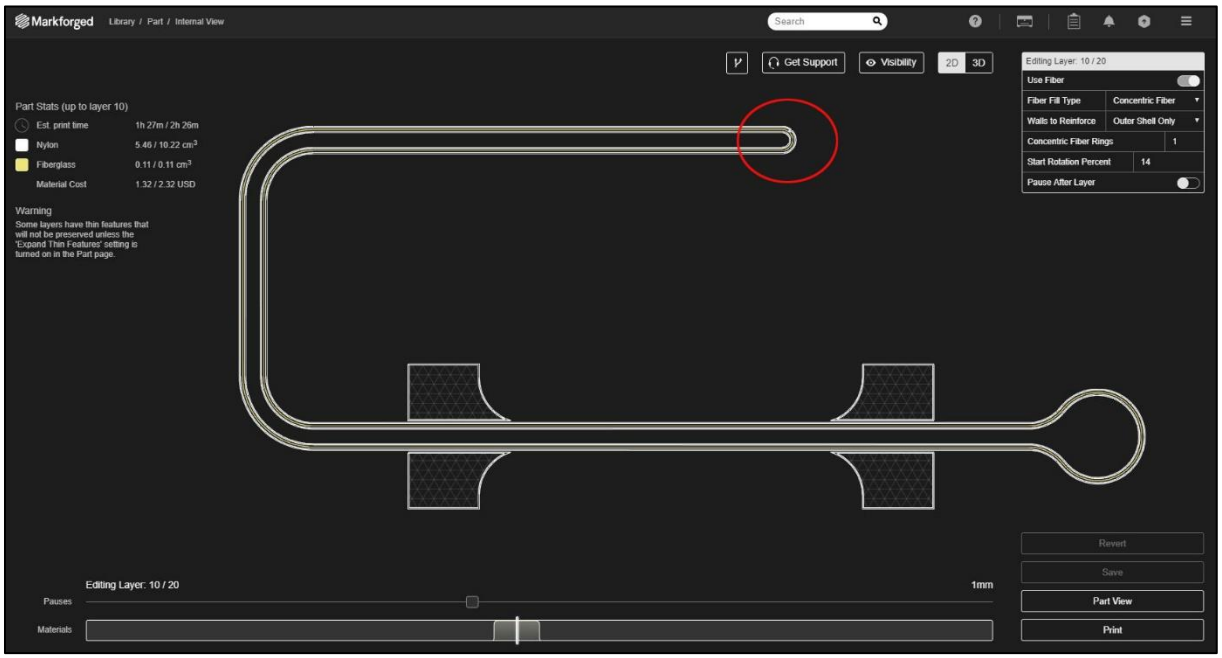

Figure 5-5: 2D Internal view of a smart component with layer settings adjusted for sensing fiber integration

Adding an automatic pause before and after the layer where the optical fiber is integrated can be used to check the structural integrity of the component and the optical fiber. In addition, the part of the fiber which will later be used for splicing the element to an fiber optical pigtail, can be placed outside the printed structure at this stage of the printing process with little effort. This step is explained in more detail within chapter 5.3.2.

The settings must be saved within the software and the file can be transmitted to the Mark One for printing.

5.3.2 Printing process guideline

This part of the guideline will focus on the printing process itself. As the Mark One printer is not capable of printing or placing spare fiber outside of the printed nylon structure, some additional actions need to be taken to produce smart components with this printer.

- Loading the optical fiber

Although the optical fiber which is integrated into the printed structure within this project is not a supported fiber material of MarkForged, it can be used for this process. The special ORMOCER® coating of the integrated fiber can survive the printing process without clogging the fiber nozzle of the 3D printer.

Load the ORMOCER® coated optical fiber to the Mark One printer as shown in Figure 5-6 accordingly to the printer's operating instructions:

1. Load material
2. Load fiber
3. Quick load fiberglass
4. Cut when the fiber reaches the fiber nozzle of the print head
5. Remove the cut-off fiber

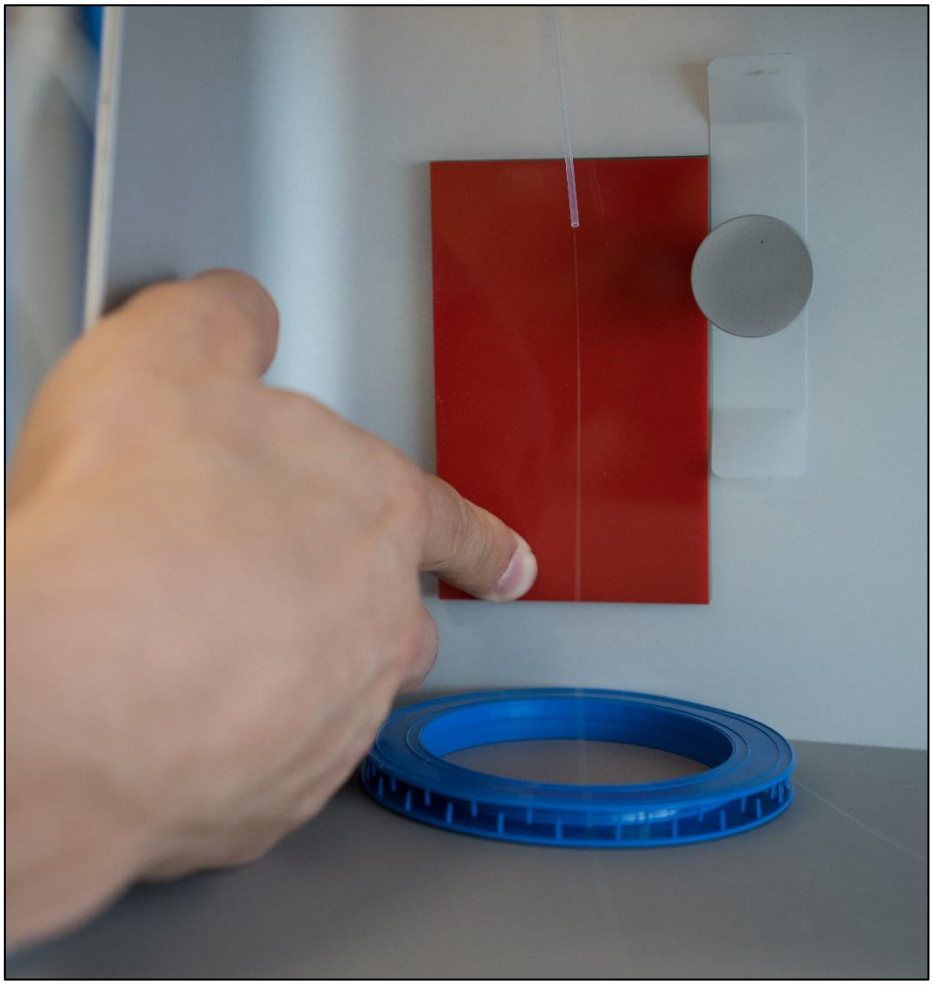

Figure 5-6: Loading the ORMOCER® coated optical fiber to the MarkForged Mark One™

As the used optical fiber is smaller in diameter than the ones recommended by MarkForged, the fiber may get stuck at the input-side of the fiber extruder. Special attention to this area shown in Figure 5-7 is recommended for successfully loading the optical fiber.

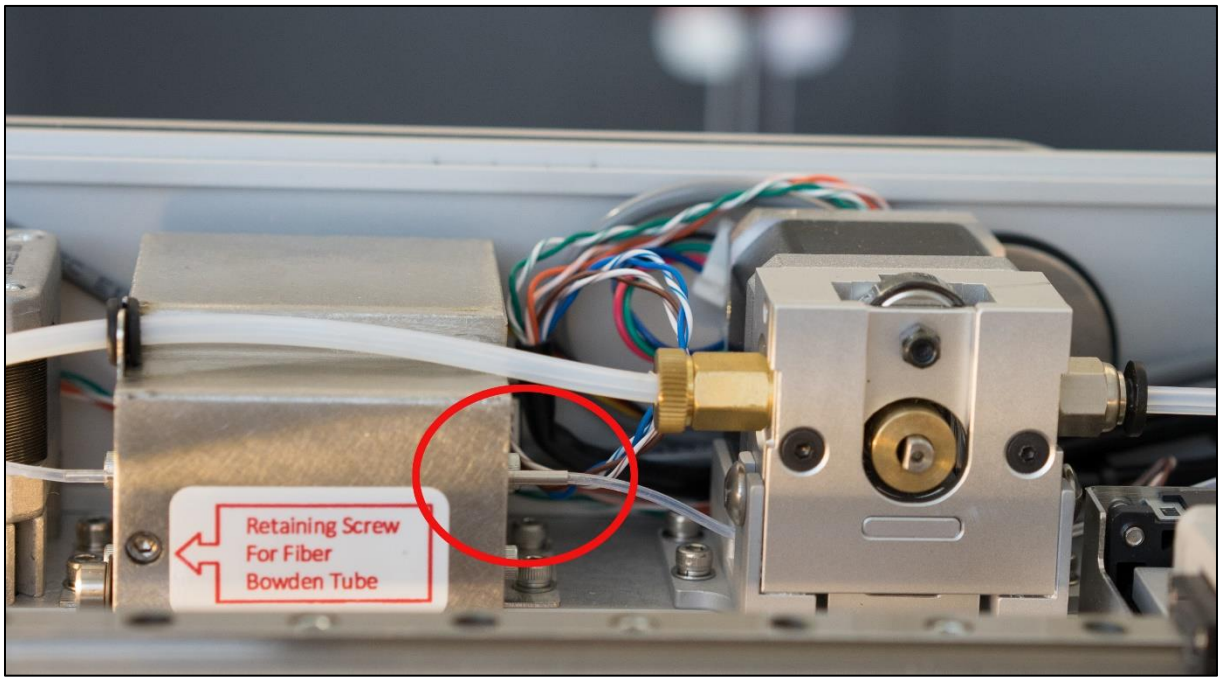

Figure 5-7: Input of the fiber extruder inside the Mark One™

- Printing process

Start the printing process with a component specially designed for printing with optical fiber used for sensing as described in chapter 5.3.1. Check for a correct start of the printing process. The manufacturing process of the component's nylon structure is done fully automatically. Pre-defined pauses during the printing process can be used for controlling the part. The fiber integration process needs to be supervised to guarantee a successful implementation of the FOS.

Immediately after the fiber printing process is finished, the printer should be paused manually. This provides the possibility of partly removing the optical fiber from the external fiber bridge as shown in Figure 5-8.

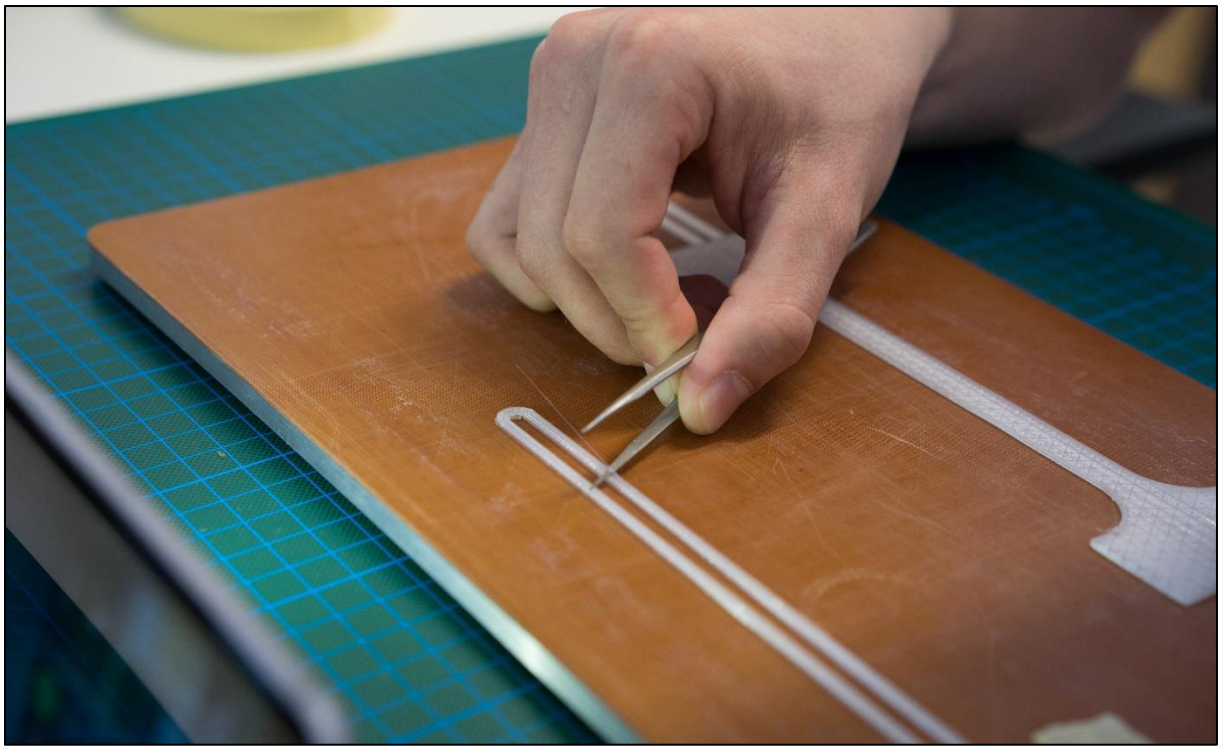

Figure 5-8: Uncovering optical fiber from the fiber bridge to provide a splicing opportunity

Enough fiber needs to be exposed to be able to splice the integrated optical fiber with an optical fiber pigtail afterwards. The uncovered fiber will be fixed to the build platform with tape to prevent it from any interferences with the upcoming nylon printing process. The continued printing process can be seen in Figure 5-9.

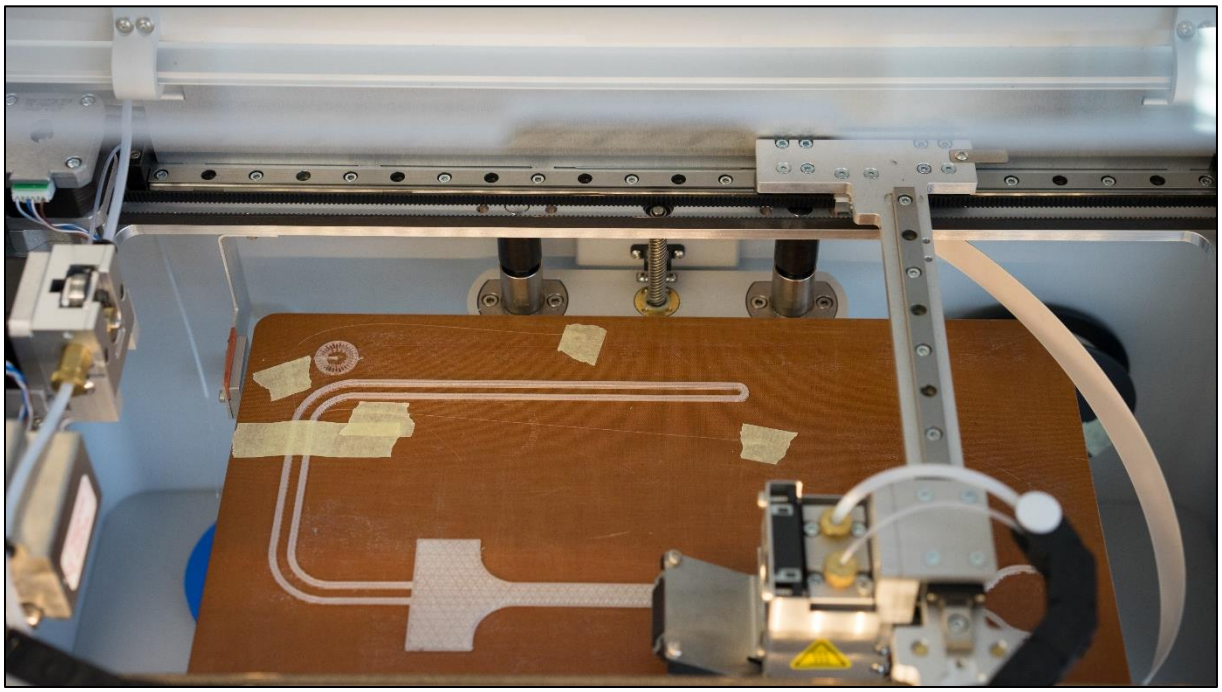

Figure 5-9: Continued printing process after integration and preparation of the optical fiber

This fiber exposing process must be repeated if more than one layer of the component is equipped with optical fibers for sensing. Afterwards, the print can be finished as usual and carefully removed from the build platform with the included optical fiber.

5.3.3 Fiber splicing process guideline

To be able to connect an additively manufactured smart component to an optical fiber measurement device, a fiber optical pigtail needs to be spliced to the bare optical fiber. Some special equipment and safety instructions are necessary for this purpose. The tools and know-how are available at the Institute of Engineering Geodesy and Measurement Systems at TU Graz.

- Preparing the fiber optic pigtail

A fiber optic pigtail is a fiber optic cable with a fiber optic connector on one end and a loose fiber on the other.

For splicing purpose, the bare fiber of such a pigtail needs to be uncovered. Therefore $\sim 130\ mm$ of the yellow protection tube are removed and the KEVLAR fabric inside is cut off. Then $33\ mm$ from the coating are removed as shown in Figure 5-10 below.

Figure 5-10: Removing the coating from the optical fiber for splicing purpose

In the next step, a $60\ mm$ splice protection tube is put onto the fiber optical pigtail. Then the bare optical fiber needs to be cut in a clean $90°$ angle. This step is done with an optical fiber cleaver as shown in Figure 5-11. The protection tube should be added before cleaving the fiber to prevent the cleaved fiber end from unnecessary damage. After cleaving, $20\ mm$ of bare optical fiber should be left for splicing.

Figure 5-11: Cleaving the bare optical fiber of the pigtail

- Preparing the optical fiber of the smart additively manufactured component

Uncover $\sim 25\ mm$ bare fiber from the ORMOCER® coating of the fiber which is integrated into the smart additively manufactured component. Cleaving the uncover fiber end will provide a clean edge for splicing it to the optical fiber pigtail. Paying attention for having enough loose fiber ($\sim 70\ mm$) between the end of the fiber and the additively manufactured material helps for preventing problems when splicing the parts in the following steps.

- Splicing the integrated optical fiber to the optical fiber pigtail

At this step, the two prepared fiber ends are placed inside the optical fiber splicer. Special attention should be payed not to harm or break the optical fiber which is integrated into the additively manufactured component. The placement of the fiber ends can be seen in Figure 5-12. On the right side you can see the fiber optic pigtail with the splice protection tube. On the left side, there is the bare fiber coming from the smart component in the background.

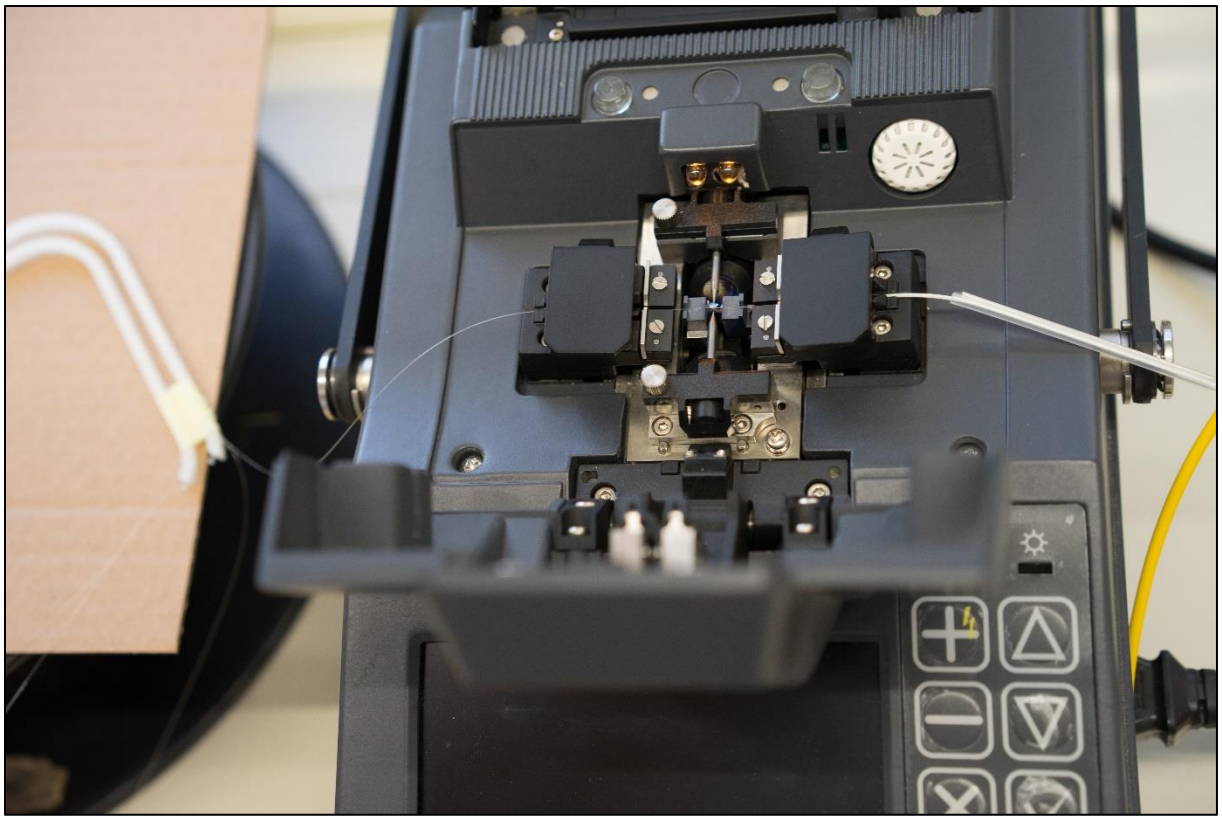

Figure 5-12: Optical fibers prepared for splicing

After successfully splicing the ends together, the splice protection tube is put over the splice and the heat shrinking tube is fixed in place.

Having correctly completed all these steps, measurements can be performed with the additively manufactured smart component.

5.4 Printed components

All additively manufactured components, developed and produced within this thesis, will be described and analysed in the following section. The first prototypes produced are mere functional prototypes to gain quick information if the concept is plausible. Therefore, components are designed with an included cavity or slot. The filament printing process is paused and the optical fiber is placed into this manufactured slot by hand and finally covered with material as the printing process is continued. Within the next steps, a suitable optical fiber needs to be selected to automate the production process. The critical issue concerning the optical fiber is the temperature load the coating of the fiber is exposed while being extruded through the printing nozzle of the Mark One. As the printer's settings are predefined and fixed, the fiber is exposed to temperatures between 260°C and 270°C. When using an optical fiber with an acrylic coating (PT05) the printer nozzle was clogging up and the fiber could not be placed correctly within the printed component's structure. Therefore, an optical single mode fiber from FBGS Technologies with a special ORMOCER® coating is used to manufacture the smart components automatized with the Mark One. To provide a systematic overview the printed

components shown in Table 5-2 are subdivided into early stage prototypes, early stage laboratory prototypes and final laboratory components.

Table 5-2: Overview of the printed components

Component	Prototype stage	Fiber coating	Purpose	Result
PT01	Early	Acrylic	Prove of concept	Concept is feasible
PT02	Early	ORMOCER®	Automated fiber integration	Fiber integration by using Mark One feasible
PT03 **PT04**	Early	Acrylic	Cylindrical component for 3D-shape sensing	Print-failure; high signal loss inside optical fiber at small curvature
PT05	Early	Acrylic	Verification of various decreasing fiber bending radii;	Fiber integration-failure due to the use of an acrylic-coated fiber
PT06	Early	ORMOCER®	Verification of various decreasing fiber bending radii	Various tested bending radii are feasible
PT07	Early laboratory	Acrylic / ORMOCER®	Comparison of automated and manually integrated optical fiber	Manually integrated fiber was damaged before tests could be performed
PT08 **PT09** **PT10**	Early laboratory	ORMOCER®	Perform tensile test on calibration system at IGMS laboratory	Measured strain reflects the applied deformation Improvements of part clamping strategy necessary
PT11 **PT12** **PT13**	Final laboratory	ORMOCER®	Integration of multiple fibers into the components; Perform tensile and bending test	Tensile and bending tests executed successfully Feasibility of concept confirmed

5.4.1 Early stage prototypes

- Prototype PT01

The first prototype produced is a very simple and small component to check the concept of inserting an optical fiber into the structure of parts produced with the method of FFF. The design consists of an elongated rectangular cuboid with a small cavity in its centre. The printing process is paused after the centre layer was finished to manually place an optical fiber with an acrylic coating into the planned cavity. Two supporting elements on both side of the cuboid where used to secure the fiber in this position. Figure 5-13 shows the internal structure and the fixation of the optical fiber before the printing process is continued to integrate the optical fiber into the component. After splicing the bare optical fiber to a pig tail, the first functional tests were made. By simply compressing the component

with a vice, the applied load caused strain along the fiber as shown in Figure 5-14. This first prove of concept was used as a foundation for further development of printable components.

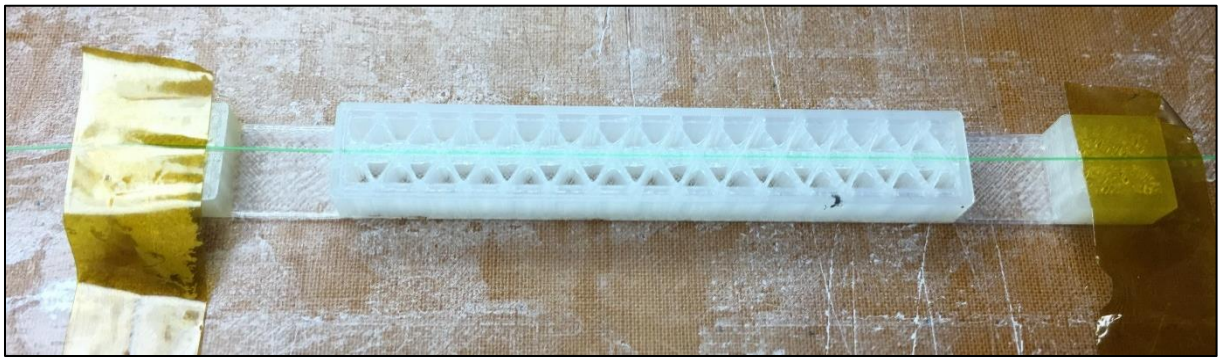

Figure 5-13 Manufacturing the first prototype PT01

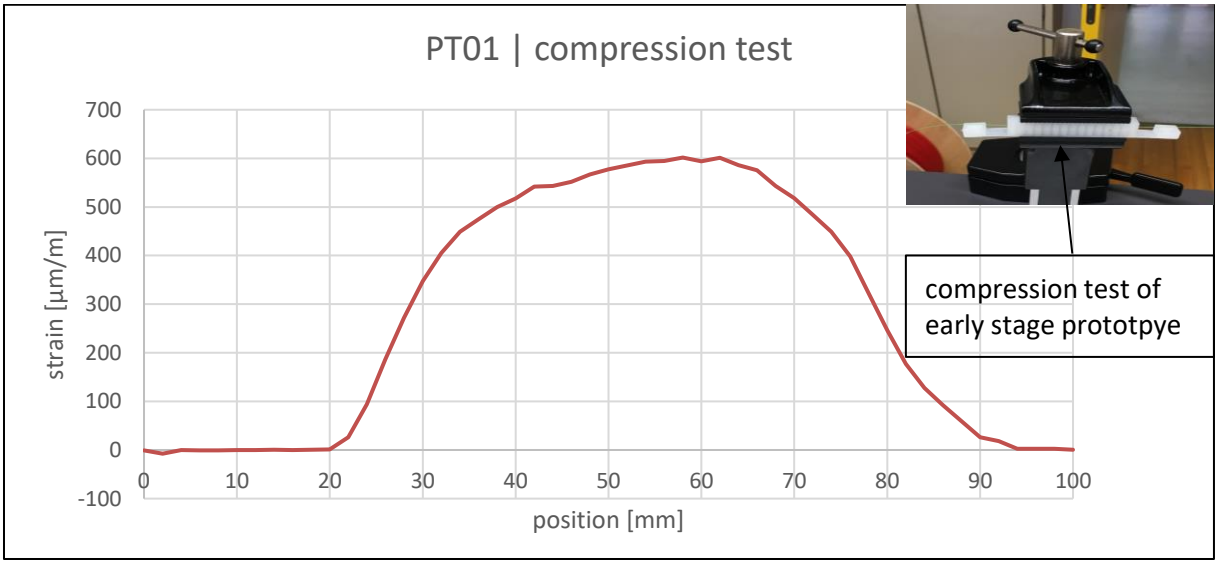

Figure 5-14 Fiber optic strain profile along an early stage prototype PT01

- Prototype PT02

For a complete automatization of the manufacturing process of smart elements, the placement of the fiber needs to be done by the printer itself. As the MarkForged Mark One provides the possibility to produce fiber reinforced components, this printer can also be used to integrate an optical fiber into the component's structure which can be used for sensing. PT02 is a relatively small and flat plastic pad with an ORMOCER® coated optical fiber integrated around its outside contour as shown in Figure 5-15.

Figure 5-15 Printed prototype PT02 with an integrated ORMOCER® coated optical fiber

The splicing process of this component was also done successfully. Some basic measurements were performed. Those results were the basis for further developments and improvements of the concept.

- Prototype PT03

To realize the concept of three-dimensional shape sensing, a cylindrical component was designed. For this purpose, a special layout for integrating an optical fiber into the structure was planned. This layout, consist of six circular distributed fibers and one central fiber inside the cylinder's structure. The integration of the fiber into the structure was performed manually. Unfortunately, the print failed due to thermal distortions of the component after the first layer of fiber was integrated. The measurements with the integrated fiber showed high losses around the relatively small curvature ($r = 6\,mm$) of the fiber.

- Prototype PT04

An iterated design of prototype PT03, where one single fiber should be placed along this path needed for three-dimensional shape sensing, was printed. Thermal distortions within such elongated structures caused this component to peel off the printer's platform and the printing process had to be stopped. Performed measurement with the integrated optical fiber delivered a similar result as those with prototype PT03. The losses around the fiber's curvature are extremely high. As mentioned above, a prototype with decreasing fiber radii will provide information concerning a minimal possible bending radius of the fiber.

- Prototype PT05

Because of the high losses around the fiber's curvature in the prototypes PT03 and PT04, a component with different decreasing radii of curvature was designed. The fiber is integrated into a structure realizing one arc with a radius $r = 60\,mm$, one with $r = 30\,mm$ and the smallest one with $r = 10\,mm$. This prototype was printed using a different acrylic coated fiber. Unfortunately, the printer's nozzle clogged up and the fiber was not integrated properly. The layout as well as the rest of the damaged optical fiber is shown in Figure 5-16.

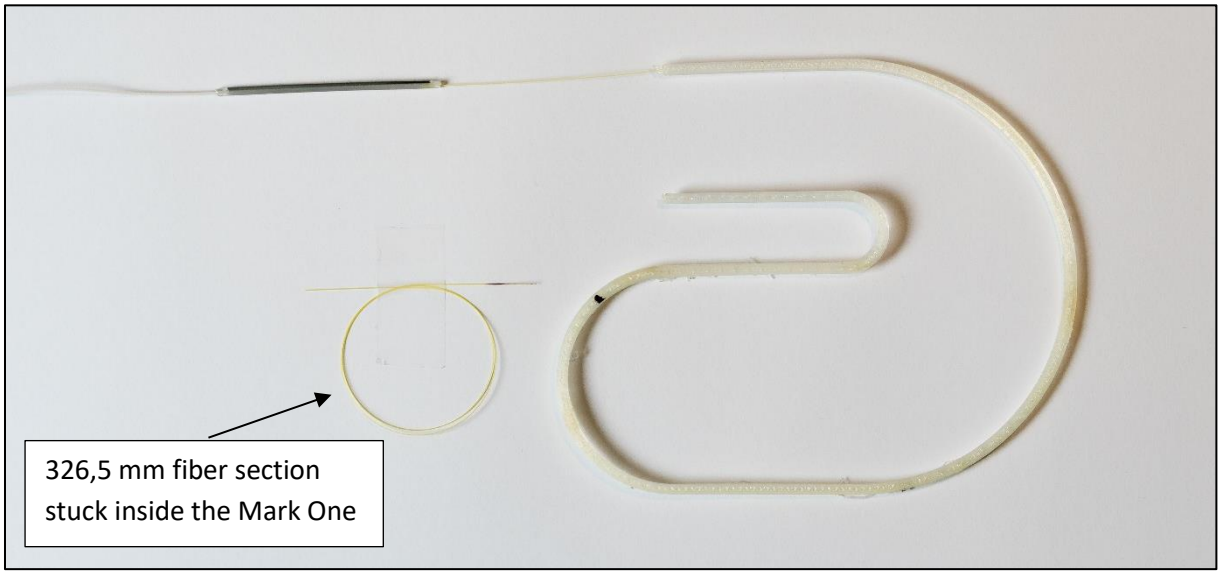

Figure 5-16 Non-functional prototype PT05 and clogged fiber at the bottom left

- Prototype PT06

Due to the malfunction within the printing process of prototype PT05, the same design is used to manufacture this component. In contrast to PT05, the fiber used for this part has an ORMOCER® coating and was successfully integrated into the component's structure. The exact dimensions of this prototype can be seen in Figure 5-17. The section on the left is specially designed to be removed during or after the additive manufacturing process expose the bare optical fiber for splicing it to a fiber optical pigtail. The measurements performed with this component showed that these realized radii of curvature are technically feasible, and an unambiguous measurement signal can be detected. Smaller radii of curvature than $r = 10\ mm$ have not been tested. Therefore, it cannot be guaranteed that components with radii of curvature with less than $r = 10\ mm$ are working properly.

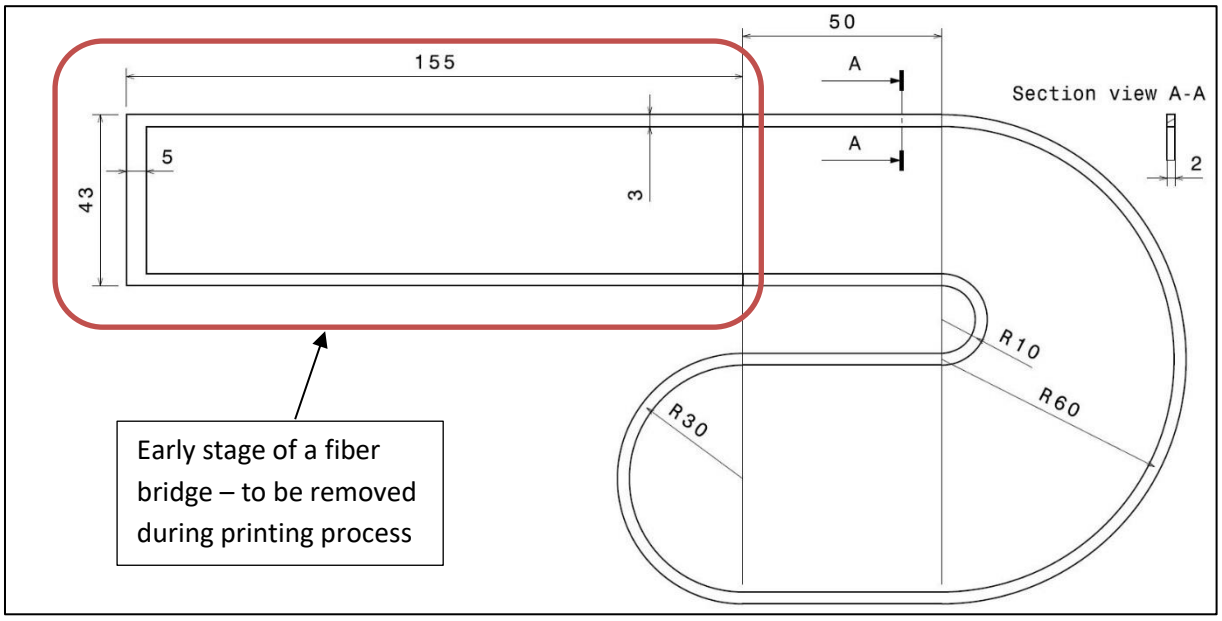

Figure 5-17 Layout and dimensions of PT05 and PT06

5.4.2 Early stage laboratory prototypes

- Prototype PT07

The purpose of this prototype is to compare the different fiber integration methods used within this thesis. Therefore, one optical fiber with an ORMOCER® coating is automatically integrated into the structure by the printer, another fiber with an acrylic coating is manually placed. The defined tensile test, planned with this prototype, was not possible as the acrylic coated fiber was damaged while performing some basic load measurements for exact localization of the component along the two fibers (Figure 5-18). In assumption that the ORMOCER® coated fiber is better integrated into the structure of the manufactured components than the manually placed acrylic coated fiber, because the ORMOCER® coating is slightly melted and fused to the filament structure during the printing process, this prototype was not re-printed for a second measurement. Tests with other prototypes will be used to prove the quality of the connection between the optical fiber and the additively manufactured plastic components.

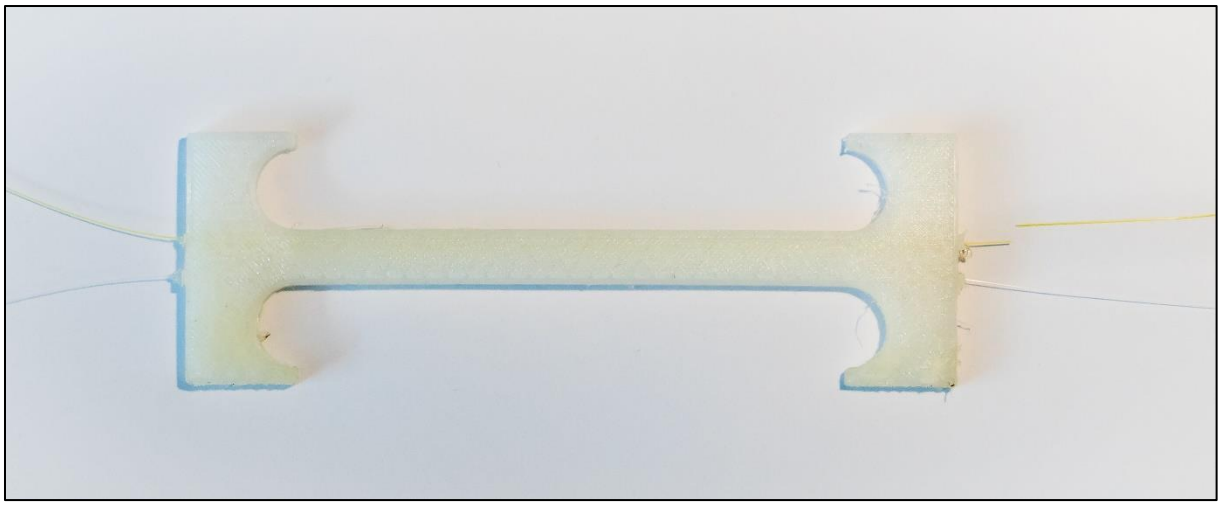

Figure 5-18 Prototype PT07 with two embedded optical fibers with different coating materials

- Prototypes PT08, PT09, PT10

These prototypes were designed and manufactured to perform tensile tests on the calibration system at the IGMS laboratory. Therefore, three prototypes as shown in Figure 5-19 are printed and spliced. Every component has one optical fiber integrated along its centre. The ORMOCER© coated optical fiber is integrated by the Mark One 3D printer. The components are then mounted to the calibration system and elongated. The results of these test are described and analysed within chapter 6. The parts have a total length of $160\ mm$. The middle section which is deformed during the laboratory tests is $100\ mm$ long.

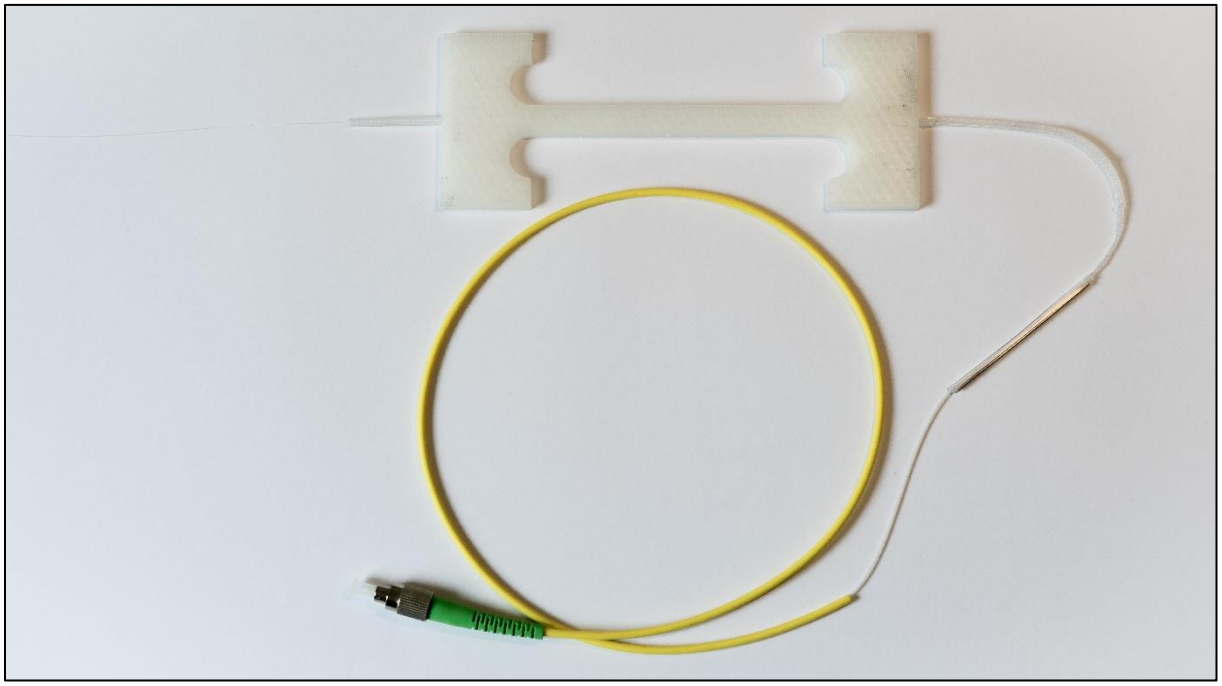

Figure 5-19: Layout of the prototypes PT08, PT09 and PT10

5.4.3 Final laboratory components

- Prototype PT11, PT12, PT13

A series of similar components is manufactured for highly accurate and comparable tests on the calibration system. Different testing modes in all three directions of the component were defined. Therefore, more than one fiber is integrated into the components. A symmetric partitioning was chosen around the centre of the parts. The four fibers are each offset by $3{,}5\ mm$ and $1\ mm$ from the neutral axis. This will also provide the possibility of performing bending measurements. The design is illustrated in Figure 5-20. It is defined similar to standard tensile test geometries used for plastic components. All displayed dimensions are shown in $[mm]$. The blue dimensions define the position of the optical fibers.

An additional redundancy for the measurement data was also accomplished by integrating multiple optical fibers.

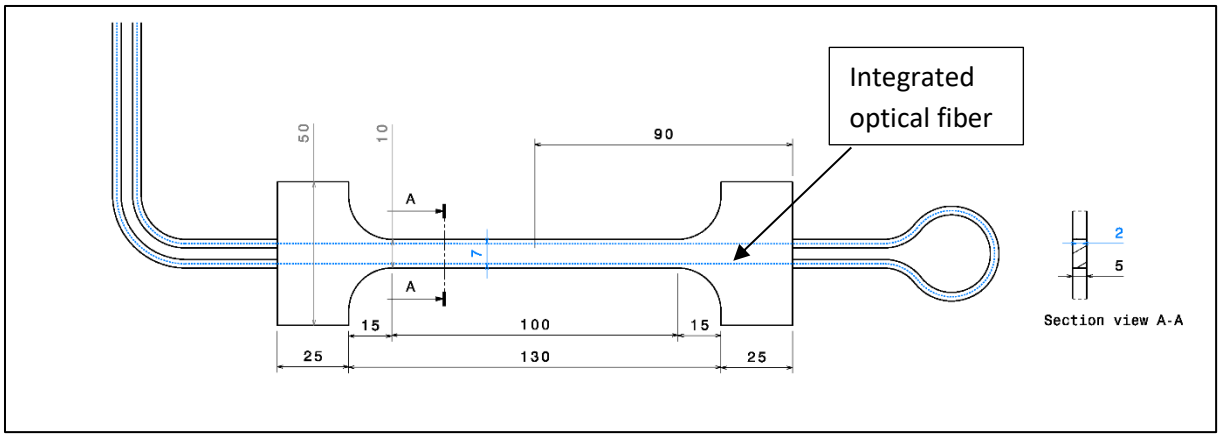

Figure 5-20: Drawing of the final laboratory prototypes PT11, PT12 and PT13

6. Laboratory measurements

As the proof of concept for additively manufacturing smart elements by integrating an optical fiber sensor into the plastic structure of FFF components is successfully accomplished with the early stage prototypes described in chapter 5.4.1, a more detailed and precise measurement setup is needed for validation and verification. Therefore, additively manufactured components with integrated optical fiber sensors are mounted to the optical fiber calibration system[62] in the laboratory of the IGMS and predefined test cycles are performed and measured. The exact setup as well as the properties of the individual prototypes which were tested will be described for every single component in detail. Table 6-1 provides an overview of all laboratory measurements performed on the optical fiber calibration system. The mentioned test modes A, B and C will be described in section 6.4.1. An analysis of the measurement results will be provided for evaluating the quality of additively manufactured smart components.

Table 6-1: Laboratory measurements

Component	Test profile	Cycles and test mode
PT08	0-250 µm in 50 µm steps	3 cycles;
	0-500 µm in 25 µm steps	3 cycles; 1h hold at 500 µm at last cycle
	0-break in 100 µm steps	
PT09	0-250 µm in 50 µm steps	3 cycles
	0-500 µm in 25 µm steps	3 cycles; 1h hold at 500 µm at last cycle
	0-break in 100 µm steps	
PT10	0-500 µm in 25 µm steps	3 cycles; 20h hold at 500 µm at last cycle
PT11	0-1000 µm in 50 µm steps	3 cycles; test modes CBACBACBA
	0-24000 µm in 1000 µm steps 0-break in 1000 µm steps	1 cycle; 1h hold at 24000 µm; test mode C
PT12	0-1000 µm in 50 µm steps	3 cycles; test modes CBACBACBA
	0-6000 µm in 250 µm steps 0-break in 1000 µm steps	1 cycle; 1h hold at 6000 µm; test mode B
PT13	0-1800 µm in 75 µm steps 0-break in 250 µm steps	1 cycle; 1h hold at 1800 µm; test mode A
	0-break in 250 µm steps	test mode A

[62] Robert Presl, 'Entwicklung Eines Automatisierten Messsystems Zur Charakterisierung Faseroptischer Dehnungssensoren' 2009, p. 102 ff.

6.1 Prototype PT08

The printed component is mounted to the calibration system with clamps which were designed to perform tension tests with thin-skinned plastic membranes. The setup is shown in Figure 6-1. The clamp mounted to the linear translation stage on the right side of the figure is moved away from the fixed clamp shown on the left side. In this way, the component is deformed. The distance is tracked through the interferometer system shown on top of the figure.

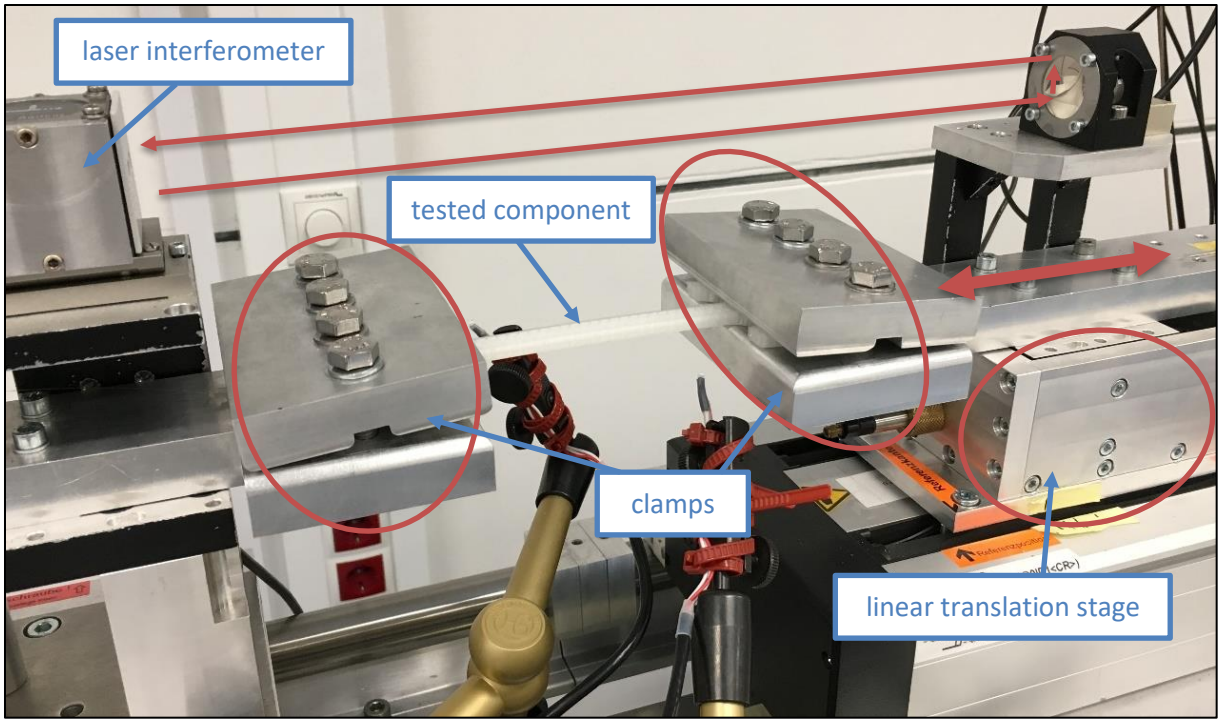

Figure 6-1: Measurement setup and calibration system

- PT08 | Test 01

For the first test, the distance between the two clamps mounted to the calibration system is increased stepwise up to a certain level. Then the distance is decreased stepwise back to the starting position. This cycle is repeated for three times.

Within the calibration system, data of the position of the linear translation stage, the measured distance of the interferometer and the force measured at the load sensor are logged with $5\ Hz$. The stepwise deformation profile measured with the calibration system's interferometer unit is shown in Figure 6-2.

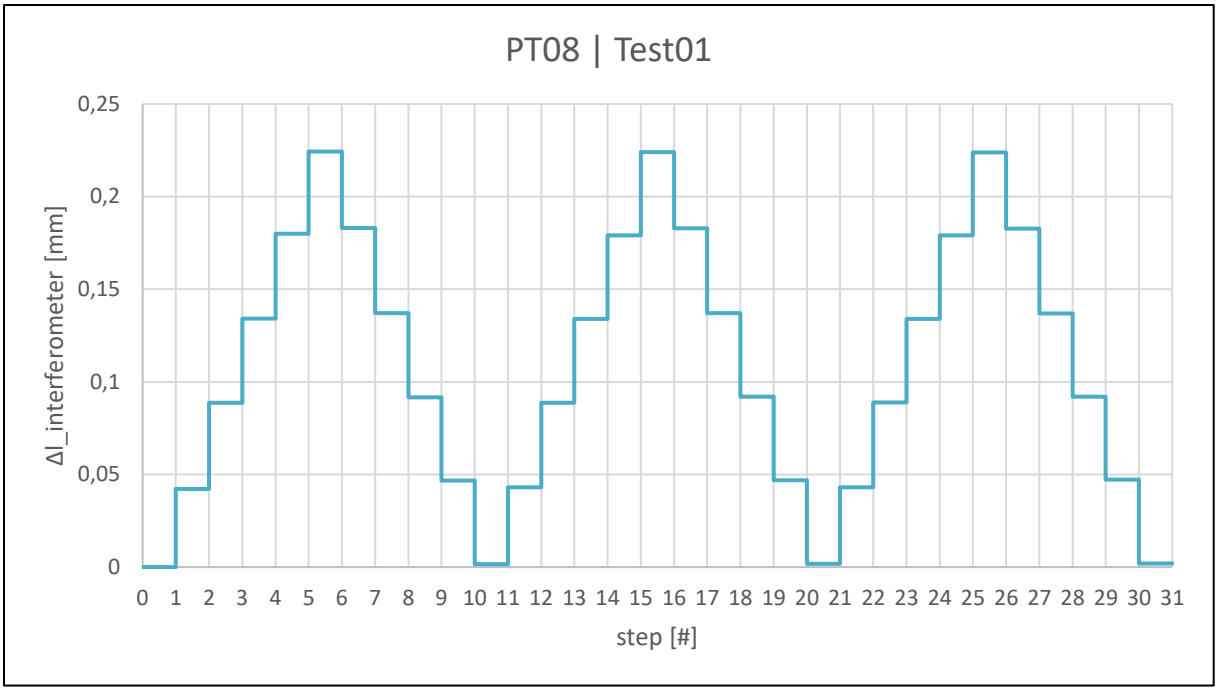

Figure 6-2: PT08 Test01 | test-scheme displayed through interferometer values over deformation steps

After every movement of the calibration system, one measurement with the LUNA OBR 4600 is performed. The strain data measured with the optical fiber is shown in Figure 6-3 for the first steps of increasing distance in cycle 1. The strain data measured when decreasing the distance stepwise back to zero is plotted as a broken line in Figure 6-3. The strain profiles for increasing and decreasing distances are nearly identical ($\Delta_{max} = 46{,}61\ \mu m/m; \Delta_{mean} = 18{,}69\ \mu m/m$) at the area of free length.

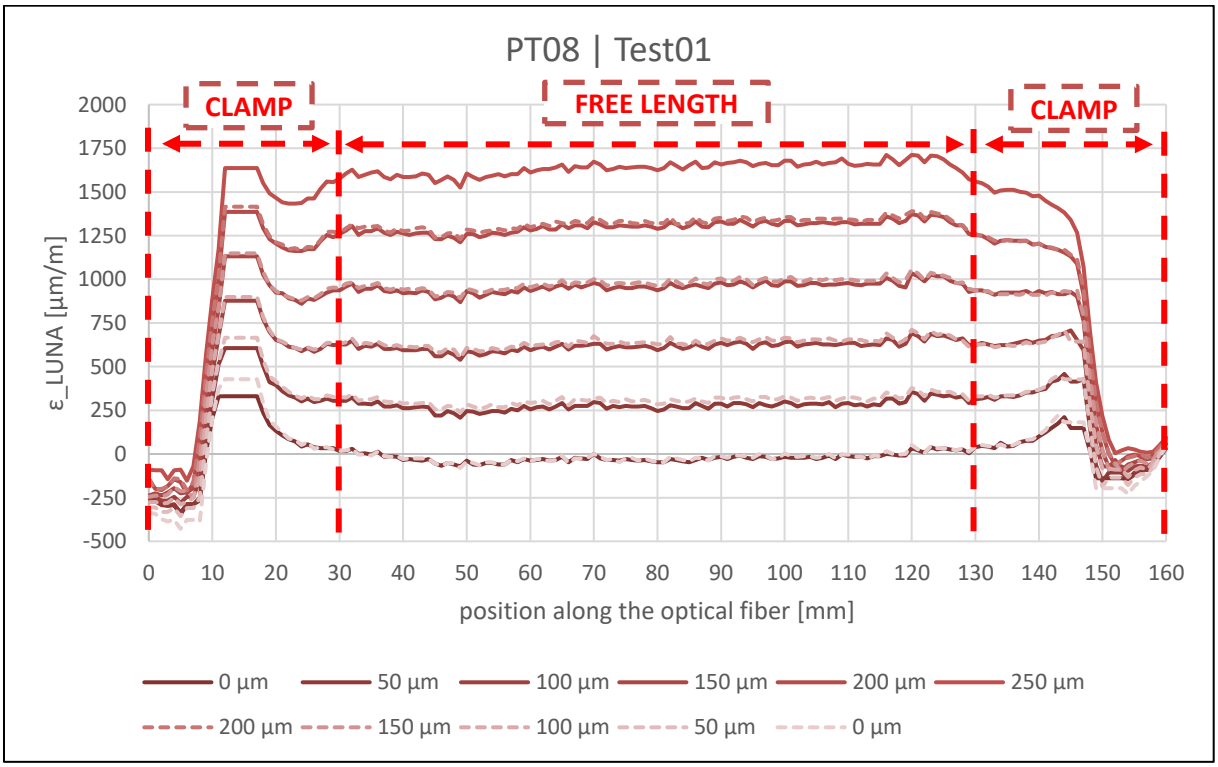

Figure 6-3: PT08 Test01 | optical fiber strain data cycle 1

The free distance between the two clamps, which are used to mount the tested component to the calibration system, is set to $100\,mm$. The initial length of the tested components is $160\,mm$. Therefore, round $30\,mm$ of the component are used to fix it to the calibration system on both ends. Analysing the strain plots of the optical fiber data, these fixation section can be detected on both ends. The area of almost constant strain per step in the middle show the free measurement section. A mean average can be derived from those strain values within the free measurement section. For this component, the free section between the clamps is used to calculate a trimmed mean. Therefore, the array of strain values is cleared up at either ends of the array by discarding a set of the highest and lowest values. An arithmetic mean is derived from the remaining data set. Through this function, single data outliers are excluded. In Figure 6-4 these mean strain data values of the first displacement cycle are plotted over the values measured using the interferometer system.

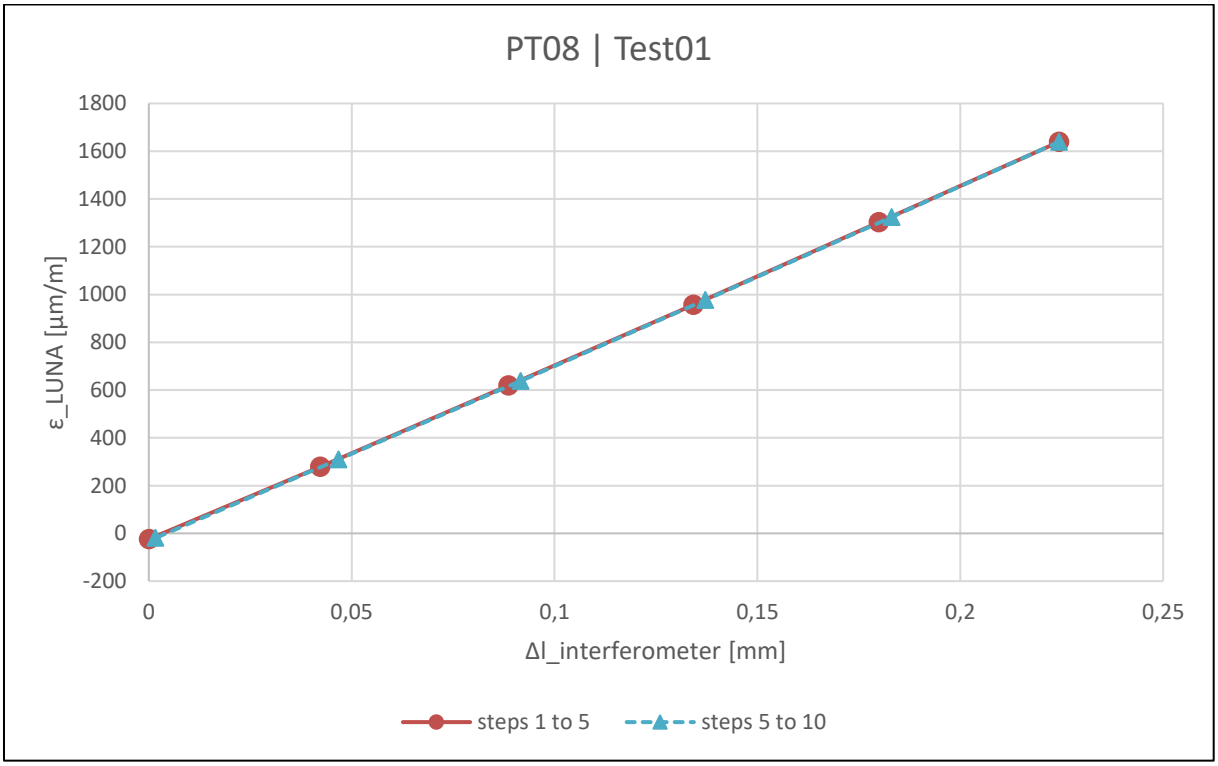

Figure 6-4: PT08 Test01 |strain (ε LUNA) over interferometer cycle 1

In order to evaluate the strain data gained from the measurements with the LUNA OBR 4600, it is necessary to compare that data to a reference measurement. In case of the performed tests, an interferometer system is used to track the applied deformation to the components. This interferometer values are then converted into strain data. The reference strain is then calculated as follow for this test:

$$\varepsilon_{referemce} = \frac{\Delta l_{interferometer}}{l_0} \tag{6.1}$$

Within this formula, $\Delta l_{interferometer}$ represents the measured interferometer reference values per step. The free length between the two clamps needs to be defined as the starting length l_0. In case of PT08, $l_0 = 100\,mm$.

For comparing the residuals of the strain calculated from the interferometer values and the strain derived from the measured optical fiber data, a $\Delta\varepsilon$ is calculated by implementing two additional compensation parameters. These characteristic parameters are named a_0 and a_1.The $\Delta\varepsilon$ is calculated as follow:

$$\Delta\varepsilon = a_0 + a_1 * \varepsilon_{reference} - \varepsilon_{LUNA} \tag{6.2}$$

The calculation of the characteristic parameters is demonstrated with the representative Figure 6-5. When subtracting the strain data gained through fiber optical sensing from the reference strain values derived from the interferometer values, the graph displayed below can be plotted. This clearly shows a linear trend within the residuals and an additional offset from a neutral axis. The parameters a_0 and a_1 are determined to compensate for these deviations by performing a linear regression analysis. As the first cycle shows a characteristic running-in behaviour, it is excluded from the calculations for the compensation parameter a_1.The parameter a_0 is used to compensate the offset resulting from the running-in behaviour. These compensation parameters need to be determined for each performed cycle test.

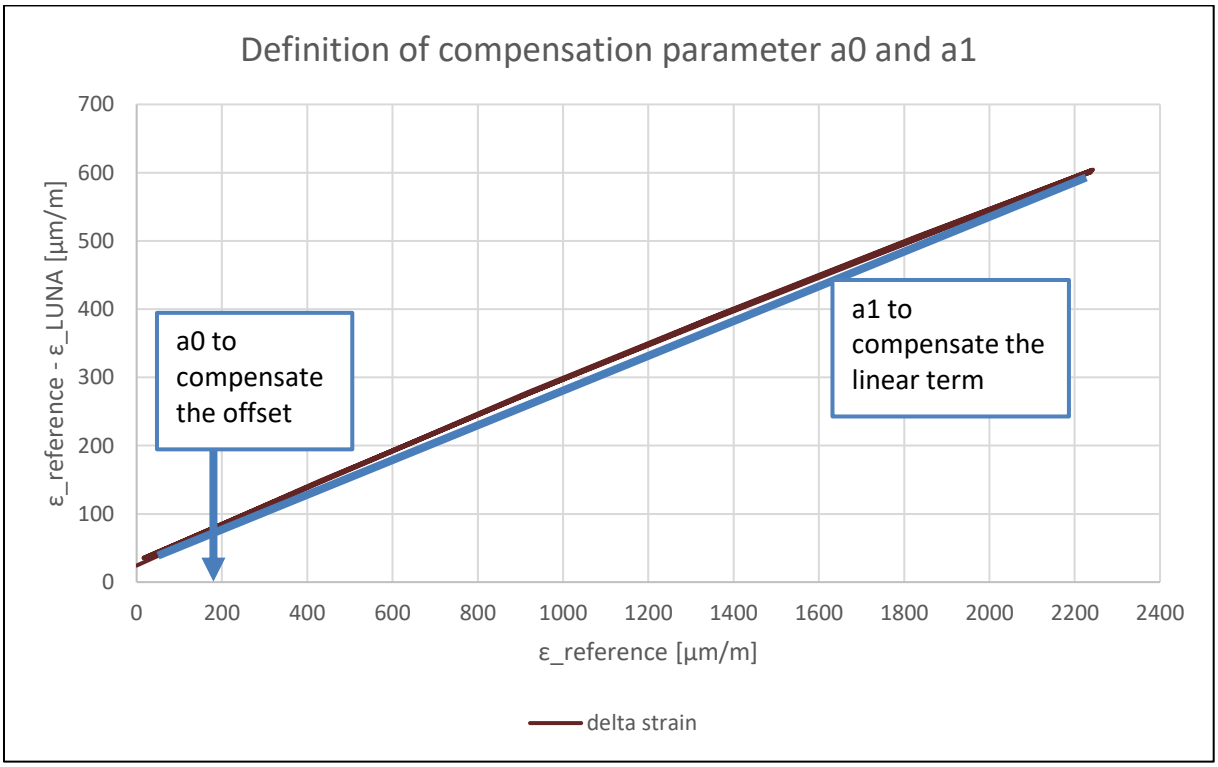

Figure 6-5: Representative graph for the explanation of compensation parameters for PT08 and PT09

The $\Delta\varepsilon$ shown in Figure 6-6 is calculated according to the linear regression analysis described above. The loading parts of the single cycles are displayed by red coloured lines, the unloading parts of the cycles are toned blue. A minimal running-in characteristic is detected at the load phase of cycle 1.

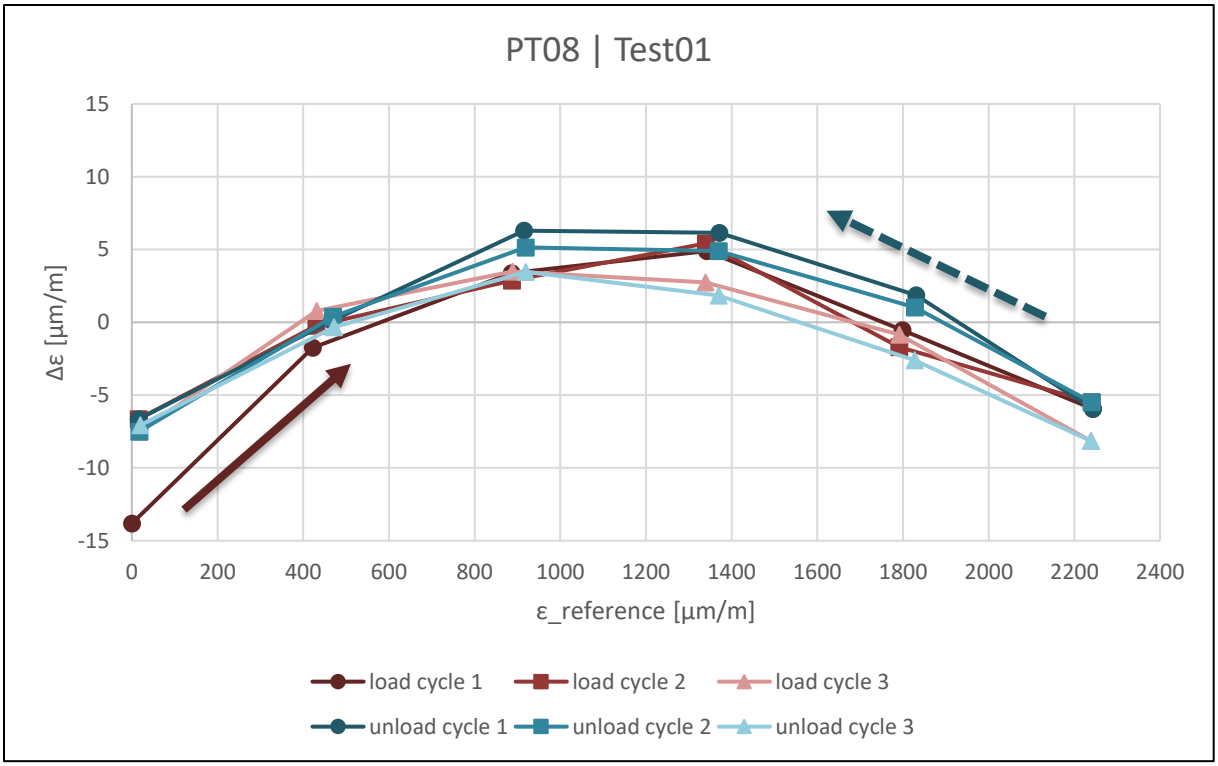

Figure 6-6: PT08 Test01 | Δε over ε reference for 3 cycles

This graph also shows, that there are quadratic residuals which are not compensated with this compensation method. The first load cycle shows the characteristic running-in behaviour. Neglecting this first cycle, the maximal difference between load and unload cycle below $5\ \mu m/m$.

- PT08 | Test 02

For this second test with PT08 a more automated approach is realized. Therefore, a cycle profile is defined within the software application of the calibration system. Every deformation step is performed for $30\ seconds$. The LUNA OBR 4600 is continuously performing measurements with $\sim 0{,}15\ Hz$. Therefore, at least two to three measurements are performed with the optical fiber sensing system per step.

An additional one hour pause at the last load stage of the three performed load cycles is implemented within this test.

The results of this test are similar to the other performed strain tests and are not displayed in detail.

- PT08 | Test 03

This test is performed to gain information about the maximal load that can be applied to smart additively manufactured components. Therefore, the displacement is increased stepwise until the fiber broke. The measured strain profiles of this test setup in Figure 6-7 show that the maximal strain to be measured with the optical strain sensing instrument is slightly below $50000\ \mu m/m$.

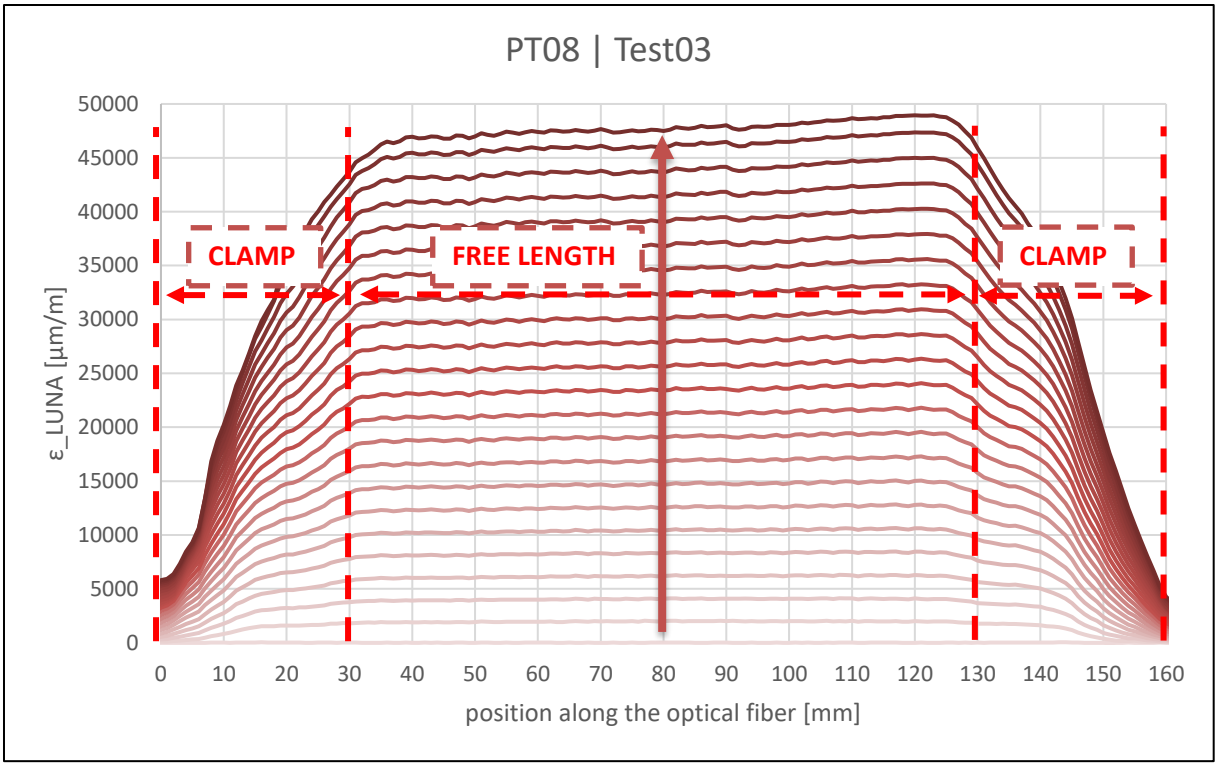

Figure 6-7: PT08 Test03 | optical fiber strain data for break test

A comparison between the mean strain data measured with the LUNA OBR 4600 system and the force detected by the load sensor of the calibration system is shown in Figure 6-8. The two data sets drift apart each other at a certain level of deformation. This is most probably caused by the fact that the plastic deformation of the additively manufactured component is not included within the analysis. As the deformation is increased, the plastic part starts to creep. Therefore, the necessary force is degrading while the strain measured with the optical fiber system is increasing.

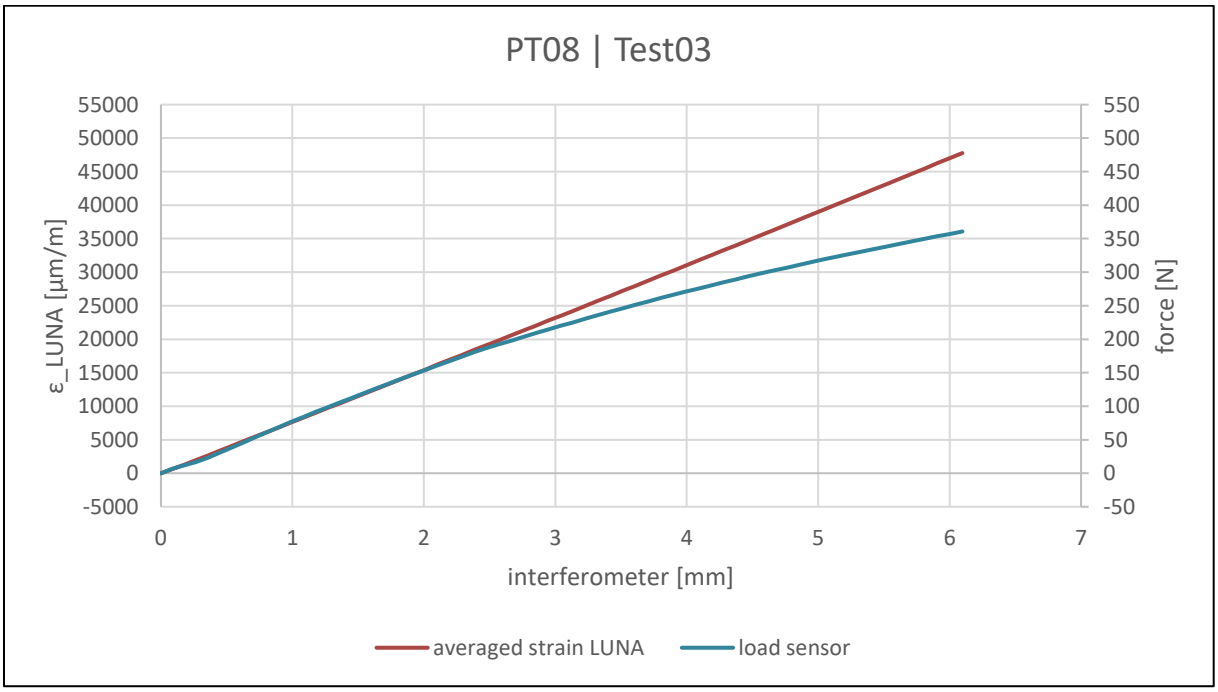

Figure 6-8: PT08 Test03 | comparison strain data LUNA vs. load sensor

6.2 Prototype PT09

A similar test series as with prototype PT08 is performed with this component. Therefore, the two component tests can be compared to each other to gain information whether their behaviour is similar and the applied fiber integration method is capable of manufacturing reproducible smart elements. The part clamping strategy for the tests with prototype PT09 is the same as shown in Figure 6-1.

- PT09 | Test 01

The calibration system is programmed to perform three load cycles from $0\ \mu m$ to $250\ \mu m$ and back in $50\ \mu m$ steps. Per step, the calibration system pauses for $30\ seconds$. The LUNA OBR 4600 performs measurements during the whole test program. The interferometer values from the calibration system are then used to calculate the reference strain of the deformed component. The displayed $\Delta\varepsilon$ over $\varepsilon_{reference}$, shown in Figure 6-9, is calculated in the same way as for prototype PT08. The cycles show a similar behaviour as within the previously tested component. The running-in characteristics are not that clearly finished after the first cycle. This can be seen at the starting points of the load cycles as the $\Delta\varepsilon$ data is not meeting at a single point at the smallest $\varepsilon_{reference}$ values.

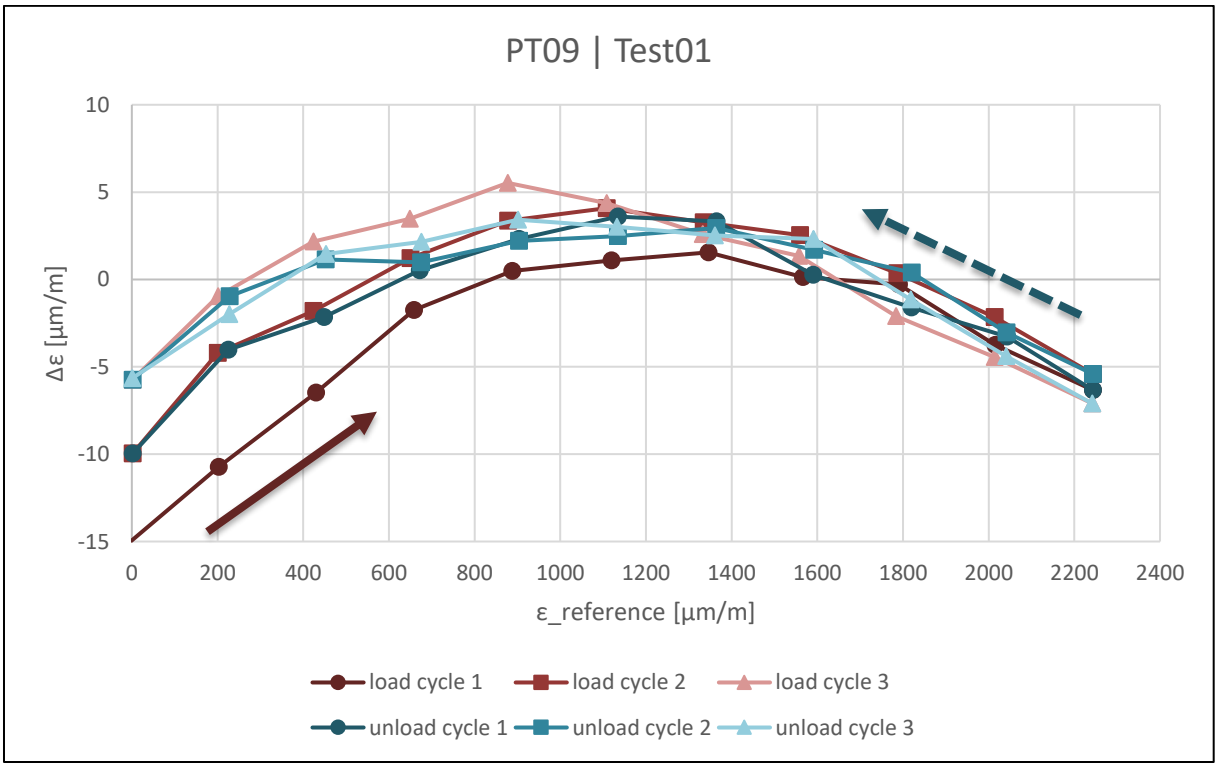

Figure 6-9: PT09 Test01 | Δε over ε reference for 3 cycles

- PT09 | Test 02

This performed cycle test with an additional one hour hold at the third cycle confirms the components measurement performance. The information gained from this test cycles will be used as input to develop a final measurement setup and clamping strategy. The measurement results are not displayed in detail within this thesis.

- PT09 | Test 03

As a final test this component is used to perform a maximum load capacity test. This test verified the smart components ability to perform strain measurements at rather high deformations. The optical fiber used for sensing failed slightly above $50000\ \mu m/m$ strain.

6.3 Prototype PT10

Another component with the same design as with prototype PT08 and prototype PT09 is used to perform this load test.

- PT10 | Test 01

The test profile of this cycle test can be seen in Figure 6-10. The duration of the whole test is $24\ hours$. At the final cycle, a $20 - hour$ break under load is integrated. The position of the linear translation stage stays at $0{,}5\ mm$ deformation, which is equal to a strain of $\sim 3350\ \mu m/m$ during this break. As shown in the figure below, the force measured with the calibration system's load sensor is degrading during this time of constant deformation. This creep characteristics is most probably due to the material properties of the measured component. In addition, the clamping strategy used with this test cannot guarantee that the part is not slipping out of the clamps during the $20 - hour$ break. On the other hand, the strain data collected during this test is properly representing the load cycle profiles as shown with the red line in Figure 6-10. During the break under load at the final cycle, the measured strain is increasing slightly.

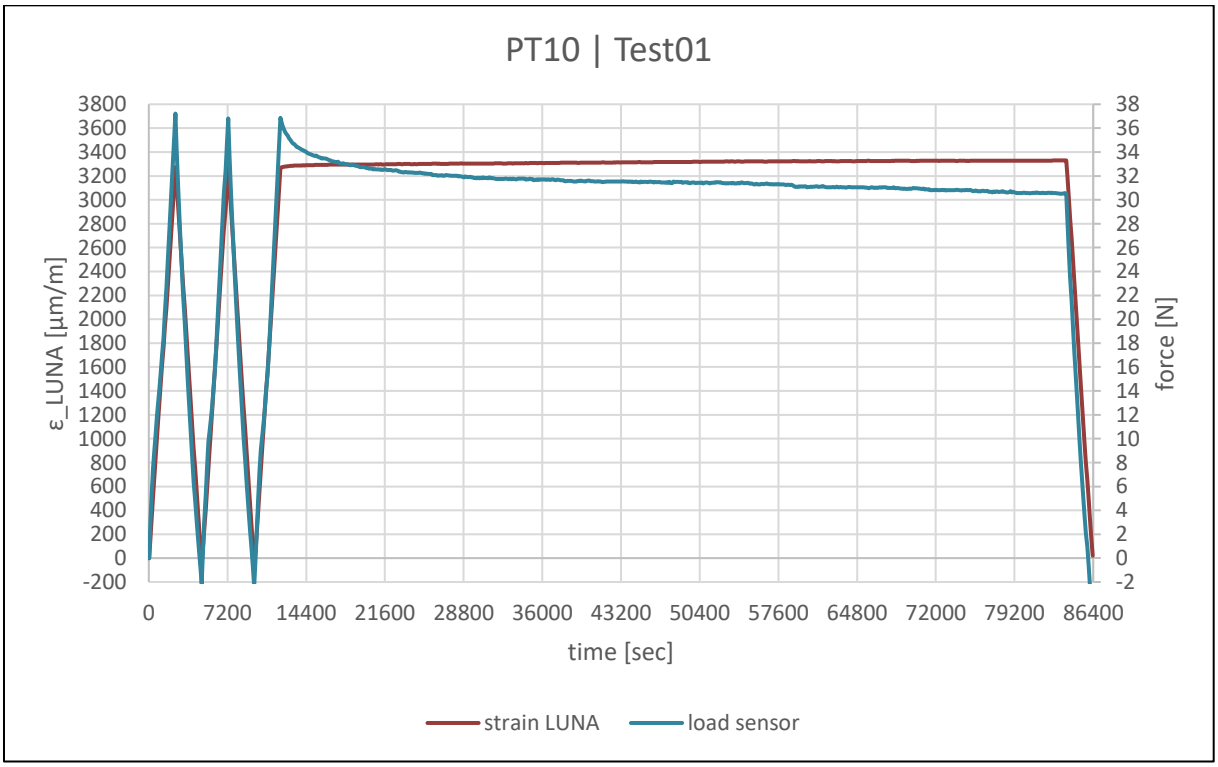

Figure 6-10: PT10 Test01 | measured strain (ε_LUNA) and force over time for 3 cycles incl. 20h hold

A more detail version of this $20 - hour$ hold area is shown in Figure 6-11. The main declination of the measured force takes place within the first hours and is not completely over at the end of the break. The inclination of the measured strain also has its maximum at the beginning of the hold phase. This increase in the measured strain most probably results from the creep behaviour of the material of the component. Through this creepage, the distance between the two clamps is incrementally increased as the smart element gets longer. This results in additional strain, which can then be detected with the FOS.

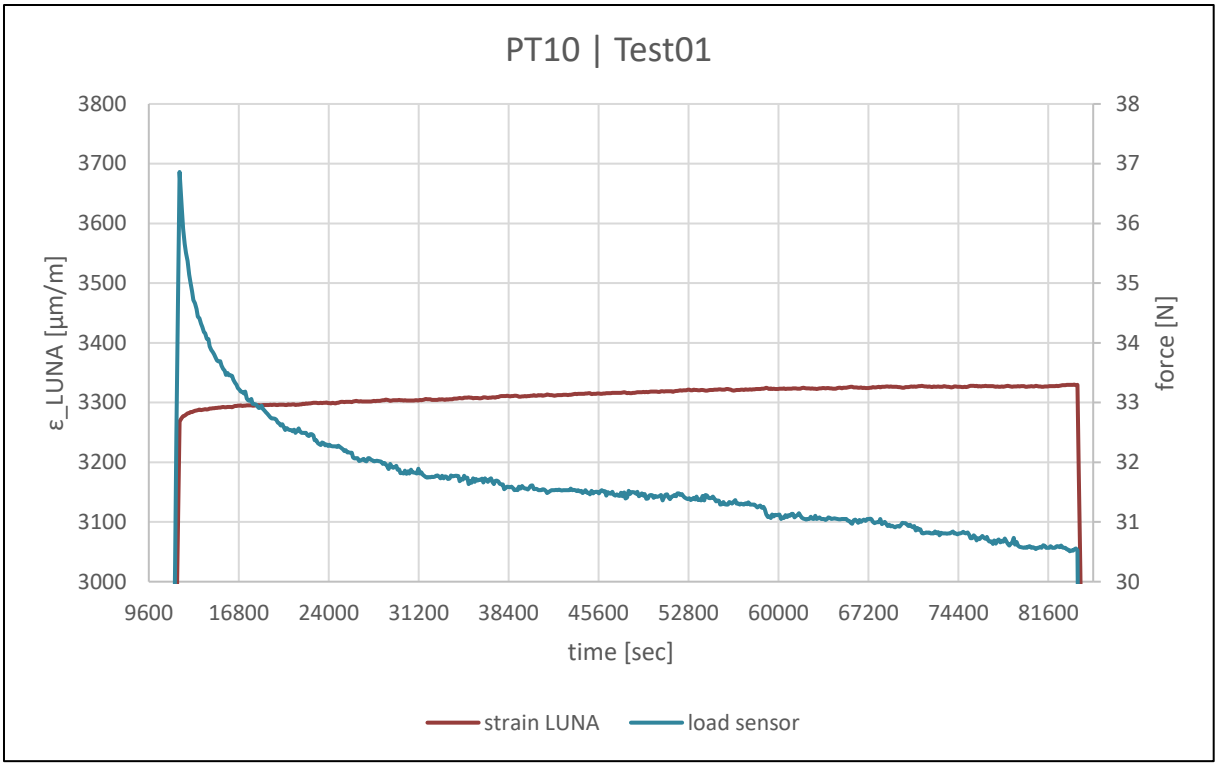

Figure 6-11: PT10 Test01 | measured strain (ε_LUNA) and force over time – hold area in detail

6.4 Prototype PT11 / PT12 / PT13

Resulting from the performed laboratory measurements on the calibration system, the implementation and manufacturing of an advanced part clamping strategy is realized. In addition to the load case – applying longitudinal deformation and strain – which was examined with the prototype PT08, PT09 and PT10, a mounting system for applying bending deformation to the components is designed. The different testing modes are labelled test mode A, test mode B and test mode C depending on the direction of deformation. The clamping and deformation setup is aligned with the smart components' geometry which are manufactured for these laboratory measurements by the IGMS.

During the laboratory measurements, only two operational optical fibers could be measured with PT13. Therefore, this prototype can only be used to perform tension tests (test mode A).

6.4.1 Test modes

As shown in Figure 6-12, a new clamping setup is designed to perform longitudinal strain test through applying elongation deformation to the tested components. The clamping strategy is improved by using aluminium blocks as clamps to fix the smart component on both ends to the calibration system. The blocks will provide an evenly distributed clamping force at the ends of the component. A small groove is integrated into the upper clamping blocks directly above the optical fibers. This should help reduce the direct clamping force onto the optical fibers inside the smart components.

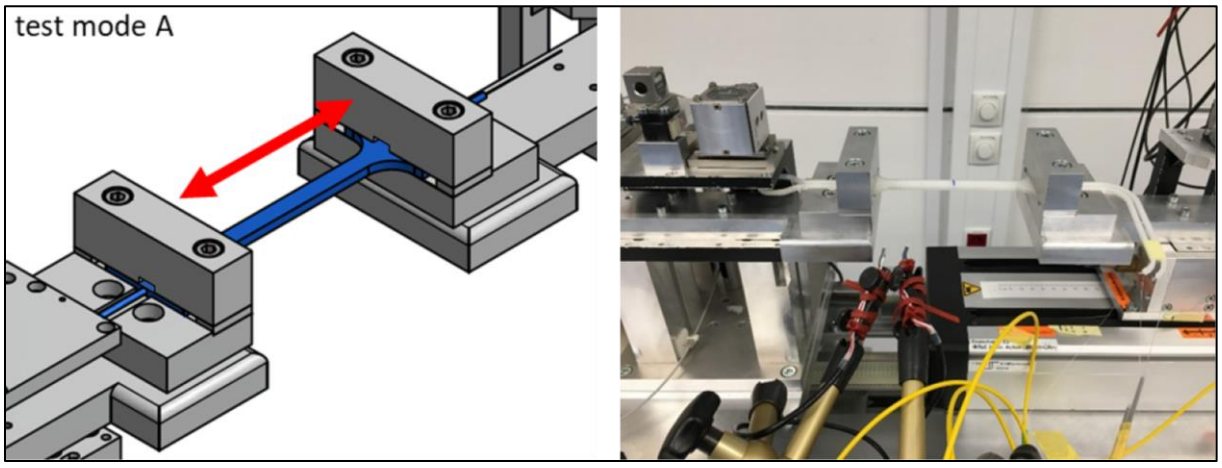

Figure 6-12: Sample drawing and picture of the measurement setup for test mode A

For test mode B, a ramming element made from aluminium is used to bend the additively manufactured component. Therefore, the pusher is mounted to the linear translation stage of the calibration system. On the second side of the system two bolts are mounted as shoulder points to support the tested component. The ramming element is then pushed towards the component to apply a bending deformation. In addition to the shoulders, the tested component is fixed against flipping over through adding a top and bottom horizontal support block. These support blocks do not apply any clamping force to the component which can move freely between them. The point of contact between the deformed component and the pusher is in the centre of the shoulders. The test setup of test mode B is displayed within Figure 6-13.

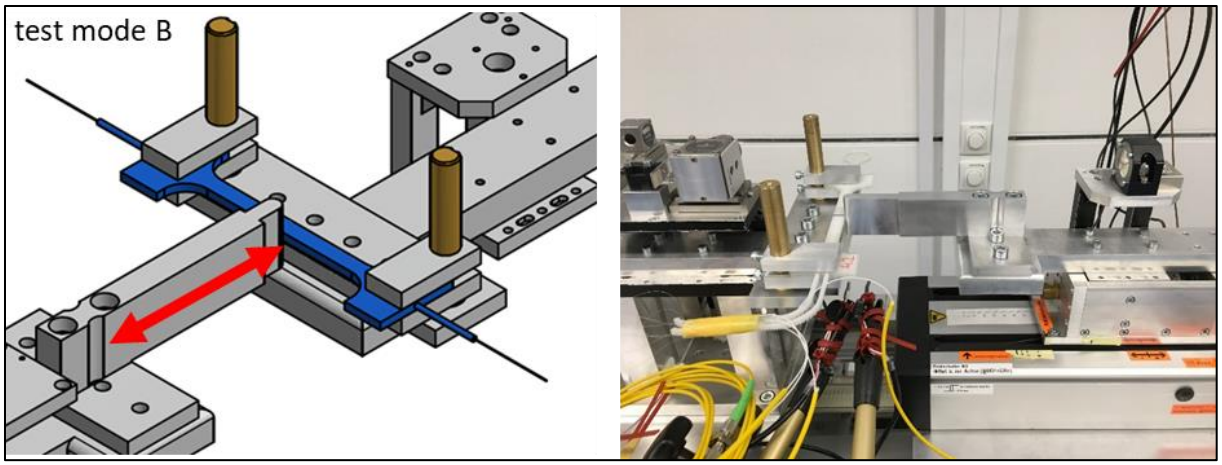

Figure 6-13: Sample drawing and picture of the measurement setup for test mode B

To complete a three-axial deformation setup, test mode C is defined like test mode B, but the measured component is turned by $90°$. As the tested components are not able to flip during the load cycles of this test mode, the horizontal supports used in test mode B are not in use. The pusher and the shoulders are the same as used before. The test setup is again shown in Figure 6-12 below. Test mode C is expected to show the smallest strain values measured with the optical fiber sensors as the sensors' distance to the strain-neutral plane is the smallest of the performed component bending tests.

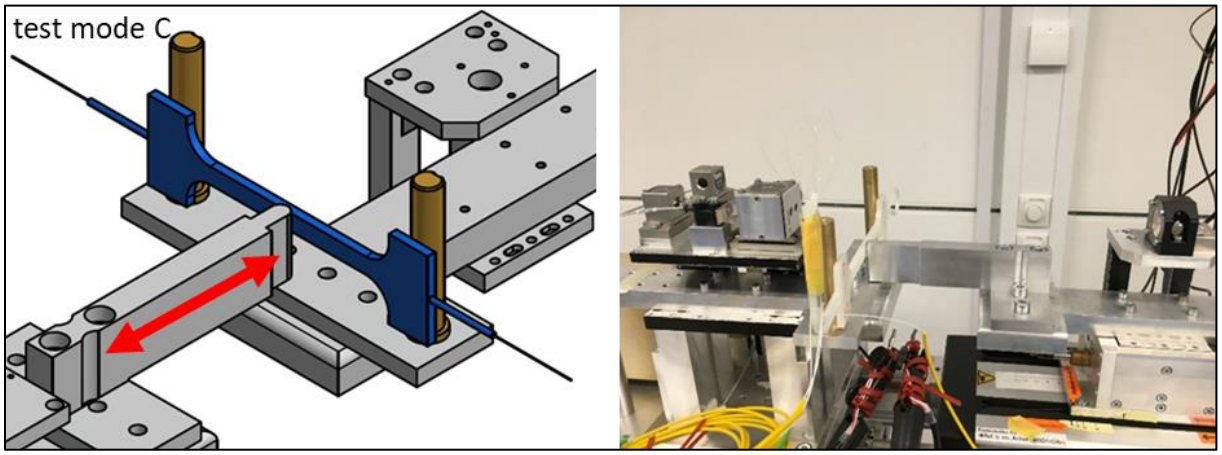

Figure 6-14: Sample drawing and picture of the measurement setup for test mode C

In order to compare the performed test at different test modes and with different additively manufactured components, the first cycle tests are executed with similar deformation steps. Every test consists of three cycles; a deformation from $0\ \mu m$ to $1000\ \mu m$ in $50\ \mu m$ steps is applied to the component at every test mode. The components are evaluated for test mode C, then test mode B and finally test mode A. Afterwards, this loop is repeated two more times. In total, every test mode is executed three times for three cycles with every measured component.

6.4.2 Measured strain profiles

The upcoming figures (Figure 6-15- Figure 6-18) show the characteristic strain profiles for the single test modes. The various profiles are displayed in continuous lines for deforming the components. The dotted profiles represent the unloading phase of the tested cycles.

The strain is measured with the LUNA OBR 4600 multiple times per deformation step. Then a mean value for the strain profiles is calculated from that measurement data. For test mode A, the components are clamped on both side to the calibration system. Between the clamps, the part is elongated step by step on a free length of $l_0 = 130\ mm$. This setup for deformation from $0\ \mu m$ to $1000\ \mu m$ is shown in Figure 6-15. For a better recognizability, only every second deformation step is displayed in this figure ($100\ \mu m$ steps). The increasing and decreasing strain per step can be seen clearly. In the areas next to the clamps, the transition between zero strain and the nominal strain value of the represented deformation step can be seen. the strain which is built up inside the clamps is decreasing delayed as shown in the figure below. Along most of the free length of the components, the measured strain is then nearly constant. For further analysis of the measured strain with the LUNA OBR 4600, an averaged strain value is calculated from these constant sections for each single deformation step.

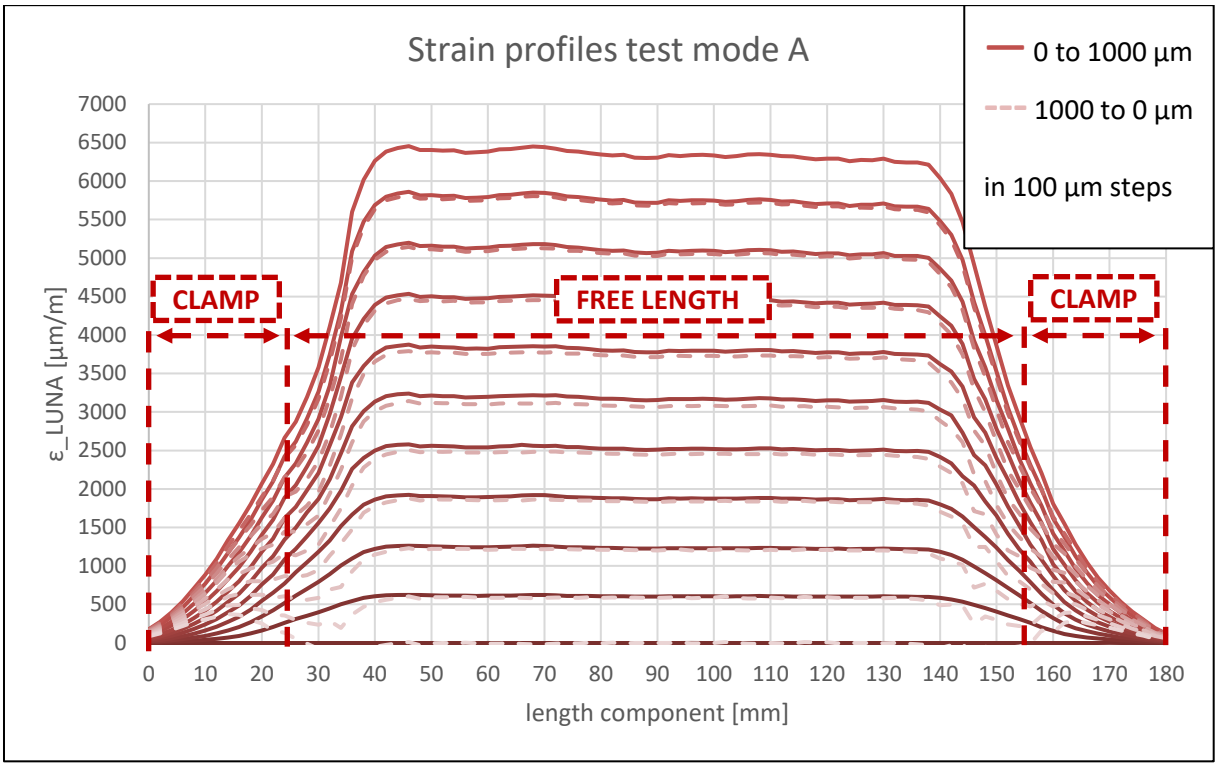

Figure 6-15: Test mode A | strain profiles

As there are four optical fibers integrated into the tested parts, all those fibers should show a nearly identical strain profile for a certain load level. As shown in Figure 6-16, the strain measured at the top two fibers, displayed in dotted orange lines, is slightly bigger than the strain measured at the two fibers at the bottom of the component. These bottom fibers are displayed in dotted blue lines. The average strain calculated from all four fibers is shown as a red continuous line. This deviation between the bottom and top fibers is most likely due to a minimal bending effect of the tested component during the applied deformation. Therefore, the values of the top fibers is slightly higher and the values of the

bottom fibers is slightly lower than the actual strain. The profiles shown in the figure before as well as the upcoming figures are all averaged in a similar way, if there are multiple fibers representing the same strain.

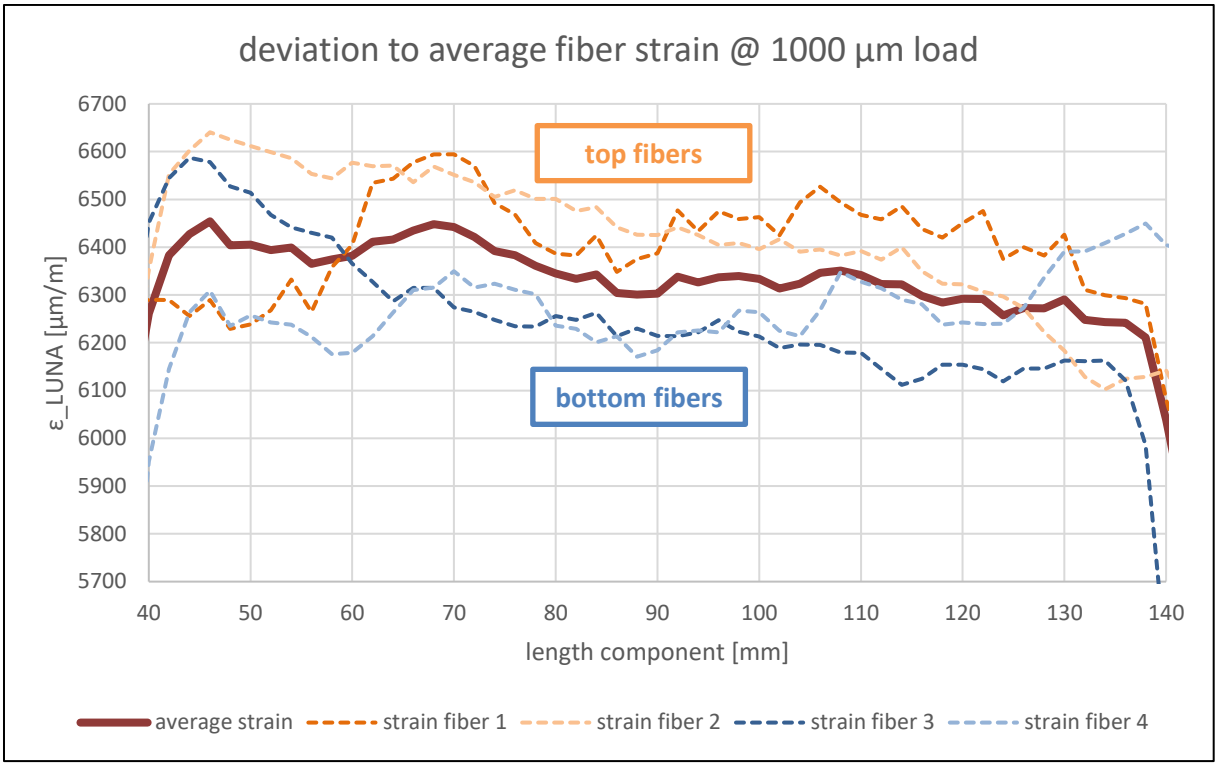

Figure 6-16: test mode A | average strain of four optical fibers

With test mode B, a bending test is performed with the components. The layout of the integrated fibers enable the detection of the positive and negative strain that occurs when a beam-like structure is bent. In Figure 6-17 the strain profiles are shown for various deformation steps. The front fibers are measuring negative strain (compression) while the rear fibers are showing positive strain (elongation). The point where the bending load is applied is at the centre of the components, in the middle of the two bearing points. At this centre point, the maximal positive and negative strain values are measured, and they are continuously decreasing towards the ends of the measured components. For further analysing the strain measured with the optical fibers, the maximum values at that centre point are used for calculations.

The unload cycles are again displayed with dotted lines. The negative strain measured with the fibers is not completely released at the end of a load-unload-cycle. This might probably indicate some kind of run-in behaviour of the components. This effect is more distinct at the front fibers.

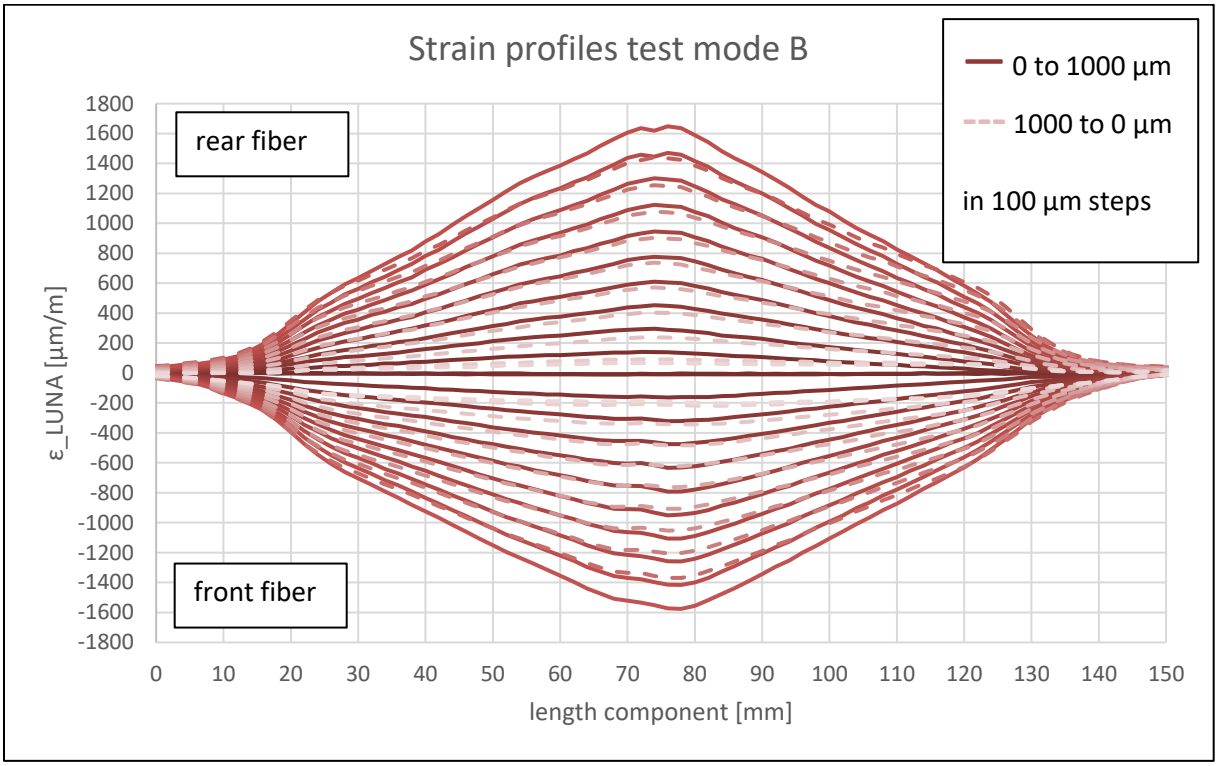

Figure 6-17: test mode B | strain profiles

Similar to the strain profiles shown in the previous figure, the maximum positive and negative strain values for test mode C are measured at the centre of the component. As shown in Figure 6-18, the detected strain within this test mode is lower than before. This results from the smaller distance of the optical fibers to the strain-neutral fiber of the components. Nevertheless, the single steps are clearly distinguishable. The absolute measured strain values on the bottom fibers are slightly less than the values measured at the top fibers. This is most probably a result of the manufacturing process of the components. In the digital model, the top and bottom fibers are equidistant to the neutral axis. But at the manufacturing process with the Mark One, the digital model is sliced into various layers that are then printed one after each other. Between those layers, the optical fibers are integrated. Within this step of manufacturing, the bottom fibers are placed closer to the strain-neutral fiber than originally designed. Therefore, less strain is applied to them during this mode of bending deformation.

The unloading strain profiles of test mode C, displayed with dotted lines, are again rather similar to the related deformation profiles. The difference between bottom and top fibers can also be seen clearly in the figure below.

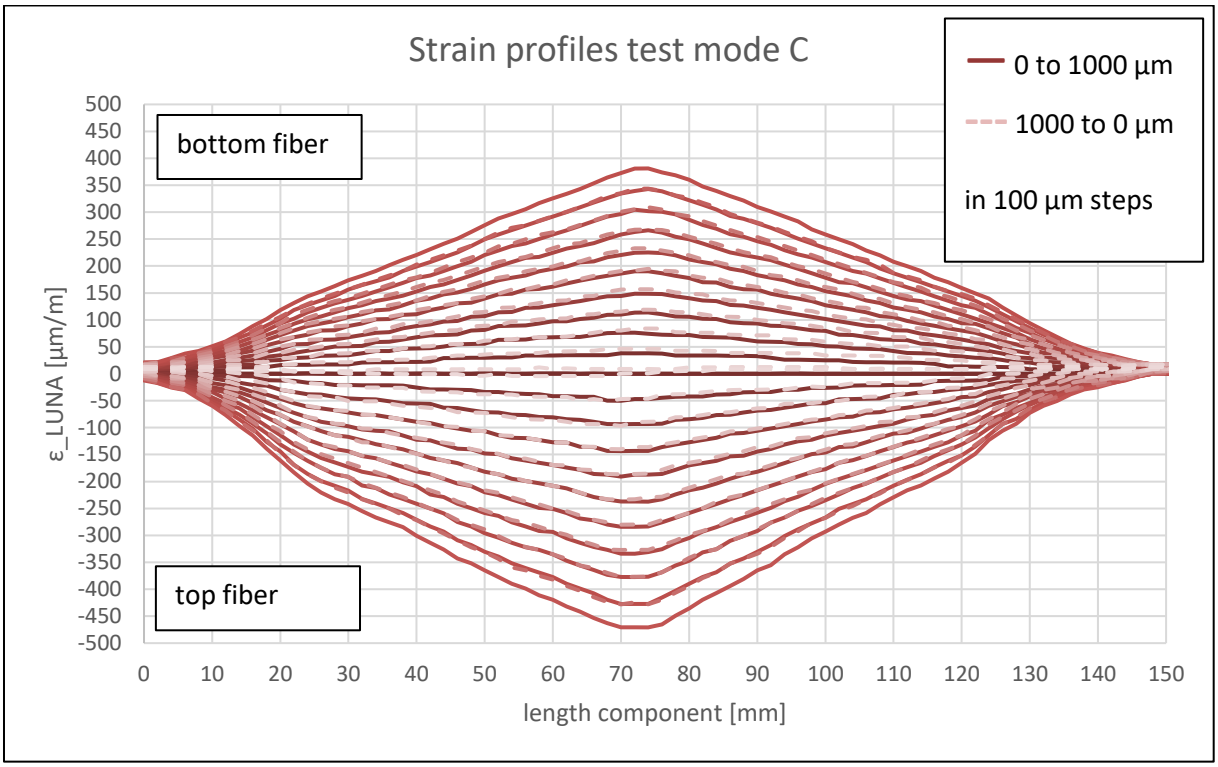

Figure 6-18: test mode C | strain profiles

6.4.3 Cycle test analysis

The performed tests with the displayed component PT11 are corresponding to the test plan. At first, three cycles are performed with test mode C, followed by three cycles with test mode B and finally three cycles with test mode A. Afterwards, these cycles are repeated two more times.

- **Tension tests | test mode A**

The three figures (Figure 6-20 - Figure 6-22) below show, that there is a characteristic running-in behaviour in each case at the first cycle. $\varepsilon_{reference}$ and $\Delta\varepsilon$ are calculated according to the formulas (6.1) and (6.2) with an initial free length of $l_0 = 130\ mm$. Figure 6-19 shows the calculation principle once more for data from the prototypes PT11, PT12 and PT13.

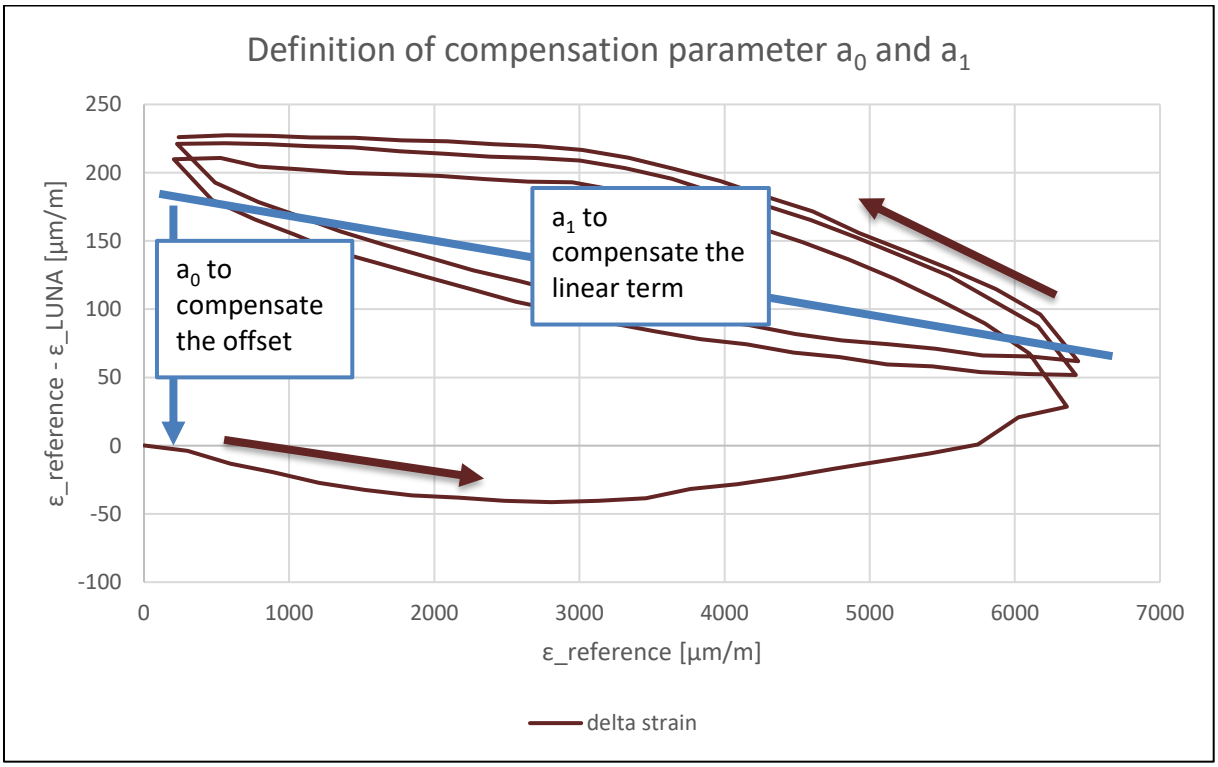

Figure 6-19: Representative graph for the explanation of compensation parameters for PT11, PT12 and PT13

The residuals of test mode A are negative for load cycles and positive for unload cycles. Neglecting the respective first load cycle, the delta between the residuals for test mode A are mostly below $\pm 100\ \mu m/m$. The maximum $\Delta_{residual} = \sim 124\ \mu m/m$.

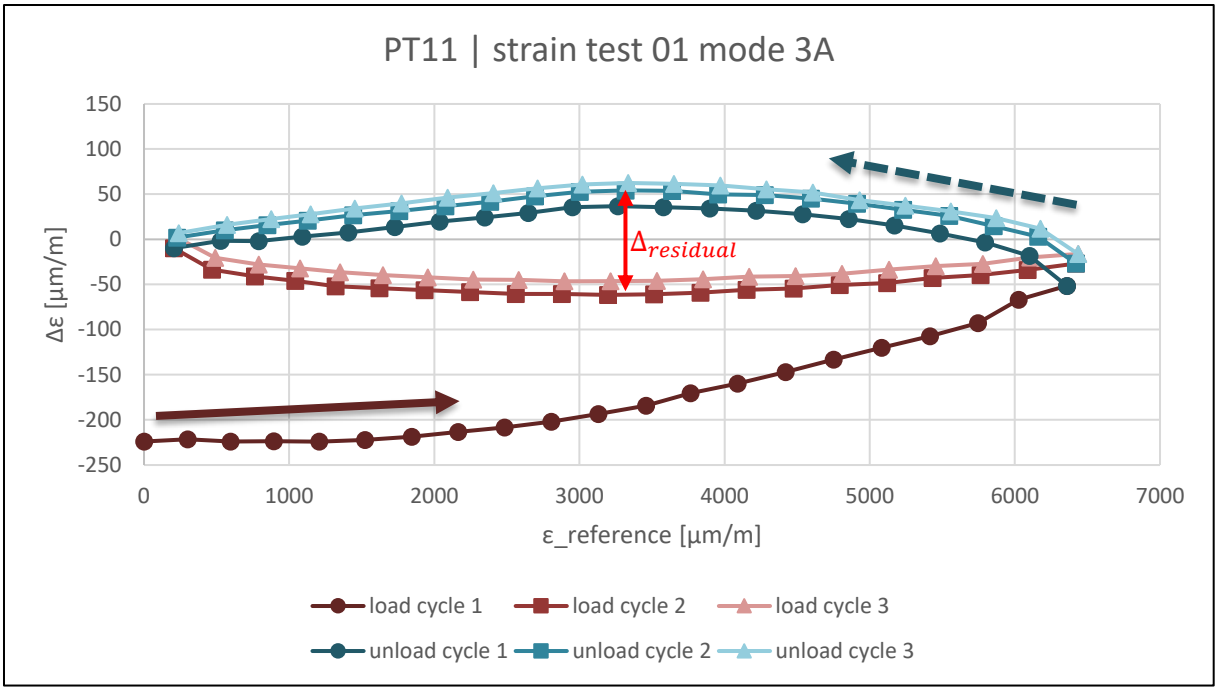

Figure 6-20: PT11 Test 01 mode 3A | Residuals of the LUNA strain values in relation to the reference strain values for 3 cycles

Normally, the running-in characteristic should only appear at the first deformation of the component. But as seen in Figure 6-21 and Figure 6-22, a similar effect is occurring in the later tests. Therefore, it is necessary to exclude the first cycles from the calculation of the compensation parameters at these tests as well. An obvious explanation for this behaviour could not be found yet. It might result from a minimal slipping of the fiber inside the component at the beginning of every performed test. This could indicate that the connection between the smart element and the coating of the optical fiber needs to be improved.

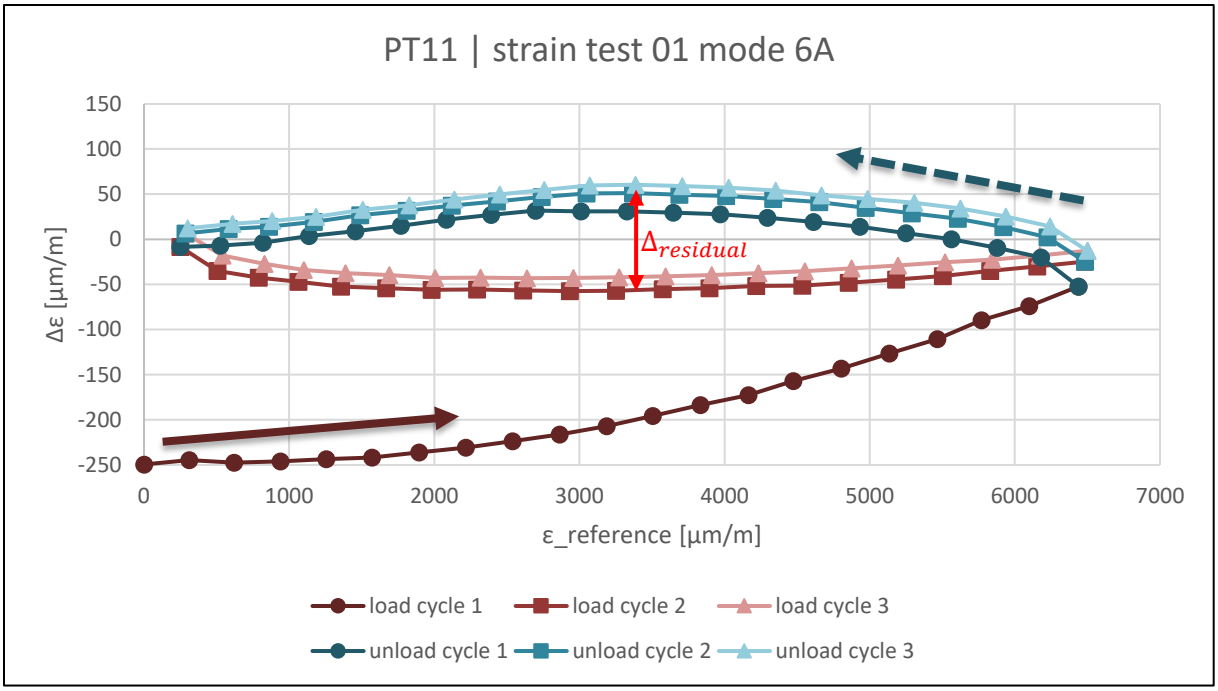

Figure 6-21: PT11 Test 01 mode 6A | Residuals of the LUNA strain values in relation to the reference strain values for 3 cycles

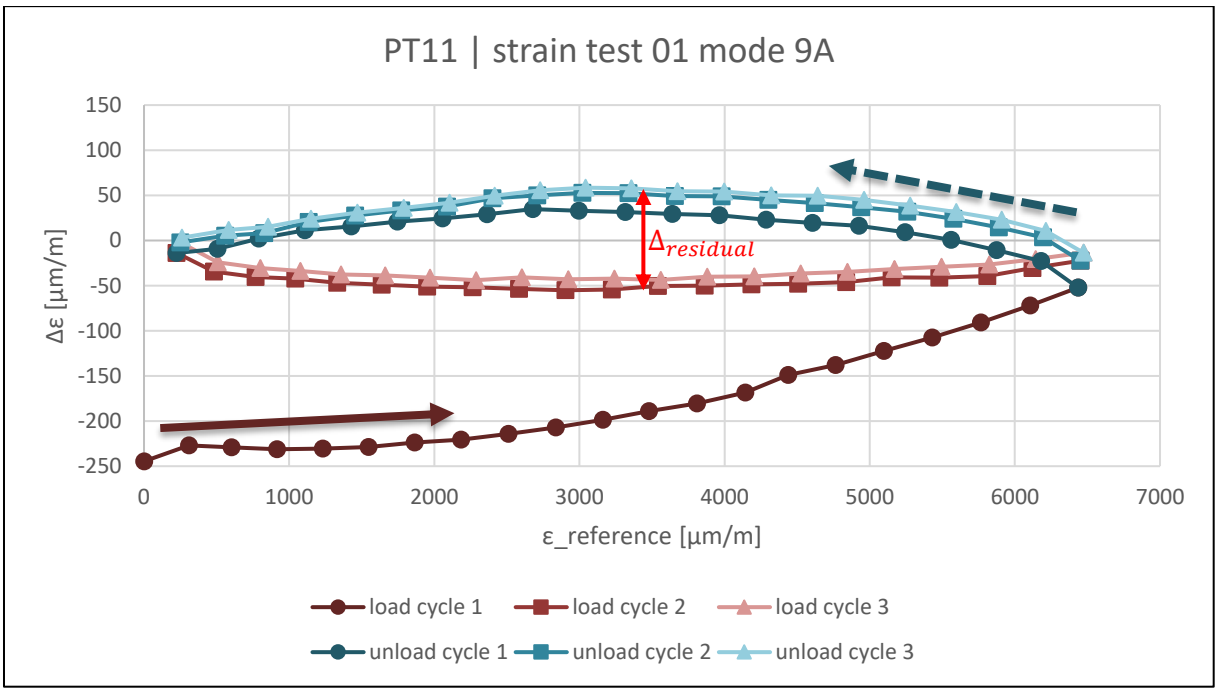

Figure 6-22: PT11 Test 01 mode 9A | Residuals of the LUNA strain values in relation to the reference strain values for 3 cycles

These compensation parameters are then determined for each performed cycle test and test mode. As shown in Table 6-2, the parameter a_0 is fluctuating relatively wide. But the more significant parameter a_1 is rather characteristic for a single component.

Table 6-2: PT11 and PT 12 | Compensation parameters for test mode A

Test	a0 [µm/m]	a1 [-]
PT11 Test 01 3A	-224,2647	1,0227
PT11 Test 01 6A	-249,6629	1,0219
PT11 Test 01 9A	-245,2000	1,0230
PT12 Test 01 3A	-249,0076	1,0456
PT12 Test 01 6A	-213,8187	1,0436
PT12 Test 01 9A	-237,7363	1,0456

From these characteristic parameters for a_1, the mean value can be calculated for every single component. This parameter can then be used to calibrate the strain data from the LUNA OBR 4600 for a tension test.

For PT11, the calculated mean parameter is: $a_{1_{mean}} = 1{,}0225$ and for PT12: $a_{1_{mean}} = 1{,}0449$.

- **Bending tests | test mode B and C**

For the bending tests – test mode B and test mode C – the residuals and the compensation parameters are determined for positive and negative strain. Therefore, the nominal strain is calculated from the interferometer values according to the Euler-Bernoulli beam theory [63]. The test modes are represented by a three-point bending test with a central load. The respective equation used for calculating $\varepsilon_{reference}$ is:

$$\varepsilon_{reference} = \frac{12 * \Delta l_{interferometer} * a_{max}}{L^2} \qquad (6.3)$$

In this equation, $\Delta l_{interferometer}$ is the distance measured with the interferometer on the calibration system, a_{max} is the maximal distance between the optical fiber and the neutral fiber of the bended beam and L is the distance between the two bearings. In case of test mode B, $a_{max} = \pm 3{,}5\ mm$ and in for test mode C $a_{max} = \pm 1\ mm$. $L = 155\ mm$ for both test modes.

As shown in Figure 6-17, the strain measured with the optical fiber system is not completely back to zero at the end of a load-unload-cycle. This results in the negative deflection of the graph shown in Figure 6-23, as the values of ε_{LUNA} are bigger than the reference strain values. For calculating the compensation parameter a_1, the data set for $\varepsilon_{refernce} < 400\ \mu m/m$ is excluded. Furthermore, the

[63] cf. Günther Holzmann, Heinz Meyer and Georg Schumpich, *Technische Mechanik Festigkeitslehre*, 2012, p. 141 ff.

strain data set of the first load cycle is also excluded due to the running-in behaviour at the first deformation of a cycle test.

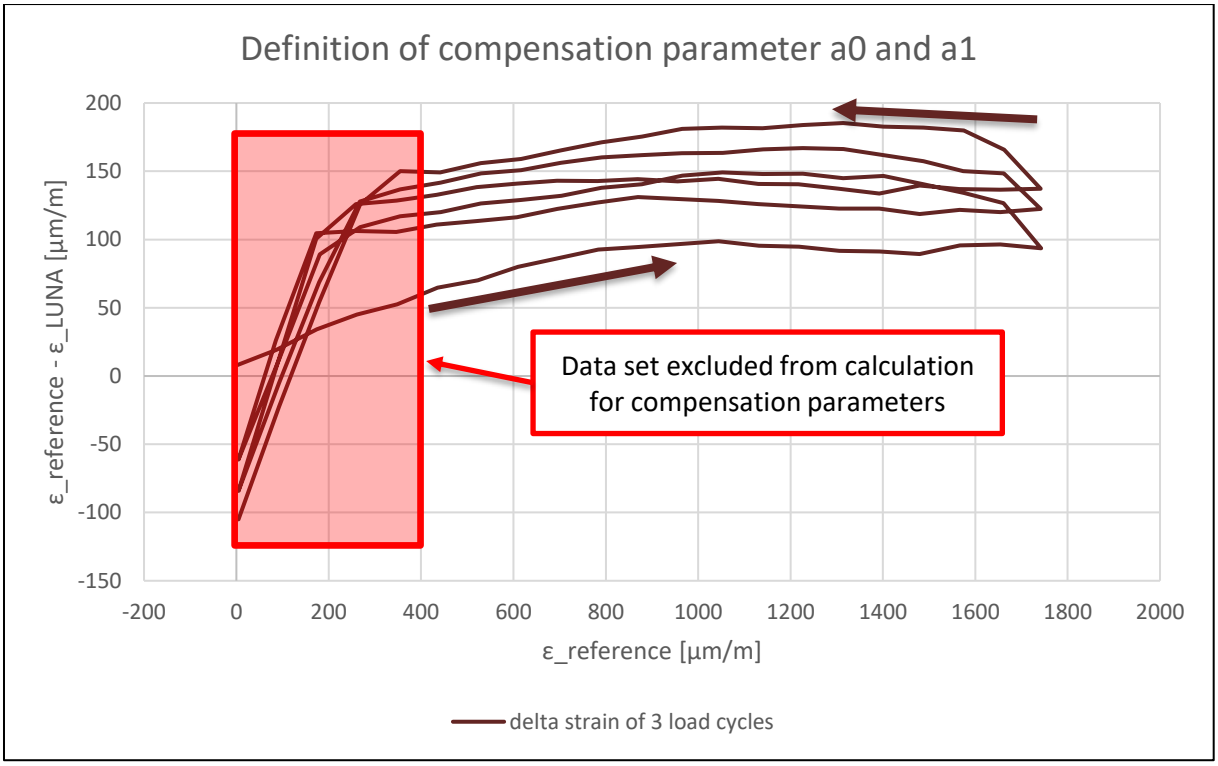

Figure 6-23: Representative graph for the explanation of compensation parameters for bending tests

As shown in Figure 6-24 and Figure 6-25 below, there is still a certain level of strain measured with the LUNA OBR 4600 even when the deformation between the single cycles should be zero. This results in the negative/positive deflections of $\Delta\varepsilon$ at the cycle ends.

Besides these deflections, a running-in behaviour of the first cycle is detected for bending tests as well. This effect is not as distinct as within test mode A. This most probably results from the lower absolute strain that is applied at test mode B and test mode C.

In general, a minimal upwards trend can be detected at the bending tests. But this trend is declining from cycle to cycle.

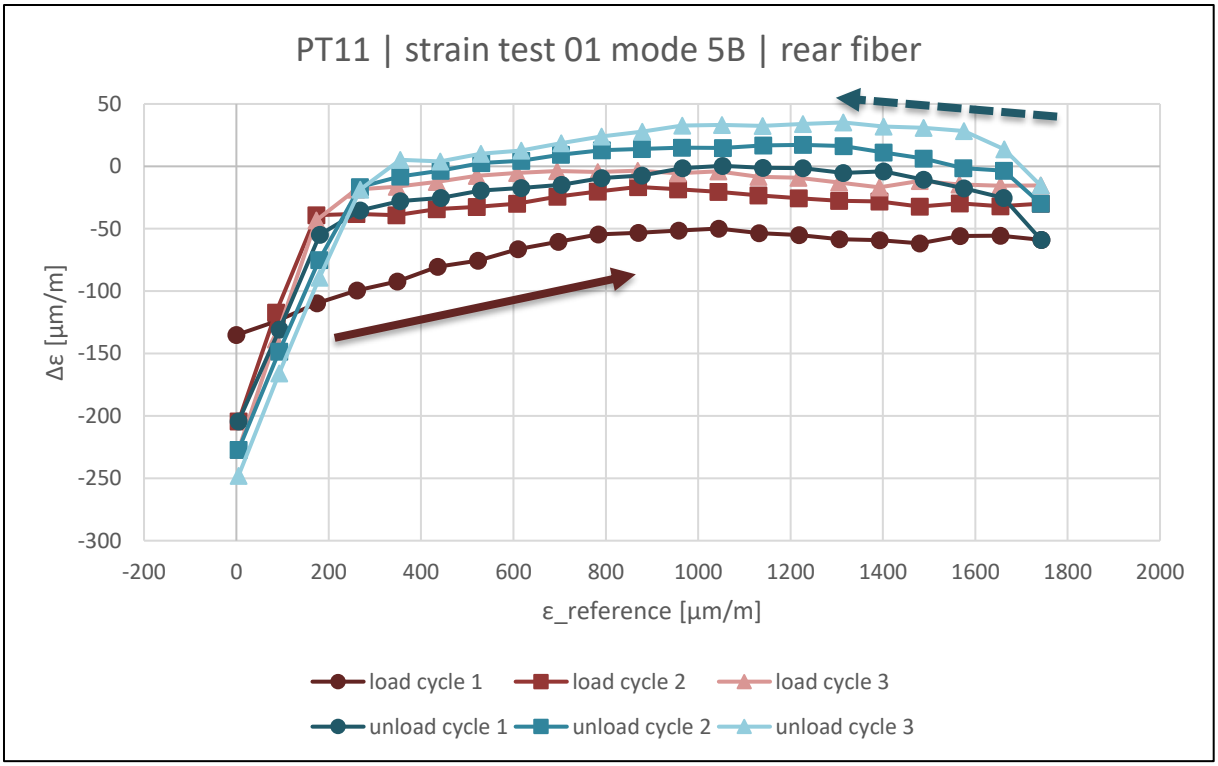

Figure 6-24: PT11 Test 01 mode 5B rear fiber | Residuals of the LUNA strain values in relation to the reference strain values for 3 cycles

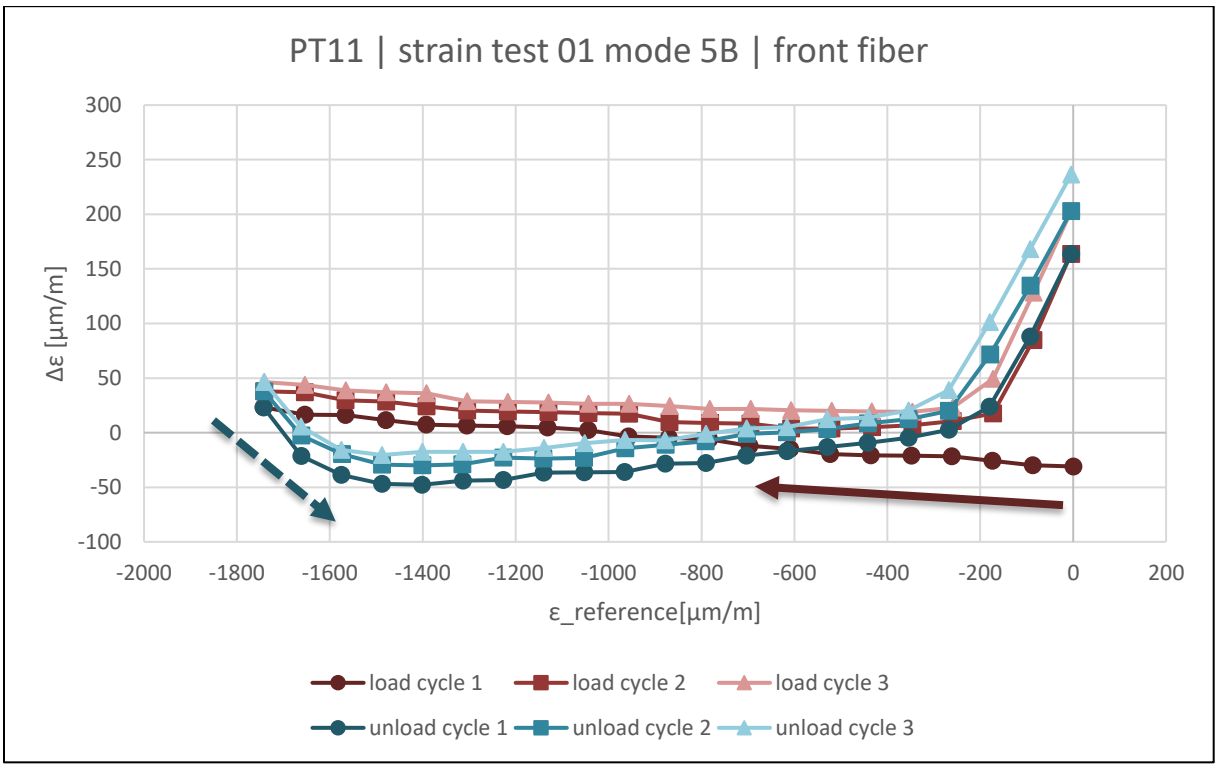

Figure 6-25: PT11 Test 01 mode 5B front fiber | Residuals of the LUNA strain values in relation to the reference strain values for 3 cycles

Table 6-3 lists the compensation parameters of PT11 and PT12 calculated for test mode B. These parameters are determined separately for the rear and front fibers. Besides the values for “PT11 Test 01 2B”, the calculated parameters are within a certain spreading with. These outliers are resulting from a permanent elevated strain level between the cycles that occurred during this specific test. Therefore, the parameters are indicated as non-valid. The compensation parameters calculated at “PT12 Test 02 8B” are also slightly off the other values due to the same effect. The strain gained from the optical fibers is not completely decreasing to zero between the load cycles at these two tests.

Table 6-3: PT11 and PT 12 | Compensation parameters for test mode B

Test	a1 rear [-]	a1 front [-]
PT11 Test 01 2B	Non-valid	Non-valid
PT11 Test 01 5B	0,9945	0,8708
PT11 Test 01 8B	1,0083	0,8679
PT12 Test 02 2B	0,9942	0,8921
PT12 Test 02 5B	1,0171	0,9328
PT12 Test 02 8B	1,0383	0,9686

The parameters displayed in Table 6-4 are determined for test mode C and show a similar characteristic behaviour of the tested components. For calibrating these components for a specific load case, an averaged value from these measurement results can be used. Nevertheless, when comparing the parameters of PT11 and PT12, there will be the necessity of calibrating each component separately.

Table 6-4 PT11 and PT 12 | Compensation parameters for test mode C

Test	a1 bottom [-]	a1 top [-]
PT11 Test 01 1C	0,7458	0,9350
PT11 Test 01 4C	0,7547	0,8621
PT11 Test 01 7C	0,7606	0,8833
PT12 Test 02 1C	0,8974	0,8678
PT12 Test 02 4C	0,8924	0,8740
PT12 Test 02 7C	0,8896	0,8919

6.4.4 Break test analysis

In order to gain additional information on the load limits and maximal detectable strain with the integrated optical fibers, the following break tests are performed for test mode A, B and C. Therefore, the components are deformed until the implemented optical fiber malfunctions.

In Figure 6-26 the strain profiles for PT13 are displayed up to the level of the first measurement errors. The different colour schemes are used to indicate certain events during the performed test. The red profiles show the deformation up to nearly $45000\ \mu m/m$. Then the component is slipping inside the clamp. Therefore, the next profile shown in blue is inconsistently closer to the previous one. The next impact occurs slightly above $50000\ \mu m/m$ where the component is again slipping out of the clamp. The upcoming strain profile, now coloured in orange, is on the same level as the previous one although the distance between the clamps is increased. The component finally fails at around $60000\ \mu m/m$. Consequently, a linear deformation of roughly 6% can be detected with these smart elements. In Figure 6-27, the sections of the displayed strain are colour equivalently to the description above. The differences between the strain calculated from the interferometer data and the optical fiber strain is marginal and only clearly detectable when the component begins to slip inside the clamp.

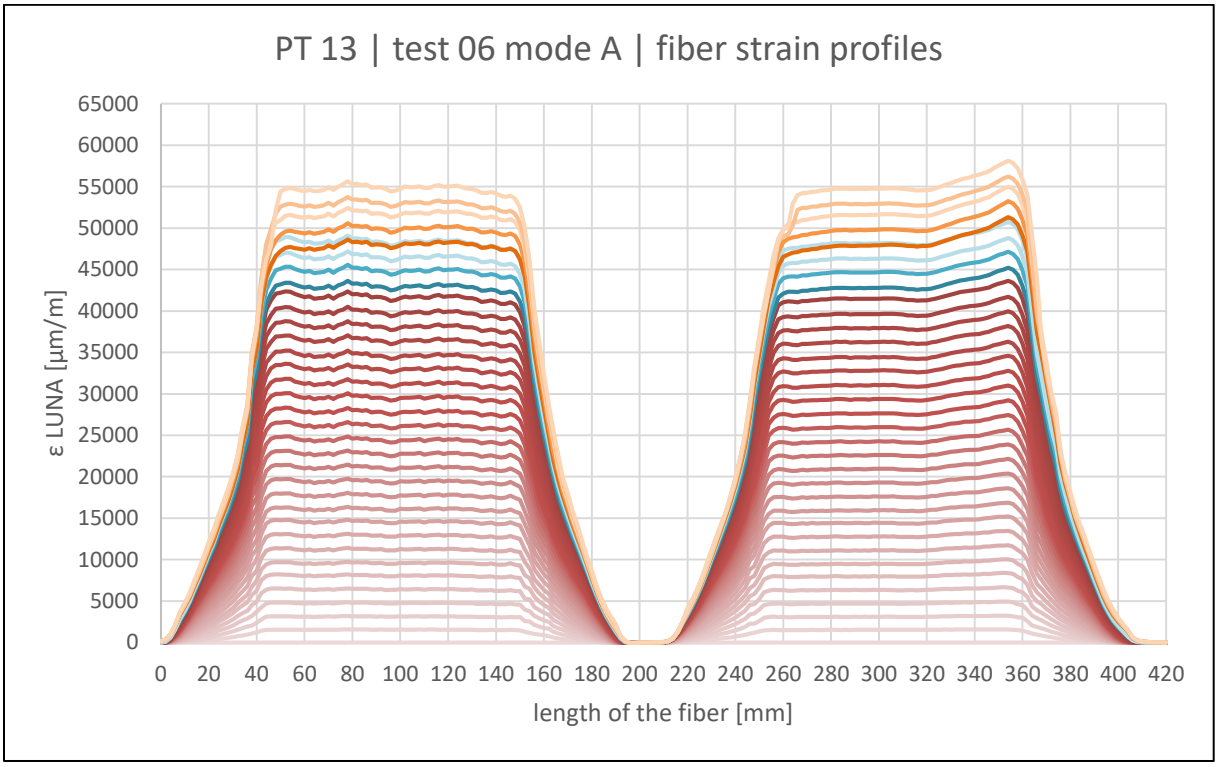

Figure 6-26: Test mode A | increasing strain profiles

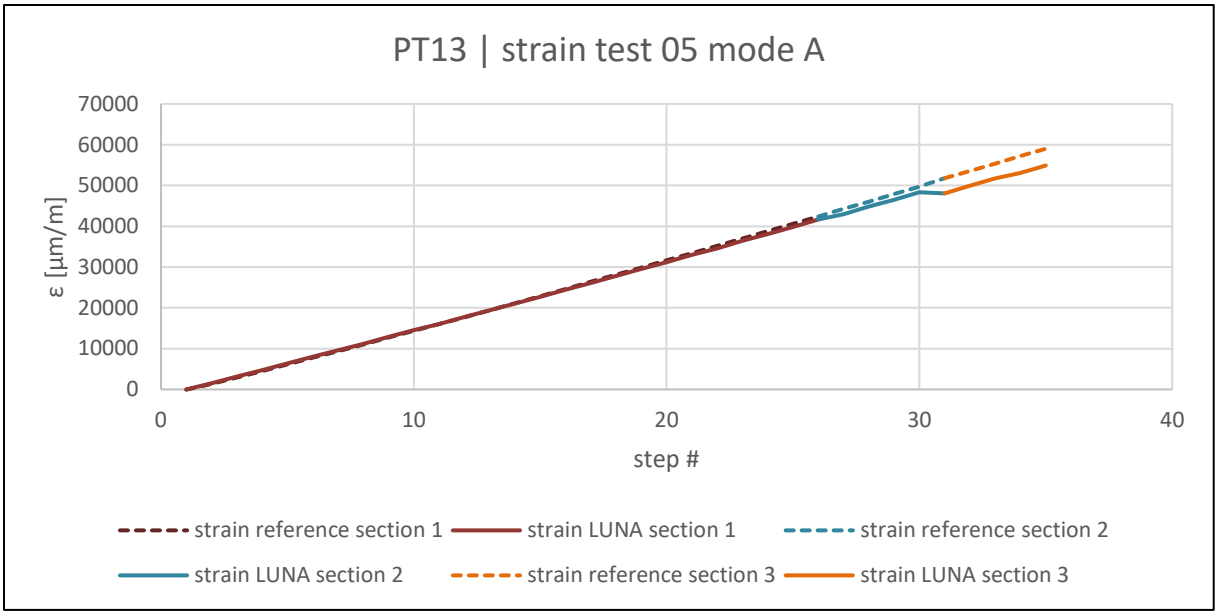

Figure 6-27: Test mode A | increasing strain refernce and strain LUNA plotted over deformation steps

The maximal applicable deformation for bending test mode B is shown in Figure 6-28. The strain profiles of all four integrated fibers of PT12 are depicted in this graphics. The positive strain at the rear fibers is slightly higher than the measured negative strain at the front fibers. This effect needs to be compensated by calibrating the smart elements. The limits for sensing strain with optical fibers for bending deformation is slightly below $30000\ \mu m/m$ in this case. This is equal to a total displacement of $\sim 15\ mm$.

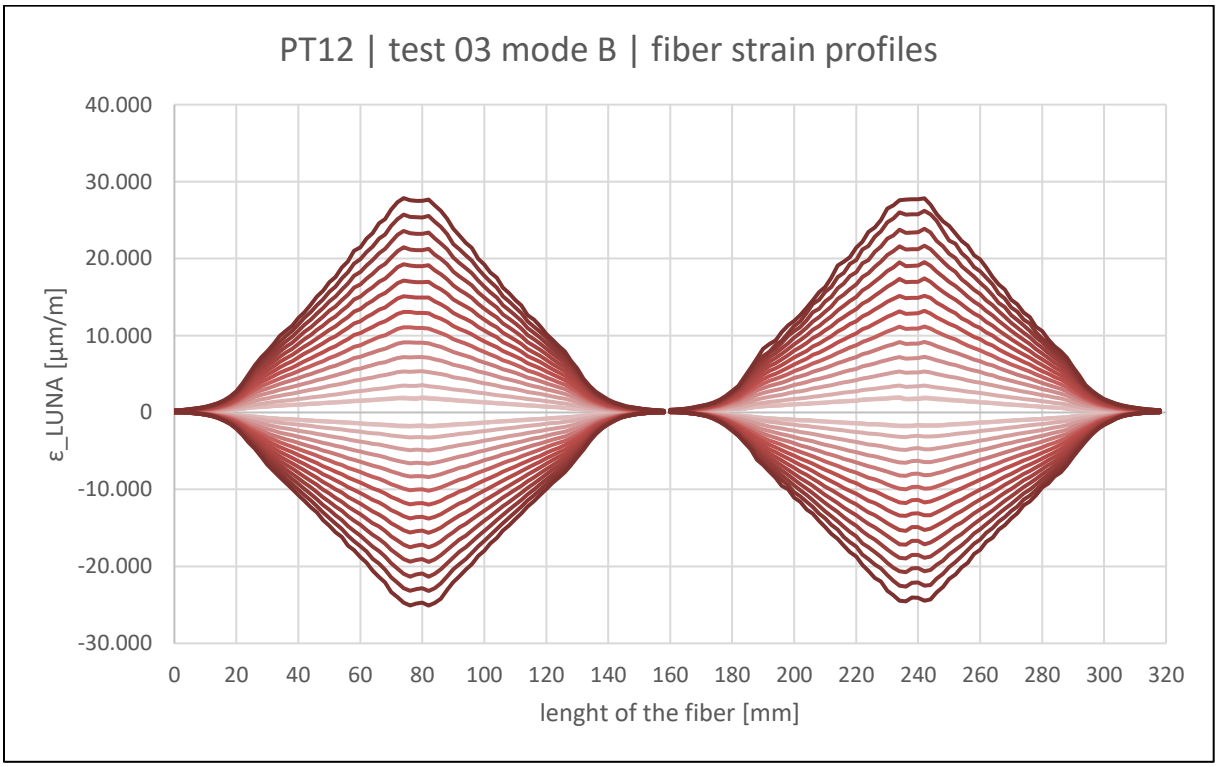

Figure 6-28: Test mode B | increasing strain profiles

The compensation as mentioned before is shown in Figure 6-29 and Figure 6-30. In the first diagram, the absolute difference between the maximal positive and negative strain measured with the LUNA OBR 4600 is $\sim 3000\ \mu m/m$. In the second diagram, the strain values are compensated by the factor a_1. This factor is gained from the cycle tests that were performed previously. In both figures, the strain measured with the optical fibers differs from the strain derived from the interferometer data at the first two deformation steps. This is a result form the performed load cycle before the break test. As already displayed in previous tests, the optical fiber strain does not fully decrease to zero between two load cycles with this test mode.

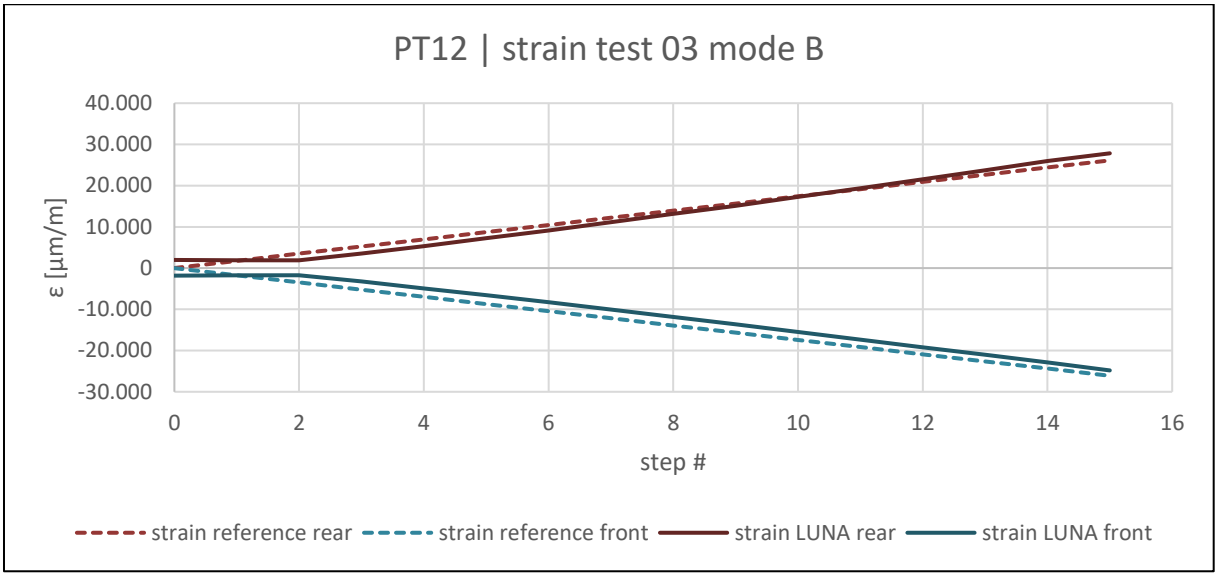

Figure 6-29: Test mode B | increasing strain reference and strain LUNA plotted over deformation steps

The compensated optical fiber strain is drifting off the strain calculated from the interferometer values at higher strain levels. As the factor a_1 is gained from cycle tests at strain levels below $2000\ \mu m/m$ it might be necessary to calibrate the components separately for higher strain levels.

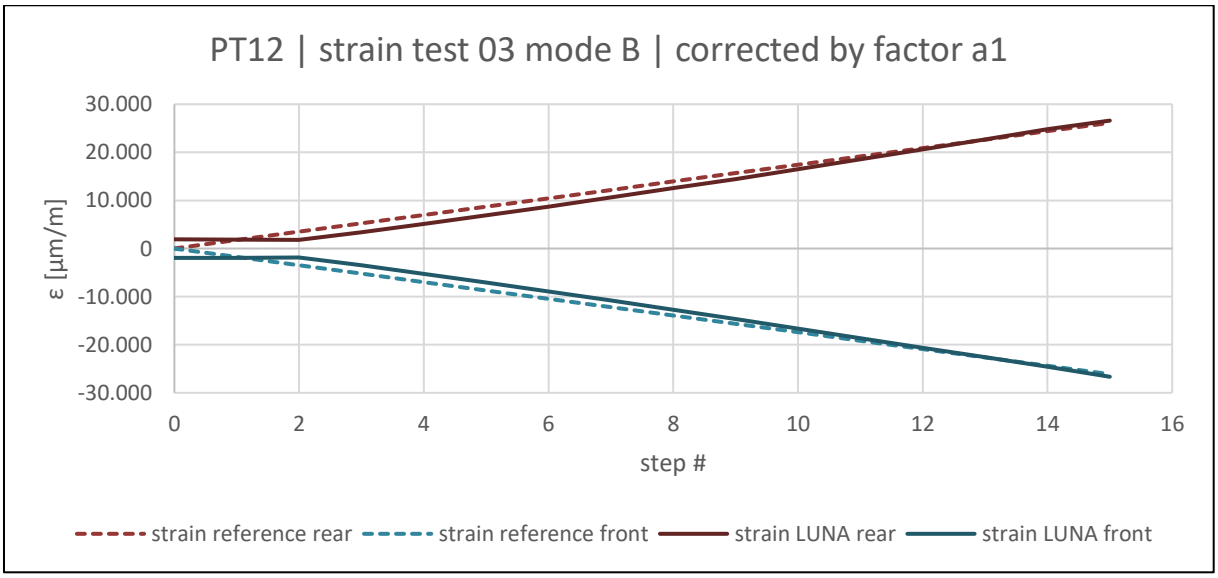

Figure 6-30: Test mode B | increasing strain reference and corrected strain LUNA plotted over deformation steps

The performed break test with bending test mode C needed to be aborted before the optical fibers reached their limits. The applied deformation was not big enough to break the optical fibers, but the test setup reached its spatial limit as shown in Figure 6-31. The total displacement applied with this test mode is $\sim 35\ mm$.

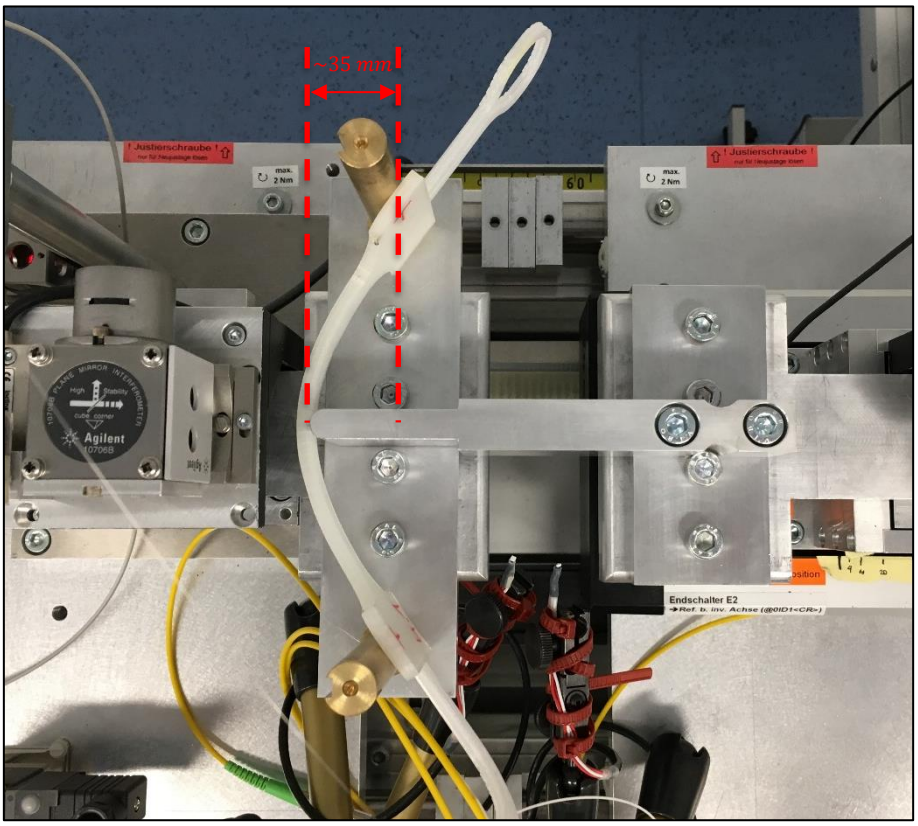

Figure 6-31: PT11 test 04 mode C | maximal applicable deformation

The strain profiles of all integrated optical fibers measured during this load test are displayed in Figure 6-32 below. The impacts of the load cycle performed right before the maximum load test are noticeable up to the fifth deformation step. The first five optical fiber strain profiles are elevated to a higher level. For comparing the strain data from the LUNA OBR 4600 and the interferometer strain data, the values are again compensated by the factor a_1 calculated earlier for PT11. As shown in Figure 6-33, the positive and negative optical fiber strain data is consistent to the calculated interferometer strain data. The absolute difference between positive and negative strain after compensation is $\sim 1000\ \mu m/m$ at this load case. An additional calibration at these high strain levels might be necessary to optimize the sensing results.

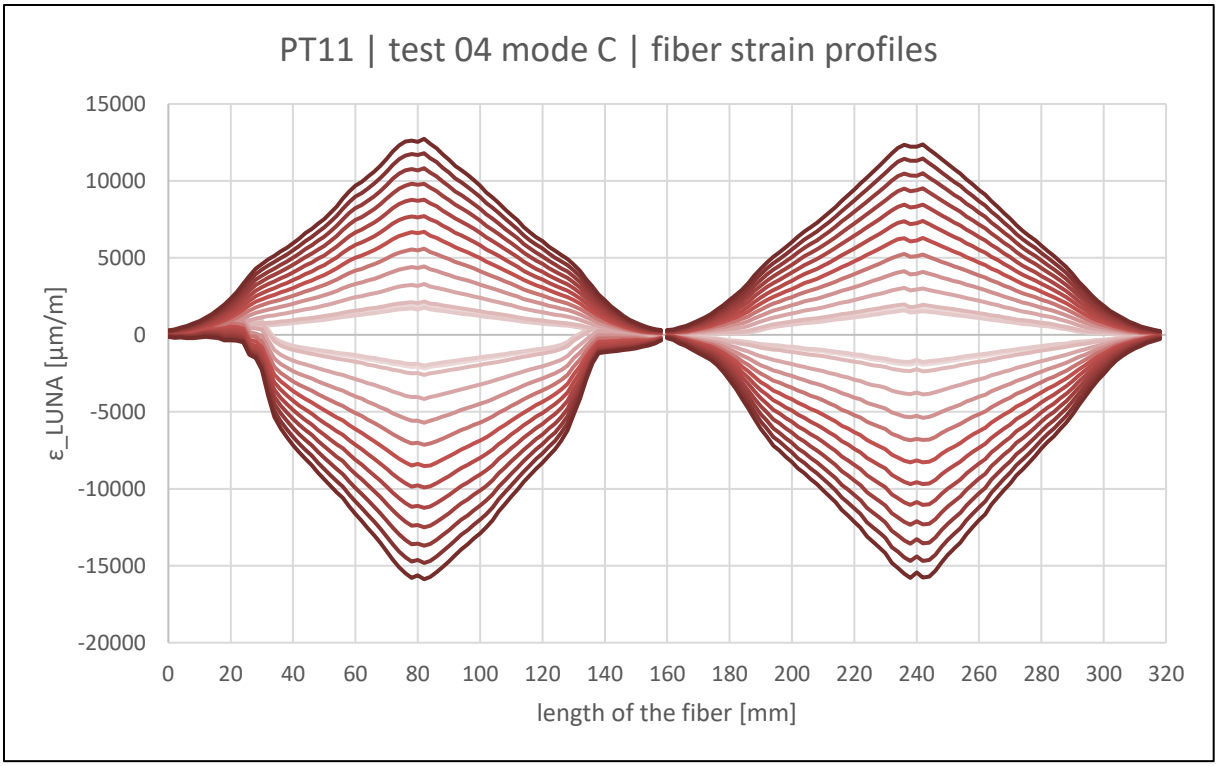

Figure 6-32: Test mode C | increasing strain profiles

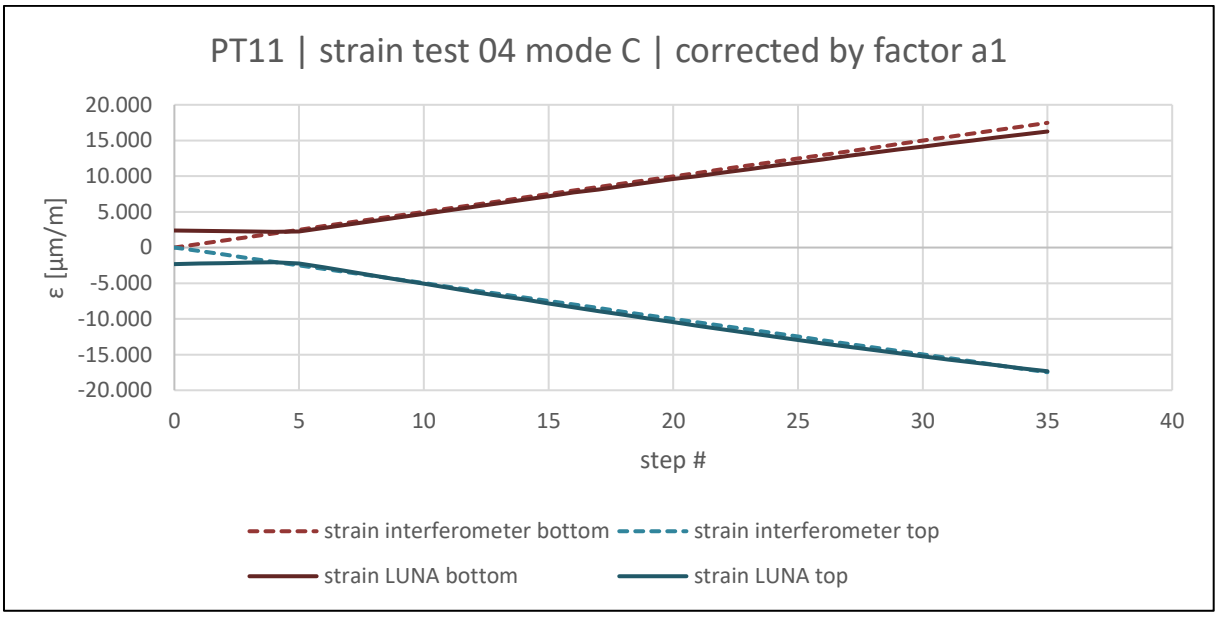

Figure 6-33: Test mode C | increasing strain reference and corrected strain LUNA plotted over deformation steps

7. Conclusion and further perspectives

The potential and the feasibility of additively manufactured smart components are confirmed successfully. After identifying the crucial aspects of the combined technologies, the first steps towards realizing this innovative concept are made. After having developed a manufacturing strategy, multiple prototypes are produced for verification and validation purpose. Laboratory tests with highly accurate reference measurements provide sufficient data for a final analysis.

7.1 Results and expertise

FOS is a well-suited sensing technology for manufacturing these smart components. They provide the possibility of integrating a minimally interfering sensing element into the structure of the produced part. Standard single mode optical fibers can be used for this purpose. Rayleigh scattering naturally occurs along the fiber core. The changes in the Rayleigh backscattering patterns can be correlated to changes in the physical parameters like temperature and strain. This effect is used to realize a highly accurate distributed sensing system with a high spatial resolution.

The LUNA OBR 4600 is identified as a suitable optical measurement system for this thesis. Combining this technology with the emerging concepts of additive manufacturing, smart components can be produced. Therefore, an integration strategy of the optical fibers into the produced elements need to be developed. The FFF process provides the optimal possibility for testing the concept. The printing process of the Mark One 3D printer is adopted in a way that an optical fiber can be placed inside the manufactured structure. As the coating of the optical fiber needs to match the printer's fabrication parameters, an ORMOCER® coated optical fiber is selected for this purpose. Guidelines are developed and provide the necessary knowledge on how smart elements can be manufactured in that way.

Although the manufacturing process is still improvised, the researched concept is proven feasible. The first prototypes can be produced with this method. Various tension and bending tests with specially designed laboratory equipment are performed with multiple components. Test cycles and modes for tension and bending tests are defined and realized with the final three components. The results from these laboratory measurements show, that the data obtained from the optical fiber measurements is corresponding to a highly accurate reference measurement. Nevertheless, compensation parameters need to be determined for the different load cases to improve the measurement results. These parameters are characteristic for every single component. The smart additively manufactured elements need to be calibrated for all expected load cases. The different tests show a distinctive running-in behaviour at the beginning of each cycle test. Test results are reproducible when similar deformation is applied to the components. Cycle tests for bending deformation have shown that the strain measured with the optical fiber is not completely decreasing to zero between two load cycles. Therefore, parts of the strain data need to be excluded from the determination of the characteristic compensation parameters. The maximal detectable strain for tensile load is around $55000\ \mu m/m$ and for bending load slightly below $30000\ \mu m/m$.

7.2 Further perspectives and possible improvements

The optical fiber integration method needs additional improvements. Therefore, a manufacturing machine specially designed to create such elements could be developed. As a first step towards such a machine, an open source FFF 3D printer could be extended with an additional print head that is used to integrate the optical fiber. With this adapted printer, additional sensitive plastic components can be produced more efficiently as the manufacturing limitations resulting from using the Mark One can be avoided. Furthermore, the integration of acrylic coated optical fibers into plastic components could be tested as the print heads operating temperature can be adjusted accordingly.

Further on, various other manufacturing technologies can be examined concerning their feasibility of producing such smart elements. As the materials of high temperature resistant fiber coatings are improving, the production of additively manufactured smart metal components might get feasible.

Improvements of the sensing instruments might enable not only static but dynamic distributed measurements. Then, the manufactured components could be used to perform vibration analyses.

The big advantages in contrast to existing electrical sensing systems is the possibility of integrating a distributed sensing element into the structure of the manufactured component. The senor can be placed at the exact location of interest and will not influence the measurement results. Furthermore, it is not influenced by electromagnetic disturbances.

List of figures

List of tables

References

Al-Azzawi, A.: Fibre Optics: Principles and Practices, Boca Raton: CRC Press, 2007.

Breuninger, J. et al.: Generative Fertigung Mit Kunststoffen: Konzeption und Konstruktion für Selektives Lasersintern, Berlin: Springer Verlag 2013.

Corning: SMF-28e+ Optical Fiber Specification Sheet, Datasheet 2014.

DeCusatis, C. M.; DeCusatis C. J. S.: Fiber Optic Essentials, 1st ed., Amsterdam [u.a]: Elsevier, 2006.

Fang, Z.: Fundamentals of Optical Fiber Sensors, 1st ed., Oxford: Wiley-Blackwell, 2012.

Fastermann, P.: 3D-Druck/Rapid Prototyping: Eine Zukunftstechnologie kompakt erklärt, 1. Aufl., Berlin, Heidelberg: Springer Verlag, 2012.

Fastermann, P.: 3D-Drucken: Wie die generative Fertigung funktioniert, 2. Aufl., Berlin, Heidelberg: Springer Verlag, 2016.

FBGS International: DTG-A3, Datasheet.

Feldmann, C.; Pumpe, A.: 3D-Druck – Verfahrensauswahl und Wirtschaftlichkeit, Münster: Springer Verlag, 2016.

Fibercore: SM1250(10.4/125)Cu, Datasheet.

Fibercore: SM1250(10.4/125)Gold, Datasheet.

fibrisTerre Systems GmbH: FTB 2505 series, Datasheet.

Gebhardt, A.; Hötter, J.S.: Additive Manufacturing: 3D Printing for Prototyping and Manufacturing, Munich 2016.

Ginu Rajan: Optical Fiber Sensors: Advanced Techniques and Applications, 1st ed., CRC Press, 2015.

Grund, M.: Implementierung von Schichtadditiven Fertigungsverfahren, 1. Aufl., Berlin, Heidelberg: Springer Verlag, 2015.

Hagl, R.: Das 3D-Druck-Kompendium: Leitfaden für Unternehmer, Berater und Innovationstreiber, 2. Aufl. 2015 ed., Wiesbaden: Gabler, 2015.

Hehr, A. et al.: Integrating Fiber Optic Strain Sensors into Metal Using Ultrasonic Additive Manufacturing, in: JOM, Vol. 70, No. 3, 2018

Holzmann, G. et al.: Technische Mechanik Festigkeitslehre, 10. Überarb. Aufl., 2012 ed. Wiesbaden: Vieweg+Teubner Verlag, 2012.

HP Development Company, L.P.: HP Multi Jet Fusion Technology, HP Technical White Paper, 2018

Klocke, F.: Fertigungsverfahren 5: Gießen, Pulvermetallurgie, Additive Manufacturing, 4. Aufl. 2015 ed., Berlin, Heidelber: Springer Verlag, 2015.

Lachmayer, R.; Lippert, R.B.: 3D-Druck beleuchtet: Additive Manufacturing auf dem Weg in die Anwendung, Berlin: Springer Verlag, 2016.

Lachmayer, R.; Lippert, R.B.: Additive Manufacturing Quantifiziert: Visionäre Anwendungen und Stand der Technik, Berlin, Heidelberg: Springer Verlag, 2017.

Löffler-Mang, M.: Optische Sensorik: Lasertechnik, Experimente, Light Barriers, Wiesbaden: Vieweg+Teubner Verlag, 2012.

López-Higuera, J.M.: Handbook of Optical Fibre Sensing Technology, Chichester: John Wiley & Sons Ltd., 2002.

Lu, X.; Soto, M. A.; Thévenaz L.: Temperature-Strain Discrimination in Distributed Optical Fiber Sensing Using Phase-Sensitive Optical Time-Domain Reflectometry, in: Optics Express Vol. 25, 2017.

Luna Innovations Inc.: OPTICAL BACKSCATTER REFLECTOMETER TM (Model OBR 4600), Datasheet 2014.

Majumder, M. et al.: Fibre Bragg Gratings in Structural Health monitoring—Present Status and Applications, in: Sensors and Actuators A: Physical, 2018.

MarkForged Inc.: Mark One Mechanical Properties Data Sheet, Datasheet 2015.

Moi-composites-srl: Apparatus and Method for Three-Dimensional Printing of Continuous Fibre Composite Materials, 2015.

Monsberger, C.: Verteilte Faseroptische Dehnungsmessung Mit Dem Hochauflösenden Luna OBR 4600, Diplomarbeit, Technische Universität Graz, 2015

Presl, R.: Entwicklung eines automatisierten Messsystems zur Charakterisierung Faseroptischer Dehnungssensoren, Diplomarbeit, Technische Universität Graz, 2009

Price, S. et al.: On Process Temperature in Powder-Bed Electron Beam Additive Manufacturing: Process Parameter Effects, in: Journal of Manufacturing Science and Engineering December 2014, Tuscaloosa 2014.

Samiec, D.: Distributed Fibre-Optic Temperature and Strain Measurement with Extremely High Spatial Resolution, in: Optical Metrology, in: Photonic international 2012, originally published in German in Photonik 6/2011, Waldbronn 2011.

Schmid, M.: Additive Fertigung Mit Selektivem Lasersintern (SLS): Prozess- und Werkstoffüberblick, 1. Aufl., Wiesbaden: Springer Vieweg, 2015.

Schmidt, T.: Potentialbewertung Generativer Fertigungsverfahren Für Leichtbauteile, Berlin, Heidelberg: Vieweg, 2016.

Schumpeter, J.A.: Theorie Der Wirtschaftlichen Entwicklung, 7. Aufl., Berlin 1987.

Sensuron: NASA UAV Deflection And Strain Monitoring, 2008.

TAIHAN: Bending Loss Insensitive Fiber ITU-T G.657, Datasheet.

Tuegel, E. J. et al.: Reengineering Aircraft Structural Life Prediction Using a Digital Twin, in: International Journal of Aerospace Engineering Volume 2011, 2011.

Udd, E.; Spillman, W.: Fiber Optic Sensors: An Introduction for Engineers and Scientists, Hoboken: John Wiley & Sons Inc., 2011.

Online References

‘3dhubs Knowledge-Base’

<https://www.3dhubs.com/knowledge-base/additive-manufacturing-technologies-overview> [accessed 18 July 2017]

‘BJ Process’

<https://s3-eu-west-1.amazonaws.com/3dhubs-knowledgebase/introduction-binder-jetting/2-bj-steps.png> [accessed 2 March 2018]

‘FDM Process’

<https://s3-eu-west-1.amazonaws.com/3dhubs-knowledgebase/intro-fdm-3d-printing/2-fdm-steps.png> [accessed 2 March 2018]

‘LENS Process’

<https://image.slidesharecdn.com/2015-11-26-slsebmlens-151222115944/95/2015-1126-sls-ebm-lens-52-638.jpg?cb=1450785661> [accessed 15 August 2018]

‘LOM Process’

<http://www.lboro.ac.uk/media/wwwlboroacuk/external/content/research/amrg/Direct Energy Deposition - process.jpg> [accessed 15 August 2018]

‘MJ Process’

<https://s3-eu-west-1.amazonaws.com/3dhubs-knowledgebase/introduction-material-jetting/2-mj-steps.png> [accessed 2 March 2018]

‘Moi - Printer Concept’

<https://uploads-ssl.webflow.com/5a588c043c31ba0001f32925/5a6db60b10ba58000189f348_project-atrops-img.jpg> [accessed 15 August 2018]

‘SLA Process’

<https://s3-eu-west-1.amazonaws.com/3dhubs-knowledgebase/introduction-sla-3d-printing/8-sla-steps.png> [accessed 2 March 2018]

‘SLS Process’

<https://s3-eu-west-1.amazonaws.com/3dhubs-knowledgebase/introduction-sls-3d-printing/2-sls-steps.png> [accessed 2 March 2018]

Appendix: Guidelines

The following guidelines provide a step by step list on how to manufacture smart components like the ones realized within this master thesis.

General limitation with the Mark One 3D printer:

- Print bed limits: 320 x 132 x 154 mm
- Minimal fiber length: ~700mm
- Minimal fiber radii: >10mm

Part design guideline

1. Design your part with a CAD program
2. Define the desired plane to be equipped with optical fiber for sensing
   2.1. Minimal distance to top/bottom of part: 0,4mm
3. Design/construction of fiber bridge
   3.1. Draw the fiber path on the previously defined plane
   3.2. Create a rectangle (3,2mm x 0,1mm in width and height) perpendicular to the fiber path
   3.3. Centre of the rectangle needs to be placed on the fiber path
   3.4. Create a “sweeping/rib” (according to CAD program) using the rectangle and the fiber path; rectangle should stay orthogonal to the fiber path
   3.5. Subtract the generated thin profile from your component
   3.6. Draw a second rectangle (3mm x 1mm in with and height) perpendicular to the fiber path
   3.7. Centre of the rectangle needs to be placed on the fiber path
   3.8. Create a “sweeping/rib” (according to CAD program) using the rectangle and the fiber path; rectangle should stay orthogonal to the fiber path
   3.9. This will be the path/bridge for your fiber
4. Construct “holes” in the “fiber plane” everywhere where no fiber should be (the Mark One tries to integrate as much fiber as possible)
   4.1. Distance to walls >3mm
   4.2. Height of holes: 0,1mm → the thickness of one layer
   4.3. There should be no area left where the printer’s software application (eiger.io) could fit in fiber except the predefined fiber path
5. Upload your part to eiger.io software provided by MarkForged (username: fablabgraz; pw: fablabgraz)
   5.1. Place the part to the print bed

5.2. Fiber plane needs to be parallel to the print bed

5.3. Settings in eiger.io:

- Layer height: 0,1mm
- Fibertype: fiberglass

5.4. Go to internal view

5.5. Choose 2D view

5.6. Select the layer where the fiber should be placed at

5.7. Settings for “edit layer box”:

- Use fiber: yes
- Fiber fill type: concentric fiber
- Walls to reinforce: outer shell only
- Concentric fiber rings: 1
- Start rotation percent: depending on part design → definitely outside the object; somewhere on the fiber bridge with enough distance to object (>30mm)
- Pause after layer: yes

5.8. Add a “Pause after layer” one layer before and one layer after fiber layer to check structural integrity and fiber integration process

5.9. Save your settings

6. Send the file to the Mark One for printing

Printing process guideline

1. Load optical fiber to MarkForged Mark One printer according to printer guideline
   1.1. Load material
   1.2. Load fiber
   1.3. Quick load fiberglass
   1.4. Troubleshooting: special attention fiber inserting to cutting/extruding tool
   1.5. Cut when fiber reaches the fiber nozzle of the print head
   1.6. Remove the cut-off fiber
2. Start printing process with part specially designed for printing with optical fiber used for sensing
3. Check for correct start of the printing process
4. Print until printer stops according to configured pause
5. Check the structure of the component
6. Print fiber layer
7. Pause the printing process immediately after the optical fiber is printed

8. Take the print bed out of the Mark One
9. Expose the optical fiber from the fiber bridge outside the component
10. Secure printed fiber outside the part to the printer bed using masking tape
11. Continue the next layers of the print and check the integrity and implementation quality of the optical fiber
12. Finish the print as usual

Fiber splicing process guideline

1. Prepare a fiber optical pigtail for splicing
   1.1. Remove ca.130mm of the yellow protection tube and the KEVLAR fabric inside
   1.2. Remove 33mm of the coating from the optical fiber
   1.3. Put on a 60mm splice protection tube
   1.4. Cleave the bare optical fiber → after cleaving, 20mm bare optical fiber should be left
2. Prepare the optical fiber of the smart component for splicing
   2.1. Uncover ca.25mm bare optical fiber
   2.2. Cleave the uncover bare optical fiber
   2.3. Pay attention for having enough loose fiber between the fiber end and the printed structure (ca.70mm) → will result in problems with the splicer
3. Place the two bare fiber ends inside the splicer and operate the splicing program accordingly
4. Protect the splice with the splice protection tube (heat shrinking process)